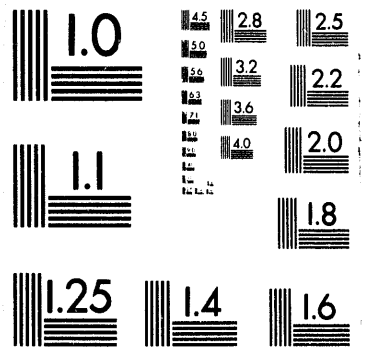
1.0
4.5
2.8
2.5
5.0
3.2
2.2
5.6
3.6
6.3
4.0
2.0
1.1
1.8
1.25
1.4
1.6

1 of 2

DOE/BC/14653--T9
A/92

INNOVATIVE TECHNIQUES FOR THE DESCRIPTION OF RESERVOIR HETEROGENEITY USING TRACERS

Second Technical Annual Progress Report
October 1991 – September 1992

By
Gary A. Pope
Getty Oil Co. Centennial Chair in Petroleum Engineering

Kamy Sepehrnoori
Frank W. Jessen Professor in Petroleum Engineering

Work Performed under Contract No. DE–AC22–90BC14653

Chandra M. Nautiyal, Contracting Officer Representative
U.S. Department of Energy
Bartlesville Project Office
P.O. Box 1398
Bartlesville, OK 74005

DISCLAIMER

This report was prepared as an account of work sponsored by an agency of the United States Government. Neither the United States Government nor any agency thereof, nor any of their employees, makes any warranty, express or implied, or assumes any legal liability or responsibility for the accuracy, completeness, or usefulness of any information, apparatus, product, or process disclosed, or represents that its use would not infringe privately owned rights. Reference herein to any specific commercial product, process, or service by trade name, trademark, manufacturer, or otherwise does not necessarily constitute or imply its endorsement, recommendation, or favoring by the United States Government or any agency thereof. The views and opinions of authors expressed herein do not necessarily state or reflect those of the United States Government or any agency thereof.

Prepared by
The University of Texas
Center for Petroleum and Geosystems Engineering
Department of Petroleum Engineering
Austin, TX 78712

MASTER

DISTRIBUTION OF THIS DOCUMENT IS UNLIMITED

INNOVATIVE TECHNIQUES FOR THE DESCRIPTION OF RESERVOIR HETEROGENEITY USING TRACERS

Contract No. DE–AC22–90BC14653

The University of Texas
Austin, TX

Contract Date: August 2, 1990
Anticipated Completion: August 1, 1993
Government Award: $224,456 (Current Year)

Principal Investigators:
Gary A. Pope
Kamy Sepehrnoori

Contracting Officer Representative:
Chandra M. Nautiyal
Bartlesville Project Office

Reporting Period: October 1, 1991 – September 30, 1992

TABLE OF CONTENTS

ABSTRACT 1

SECTION 1: A SINGLE-WELL TRACER TEST TO ESTIMATE WETTABILITY 2
- SUMMARY 2
- INTRODUCTION 2
- EFFECTS OF WETTABILITY ON RESERVOIR PROPERTIES 3
  - Relative Permeability 3
  - Capillary Pressure 3
  - Dispersivity 3
- USE OF TRACERS IN RESERVOIR PROPERTY MEASUREMENT 4
- TEST PROCEDURE AND DATA DESCRIPTION 4
  - Test Description 4
  - Tracer Data 5
  - Reservoir Data 5
- SIMULATION RESULTS 6
  - Water Cut 6
  - Tracer Production 7
  - Bottomhole Pressure 7
- CONCLUSIONS 8

SECTION 2: A TYPE-CURVE APPROACH TO ANALYZING TWO-WELL TRACER TESTS 32
- SUMMARY 32
- INTRODUCTION 32
- APPROACH 33
  - Experimental Frequency Response 33
  - Theoretical Frequency Response 34
  - Type-Curve Matching 37
- RESULTS 37
  - Type Curves 37
  - Multiple Realizations 38
  - Radioactive Decay 38
  - Residual Phase Saturation 39
  - Data Analysis 39
- FIELD APPLICATION 39
  - Type-Curve Inference 40
  - Prediction of Field Tracer Response 40
- DISCUSSION 41
- CONCLUSIONS 42

SECTION 3: HETEROGENEITY AND MIXING IN FLOW THROUGH RESERVOIRS 60
- SUMMARY 60
- OBJECTIVE AND APPROACH 60
  - Approach 60
- ANALYSIS AND RESULTS 61
  - From Channeling to Dispersion 62
  - Separating Channeling from Dispersion 62
  - Comparison with a Heuristic Model 63
- SUMMARY AND CONCLUSIONS 64

SECTION 4: SIMULATION OF TRACER FLOW UNDER FIELD CONDITIONS 72
- SUMMARY 72
- RESULTS 73
- CONCLUSIONS AND FUTURE WORK 74

NOMENCLATURE 91

REFERENCES 93

ABSTRACT

This second annual report on innovative uses of tracers for reservoir characterization contains four sections each describing a novel use of oilfield tracers. The first section describes and illustrates the use of a new single-well tracer test to estimate wettability. This test consists of the injection of brine containing tracers followed by oil containing tracers, a shut-in period to allow some of the tracers to react, and then production of the tracers. The inclusion of the oil injection slug with tracers is unique to this test, and this is what makes the test work. We adapted our chemical simulator, UTCHEM, to enable us to study this tracer method and made an extensive simulation study to evaluate the effects of wettability based upon characteristic curves for relative permeability and capillary pressure for differing wetting states typical of oil reservoirs. The response of this single-well test was evaluated based upon the production of oil, water, and several tracers of different types and the bottom hole pressure during injection, shut-in and production periods. Alternative design factors such as the length of the shut-in time were optimized. The accuracy of the test was determined as a function of each response variable individually and all of them collectively. We conclude that this is a very robust test with good potential of the in-situ estimation of reservoir wettability. The second section of this report describes a new method for analyzing interwell tracer data based upon a type-curve approach. Theoretical frequency response functions were used to build type curves of "transfer function" and "phase spectrum" that have dimensionless heterogeneity index as a parameter to characterize a stochastic permeability field. We illustrate this method by analyzing field tracer data. The third section of this report describes a new theory for interpreting interwell tracer data in terms of channeling and dispersive behavior for reservoirs. Once again, a stochastic approach to reservoir description is taken. The long wavelength response of the tracer is used to estimate the deterministic component of the permeability field that manifests itself as channeling (flow in layers of long correlation length). The short wavelength response of the tracer is used to estimate the random component of the permeability field that manifests itself as dispersion on a macroscopic scale. This theory gives us a quantitative estimate of these components from interwell tracer data. The fourth section of this report describes our simulation of perfluorocarbon gas tracers. This new tracer technology developed at Brookhaven National Laboratory is being tested at the Elk Hills Naval Petroleum Reserve No. 1 in California. We report preliminary simulations made of these tracers in one of the oil reservoirs under evaluation with these tracers in this field. Our compostional simulator (UTCOMP) was used for this simulation study.

SECTION 1

A SINGLE-WELL TRACER TEST TO ESTIMATE WETTABILITY

Authors: L.E.A. Ferreira, F.J. Descant, M. Delshad, G.A. Pope, and K. Sepehrnoori

SUMMARY

A single-well backflow tracer test to estimate reservoir wettability, first studied by Descant (1989), has been modified and extended by Ferreira (1992). This test consists of the injection of, first brine, containing tracers and then oil containing tracers. The tracers used are esters, similar to those used in the measurement of residual oil saturation, and nonreactive aqueous and oleic tracers for material balance control. The esters hydrolyze during a shut-in time and then the well is produced. The tracer production data, water cuts, and bottomhole pressures are all sensitive to wettability-dependent properties. The most important by far is relative permeability, but capillary pressure and mixing behavior (dispersion and capacitance) are also important. In the absence of fluid drift, reservoir properties such as permeability and porosity have little influence on the test results. From the results of the test, the preferential reservoir wettability may be directly inferred. By matching the test data using a compositional reservoir simulator, these properties can be estimated and used to infer wettability or simply used directly in subsequent simulations of the reservoir performance.

We illustrate this process using our chemical flooding simulator UTCHEM (Bhuyan *et al.*, 1988; Datta Gupta *et al.*, 1986; Descant, 1989; Pope *et al.*, 1987; Saad *et al.*, 1990). The CPU time on a CRAY Y-MP required for each simulation was 10 seconds for a 1D-radial (31 blocks), 3 minutes for a 2D-areal (609 blocks), and 9 minutes for a 3D (1,827 blocks) simulation, so many cases can be affordably studied.

INTRODUCTION

Wettability has been considered the most important factor that controls the location, distribution, and characteristics of the flow of fluids in a reservoir (Anderson, 1986). Changes in the wetting conditions of the samples in core analysis have been shown to affect the transport properties of a reservoir such as relative permeability and capillary pressure, dispersion of tracers, waterflood behavior, tertiary recovery, irreducible water saturation, residual oil saturation, and electrical properties (Anderson, 1986a; Anderson, 1986c; Anderson, 1987a; Anderson, 1987b).

Although wettability can be measured in the laboratory using cores (Andersen *et al.*, 1988; Anderson, 1986b; Honarpour *et al.* 1986), the wetting condition of the cores may be subject to error, mainly because of inadequate well coring fluid and handling techniques, problems with packing and preserving the cores, laboratory procedures for cleaning and preparing the samples, test temperature, and test fluid and test techniques (Owens and Archer, 1971). Thus, an in-situ method would obviously be of great advantage. The only in-situ method that we are aware of besides the one proposed here is that of Desbrandes and Bassiouni (1989, 1990), who proposed using a wireline formation tester.

Wettability impacts the economics of any recovery process because it affects the efficiency of the displacement of oil by water (Erlich *et al.*, 1974), alters the predicted breakthrough time and the required amounts of injected fluid to achieve a given reduction in oil saturation (Stalkup, 1983), influences the choice of the kind of chemicals to be used in an enhanced recovery process

(Mungan, 1966), and affects the estimated reserves of the reservoir (Cockcroff *et al.*, 1989). Therefore, it is of great importance to know the reservoir wettability in order to predict the correct performance of the reservoir under study. An in-situ evaluation of reservoir wettability thus would be an attractive alternative, not only because it is unaffected by extraneous fluids but it also would sample a much larger volume of the reservoir. The combined use of laboratory and well tests is the most likely to yield definitive results.

EFFECTS OF WETTABILITY ON RESERVOIR PROPERTIES

Anderson (1986a, 1986c, 1987a, 1987b) has performed an extensive review of the literature on wettability and presented an excellent summary of hundreds of works done in order to establish the relationships of reservoir properties to the wetting condition of the core samples We will briefly review effects of wettability on some of the transport properties of a reservoir.

Relative Permeability

In his review of the wettability effects on relative permeability, Anderson (1987b) showed that relative permeabilities are functions of wettability, pore geometry, fluid distribution, saturation, and saturation history. He also showed that in uniformly wetted cores the effective oil permeability at a given initial water saturation decreases as the wettability varies from water-wet to oil-wet. Also, the water relative permeability increases as the core becomes more oil-wet. These changes have been shown to occur in experiments with artificial porous media (Jennings, 1957; Morrow *et al.*, 1973) and with wettability-altered cores (Bhuyan, 1986; Deans, 1971; Smith *et al.*, 1988). The relative permeability curves of strongly water-wet and strongly oil-wet rocks have some distinct characteristics. Craig (1971) showed examples of both types and established some rules of thumb to help identify the wettability tendency.

Capillary Pressure

The effects of wettability on the capillary-pressure/saturation relationship are so important that two of the methods to quantify the wetting condition of a sample make use of capillary pressure curves (Amott, 1959; Deans, 1978). Anderson (1987b) reinforced the necessity of using native- or restored-state cores with crude oil and reservoir brine to measure capillary pressures because these conditions best match those in the reservoir. Some examples of strongly water-wet, strongly oil-wet, and intermediate-wet capillary pressure curves are presented by Craig (1971) from a study by Killins *et al.* (1953).

Dispersivity

Dispersion is the mixing of two miscible fluids caused by diffusion, local velocity gradients, locally heterogeneous streamline lengths, and mechanical mixing in pore bodies (Lake, 1989). Dispersivity is a measure of this mixing and depends on many factors, but mainly on the pore-level heterogeneity of the medium and the pore-level phase distribution. Dependence of longitudinal dispersivity on wettability has been observed in laboratory experiments (Delshad *et al.*, 1985; Maini *et al.*, 1986; Saad *et al.*, 1990; Salter and Mohanty, 1982; Wang, 1986). The effects of wettability are easier to observe in small cores, where the scale of the heterogeneities is small. The longitudinal dispersivity of each phase generally increases as the phase saturation decreases (Delshad *et al.*, 1985; Maini *et al.*, 1986; Saad *et al.*, 1990; Salter and Mohanty, 1982; Wang, 1986).

USE OF TRACERS IN RESERVOIR PROPERTY MEASUREMENT

Tracers have been used to help understand the flow behavior of fluids in reservoirs, and for reservoir characterization. Tracer tests can be of two types: interwell and single-well tests. In interwell tests, tracers are injected into one or more wells and information on production data is collected from other wells. The data gathering from producing wells can be used to estimate residual oil saturation (Cooke, 1971) and diagnose interwell reservoir heterogeneities (Abbaszadeh-Denghani and Brigham, 1984; Allison *et al.*, 1991; Wagner, 1977). In single-well tracer tests, tracers are injected into and produced from the same well. Single-well tracer tests have been used to estimate residual oil saturation Deans, 1971; Deans and Majoros, 1980), connate water saturation (Deans and Shallenberger, 1974; Mut and Deans, 1983), fluid drift (Tomich and Deans, 1974), brine salinity (Mut and Deans, 1983), and residual gas saturation (Deans and Bragg, 1977; Deans *et al.*, 1976).

Deans (1978) has also shown that in two-phase flow the partitioning tracers have velocities related to their partition coefficients and that they can be used to define points on the fractional flow curve. Nonreversing flow behavior (Rowney, 1989) has been demonstrated experimentally, like the single-well chemical test for measuring low saturations of highly saline brine. A single-well tracer test can also be used to estimate the permeability variation in layered reservoirs when fluid drift is present (Pope and Sepehrnoori, 1987; Ferreira, 1992).

TEST PROCEDURE AND DATA DESCRIPTION

Test Description

The single-well tracer test to estimate reservoir wettability, first studied by Descant (1989), has been modified and extended by Ferreira (1992). It consists of an injection of reservoir brine containing an ester and a nonreactive aqueous tracer, followed by an injection of a tracer-free water buffer. Then reservoir crude containing another ester and a nonreactive oleic tracer is injected, followed by an injection of a tracer-free oil buffer (Fig. 1). The well is then shut in for a period of time to allow the esters to hydrolyze into alcohols. Then the well is produced. Tracer data, water cuts, and bottomhole pressures are registered.

The idea behind the sequential injection of both water and oil is to expose the reservoir rock to the whole spectrum of saturations from residual oil to residual water. For reservoirs initially at high oil saturation, the injection of the oil slug may not be necessary. Since the wetting condition of the formation affects the transport properties of the reservoir, different wettabilities will provoke a different and characteristic behavior during injection, shut-in, and production periods, making it possible to infer the reservoir wettability. In the absence of fluid drift, those factors such as permeability and porosity that affect both water and oil will have little influence, whereas factors such as relative permeabilities that are different for water and oil result in a strong differential signal.

Since wettability affects the relative permeability and capillary pressure of a reservoir rock, the fractional flow characteristics of formations that have distinct wettabilities are different. Because of this difference in fractional flow, the tracers have different velocities and breakthrough times. The distinct behavior of the tracers, producing cuts, and bottomhole pressures under different wetting conditions is the basis for this test, and makes it possible to identify the preferential wettability of the reservoir rock.

We illustrate the application of this method for strongly water-wet, strongly oil-wet, and intermediate-wet formations. In the simulations presented here, we assumed absence of fluid drift

in the reservoir. Results of simulations that include fluid drift and capacitance (non equilibrium mass transfer) are given by Ferreira (1992). Capacitance actually adds to the differential signal, but is a second-order effect that does not change the results substantially.

Tracer Data

The tracer properties used in these simulations are given in Table 1. Methanol is used to illustrate an aqueous-phase material balance tracer (nonpartitioning and nonreacting), and octanol is used to illustrate an oil-phase material balance tracer. Any suitable material balance tracers could be used without changing any of the results shown in this paper. The esters used are ethyl acetate (EtAc) and propyl acetate (PrAc), which partition and react. Their product alcohols are ethanol (EtOH) and n-propanol (NPA), respectively, which do not partition or react under the conditions simulated. The particular choice of reacting tracers that would be best under given reservoir conditions will depend on such variables as temperature and may be other esters than the ones illustrated here, or even completely different chemicals provided that a reaction of suitable duration occurs within the phases or with the formation so that an irreversibility is established in the reservoir flow.

Reservoir Data

We illustrate a simulated test that was designed to investigate a region of approximately 5 ft away from the wellbore. Fluids are injected for 0.6 days, the shut-in time is 5.4 days, and the production time is 5 days, so the total time for the test is 11 days. Input data common for all simulations are given in Table 2. Variable input data for homogeneous radial, heterogeneous two-dimensional (2D) areal, and heterogeneous three-dimensional (3D) simulations are given in Tables 3 and 4. Figure. 2 shows the permeability field that was used for the 2D areal simulations. The Turning Bands Method was used to generate a permeability field on a 3 ft by 3 ft grid. Table 4 gives the sizes of the 21x29 gridblocks that were used in these 2D simulations. To obtain the permeabilities for the larger gridblocks, the geometric average of the small gridblock permeabilities was used. The well is located in the fine gridblock region (block 11,11). The 3D permeability fields were generated by the same method for each of three layers with differing mean permeabilities.

The relative permeabilities for all three wetting conditions simulated were calculated using a Corey-type model:

$$k_{rj} = k_{rj}^{o} (S_{nj})^{e_j} , \tag{1}$$

where

$$S_{nj} = \frac{S_j - S_{jr}}{1 - S_{wr} - S_{or}} , \qquad j = w,o . \tag{2}$$

The relative permeability curves shown in Fig. 3 are similar to those in Craig (1971). Two simulations with relative permeability curves showing hysteresis (Runs R1W18B and R1O18B) are included. The input data for these two simulations are the same as those of Runs R1W01 and R1O01, except that the curvature of the relative permeability was $e_o = 1.1$ for the oil drainage curve of the water-wet rock and $e_w = 1.9$ for the water drainage curve of the oil-wet rock.

The capillary pressure curves used in these simulations (Fig. 5) are also similar in shape to the curves in Craig (1971). They were calculated using the following relationships for water- and oil-wet rocks, respectively:

$$P_{c,ow} = c_{pcw}\left(\frac{\phi}{k_h}\right)^{1/2} (1-S_{nw})^{n_{pcw}} \tag{3}$$

$$P_{c,ow} = c_{pco}\left(\frac{\phi}{k_h}\right)^{1/2} (1-S_{no})^{n_{pco}}, \tag{4}$$

where S_{nw} and S_{no} are calculated using Eq. 2. For the intermediate-wet case, we used Eq. 3 for S_{nw} values from 0 to 0.8 and Eq. 4 for S_{nw} values greater than 0.8.

SIMULATION RESULTS

The results of simulated single-well backflow tracer tests are shown for water cut, tracer production, and bottomhole pressure. First the homogeneous radial simulations are discussed, then the heterogeneous 2D and 3D simulations. The radial simulations were done first since they take little computer time (about 10 seconds) and are simple to set up and interpret. The 2D and 3D simulations were for the purpose of investigating effects such as heterogeneity and crossflow from transverse dispersion, capillary pressure, and gravity. In all cases, we used an option in our finite-difference simulator to approximate the convective derivatives with a third-order correct method (Saad *et al.*, 1990) so that relatively few gridblocks were needed to eliminate the effects of numerical dispersion.

Water Cut

Produced water cuts for the radial simulations are shown in Fig. 5. The scales on the x axis are time and the ratio of the volume of the produced fluid to the volume of the oil slug injected (dimensionless). The contrast between water- and oil-wet reservoirs is very clear and the curves have characteristics that help identify the preferential wettability of the reservoir rock. For these simulations, the initial water cut was 0.5 for all wetting conditions, so the initial saturation distribution is different since the relative permeabilities are different. The saturation profiles at the end of the injection period are shown in Fig. 6. Near the wellbore, the water saturation is close to its residual value, and the capillary pressures are close to their maximum and minimum values for the water- and oil-wet cases, respectively.

During the shut-in period, because of the capillary pressure gradients, there is a countercurrent flow to balance the pressures, and the saturations change as shown in Fig. 7 at the end of the shut-in period.

The characteristics of the produced water cuts (Fig. 5) can be understood from the saturation profiles. For the water-wet case, the water saturation is almost uniform near the well, so the initial water cut is almost constant. Once a volume equivalent to the volume of the injected oil has been produced, the saturation changes rapidly, so the water cut also increases rapidly, followed by a more gradual change to its initial value. For the oil-wet case, the initial water cut is zero. There is a sharp increase before the production is equivalent to the injected oil volume, followed by a gradual increase to the initial water cut. Although not shown here, similar features were observed when hysteresis in the relative permeability curves was included.

The behavior of the 2D areal simulations (Fig. 8) was very similar to that of the homogeneous radial simulations. This indicates that the test is not sensitive to heterogeneity. Thus, radial simulations are useful for initial design purposes.

Tracer Production

The product tracer concentration histories are shown in Figs. 9 and 10. These curves have characteristics that help identify the reservoir rock wettability. For the strongly oil-wet case, the produced concentration increases sharply and the peak concentration occurs before production reaches injected oil volume. In contrast, when the rock is water-wet, tracer concentrations increase gradually and the peak concentration occurs after production of the injected oil volume.

Another indication of the formation wettability can be seen by comparing the aqueous-phase tracer concentration histories of the product alcohol and the ester as shown in Fig. 11. The black arrows show the ester peak concentrations and the white arrows show the product alcohol peak concentrations. When the reservoir rock is water-wet (Fig. 11), the ethyl acetate is produced before the ethanol. This happens because these tracers do not separate much during the injection and shut-in periods, as seen in Fig. 12. During production, the oleic phase has a higher velocity than the aqueous phase because of fractional flow characteristics, and since the ethyl acetate partitions between the phases and favors the oleic over the aqueous phase, it is produced first. When the formation is oil-wet, the propyl acetate is produced after the propanol (Fig. 13). This happens because these tracers separate more during the injection and shut-in periods (Fig. 14) than in the water-wet case and because the aqueous phase velocity is higher than the oleic phase velocity; thus the propanol arrives earlier than the propyl acetate.

The material balance tracers did not show a significantly different signal for the different wetting conditions.

The results of the simulations with hysteresis are shown in Figs. 11 and 13. The effect of hysteresis is small and the same qualitative results are still observed. The esters arrive earlier than the alcohols for the water-wet rock (Fig. 11) and later than their product alcohols when the rock is oil-wet (Fig. 13).

These radial simulations were repeated in both two and three dimensions. The results shown in Figs. 15 and 16 indicate that there is still a significant difference between the wetting conditions as measured by the separation of the tracer curves. The Dykstra-Parsons coefficient (V_{DP}) for the two-dimensional simulation was 0.54 (a variance of the log normal permeability distribution corresponding to 0.82). The three-dimensional case consisted of three layers with mean permeabilities of 102, 248, and 304 md and variances of about 0.64 within each of these layers. The ratio of the vertical to horizontal permeability was 0.2.

Bottomhole Pressure

Pressure transient analysis methods for two-phase flow in injection wells (Abbaszadeh-Denghani and Kamal, 1989; Namba and Horne, 1989) have also been used to estimate relative permeability. We illustrate the effect of relative permeability on the pressure response for one of the water-wet cases (Run R1W01) and one of the oil-wet cases (Run R1O10) that we have already discussed with respect to tracer and fluid production behavior. During water injection (Fig. 17), the total relative mobility for the water-wet rock in this case is always decreasing (Fig. 18). Thus, the bottomhole pressure required to inject water is always increasing. However, for the oil-wet rock considered, the total relative mobility has a minimum value. So, initially the pressure increases until a pressure gradient is established. After the water saturation increases, the total relative mobility goes through its minimum value and then the bottomhole pressure starts decreasing.

During oil injection (Fig. 19), the bottomhole pressure decreases when the rock is water-wet because now the total relative mobility increases. For the oil-wet case, the pressure initially

increased because the total relative mobility is decreasing. Then it starts to decrease after the water saturation decreases and the total relative mobility goes through its minimum value.

The simultaneous matching of pressure along with both tracer and fluid production response should yield a more definitive estimation of the relative permeability than any one of these by themselves. Although we show only the injection pressure response (Figs. 17 and 19), the pressure response during shut-in and production times should also be matched.

CONCLUSIONS

We have shown how a single-well tracer test can be used to estimate reservoir wettability. Although the tracer signal is the primary signal for interpretation purposes, both producing water cut and bottomhole pressure measurements can be included in this test to aid in the interpretation. We have used a finite-difference simulator to illustrate the sensitivity of each of these responses to the wettability of the formation as reflected in its relative permeability and capillary pressure properties. These simulations indicate that the proposed test is not sensitive to at least moderate degrees of permeability variation. Simple one-dimensional radial simulations can be done very easily and quickly for preliminary design purposes, followed by two- and three-dimensional simulations to evaluate potential complications such as heterogeneity, crossflow, and drift. The results of a simultaneous history match of such a single-well test could then be used directly in future reservoir simulation studies. This approach should result in a far more definitive evaluation of the effects of wettability than the usual simulation history match because the production of tracers from a single-well tracer test both is a much stronger signal than pressure and production data and is much less subject to non unique interpretation problems because of complex reservoir characteristics and fluid flow between wells. Furthermore, although laboratory data should be taken if cores are available and used as much as possible consistent with the particular problems that may have occurred during coring and storage, this method avoids the problems associated with small samples, altered wettability during handling, storage and measurements, and incomplete or insufficient core from representative locations in the reservoir.

Table 1. Tracer Properties

Tracer Type	Partition Coefficient	Reaction Rate ($days^{-1}$)	Injected Concentration (vol%)
Methanol (Mat. Bal.)	No	No	1.0
EtAc (Ester)	5.0	0.06	1.0
EtOH (Product)	No	No	No
Octanol (Mat. Bal.)	No	No	1.0
PrAc (Ester)	10.0	0.07	1.0
NPA (Product)	No	No	No

Table 2. Reservoir and Test Parameters

Injection and Production Rate	200 bbl/day
Water Tracer Slug	20 bbl
Water Buffer	40 bbl
Oil Tracer Slug	20 bbl
Oil Buffer	40 bbl
Injection Time	0.6 days
Shut-In Time	5.4 days
Production Time	5.0 days
Oil Compressibility	15.0×10^{-6} psi^{-1}
Water Compressibility	3.0×10^{-6} psi^{-1}
Rock Compressibility	3.0×10^{-6} psi^{-1}
Porosity	25%
Thickness	24 ft
Initial Water Cut	0.5
Longitudinal Dispersivity	0.1 ft
Transverse Dispersivity	0.003 ft
Oil Viscosity	1.0 cp
Water Viscosity	0.7 cp

Table 3. Reservoir and Simulation Data

Run No.	R1W01	R1O01	R1W02	C1W57	C1O57	C1W60	C3W01			C3O01		
							Layer 1	Layer 2	Layer 3	Layer 1	Layer 2	Layer 3
S_{or}	0.28	0.32	0.28	0.28	0.32	0.28	0.28	0.28	0.28	0.32	0.32	0.32
S_{wr}	0.25	0.10	0.25	0.25	0.10	0.25	0.25	0.25	0.25	0.10	0.10	0.10
k^o_{ro}	1.0	1.0	1.0	1.0	1.0	1.0	1.0	1.0	1.0	1.0	1.0	1.0
c_o	1.4	2.1	1.4	1.4	2.1	1.4	1.4	1.4	1.4	2.1	2.1	2.1
k^o_{rw}	0.1	0.76	0.3	0.1	0.76	0.3	0.1	0.1	0.1	0.76	0.76	0.76
c_w	1.4	2.2	1.4	1.4	2.2	1.4	1.4	1.4	1.4	2.2	2.2	2.2
c_{pcw}	15	0	15	15	0	15	15	15	15	0	0	0
n_{pcw}	4	0	4	4	0	4	4	4	4	0	0	0
c_{pco}	0	-15	-10	0	-15	-10	0	0	0	-15	-15	-15
n_{pco}	0	6	6	0	6	6	0	0	0	6	6	6
S_{wi}	0.6264	0.3893	0.5543	0.6264	0.3893	0.5543	0.6264	0.6264	0.6264	0.3893	0.3893	0.3893
k_{avg}	227.8	227.8	227.8	240.4	240.4	240.4	101.9	248.1	304.2	101.9	248.1	304.2
V_{DP}	0.05	0.05	0.05	0.54	0.54	0.54	0.55	0.59	0.54	0.55	0.59	0.54
λ_D	0.11	0.11	0.11	0.2	0.2	0.2	0.2	0.2	0.2	0.2	0.2	0.2
$M^o(1)$	0.14	1.1	0.4	0.14	1.1	0.4	0.14	0.14	0.14	1.1	1.1	1.1
$M^o(2)$	7.0	0.92	2.3	7.0	0.92	2.3	7.0	7.0	7.0	0.92	0.92	0.92
cPc	8.2	8.2	8.2	30.	30.	30.	30.	30.	30.	30.	30.	30.
Pe,l	1711.	1711.	1711.	5010.	5010.	5010.	5010.	5010.	5010.	5010.	5010.	5010.
Pe,t	-	-	-	37371.	37371.	37371.	37371.	37371.	37371.	37371.	37371.	37371.
$cN_{RL}(1)$	2855.	376.	952.	3518.	463.	1173.	4208.	6567.	7272.	332.	518.	574.
$cN_{RL}(2)$	408.	408.	408.	503.	503.	503.	601.	938.	1039.	361.	563.	623.

(1) During water injection
(2) During oil injection

Table 4. Simulation Grid Data

1D - Radial

Number of gridblocks	31
r_w	0.25 ft
r_e	171.2 ft
Dr's for blocks No.	
1	0.25 ft
2	2.0 ft
3-11	1.0 ft
12-16	2.0 ft
17-21	3.0 ft
22-26	5.0 ft
27-29	10.0 ft
30	20.0 ft
31	40.0 ft

2D - Areal and 3D

Number of gridblocks	609 (21 x 29) for 2D 1827 (21 x 29 x 3) for 3D
r_w	0.25 ft
Lx	237 ft
Ly	501 ft
Dx's for blocks No.	
1-2	33.0 ft
3-5	12.0 ft
6-16	3.0 ft
17-19	12.0 ft
21-21	33.0 ft
Dy's for blocks No.	
1-2	33.0 ft
3-5	12.0 ft
6-16	3.0 ft
17-19	12.0 ft
20-29	33.0 ft
Dz's for blocks No.	
2D 1	24.0 ft
3D 1-3	8.0 ft

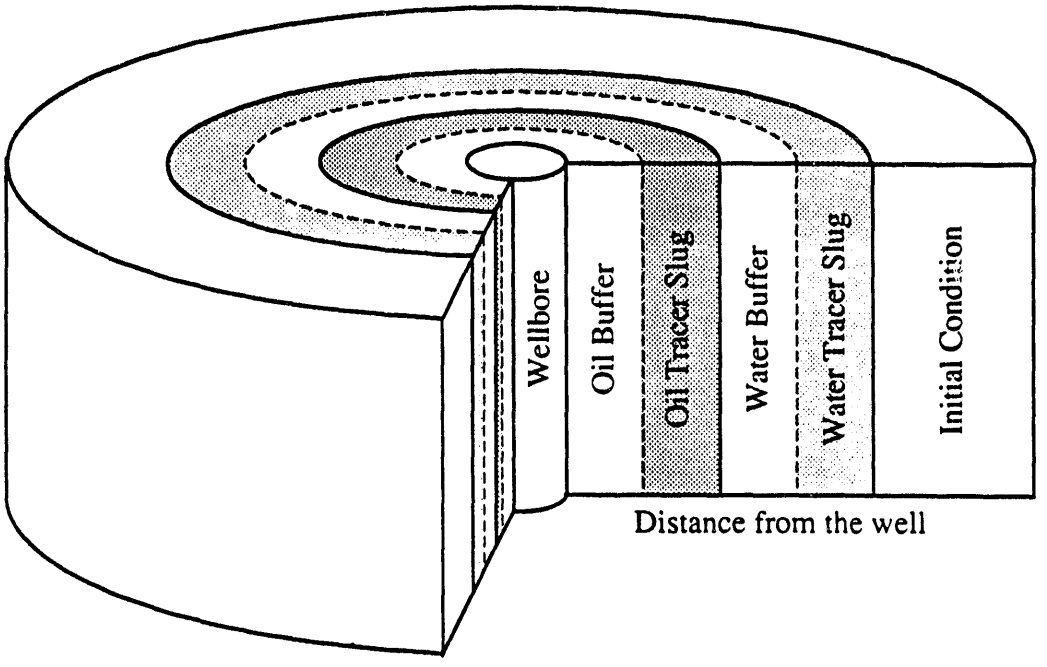

Fig. 1 Injection sequence scheme

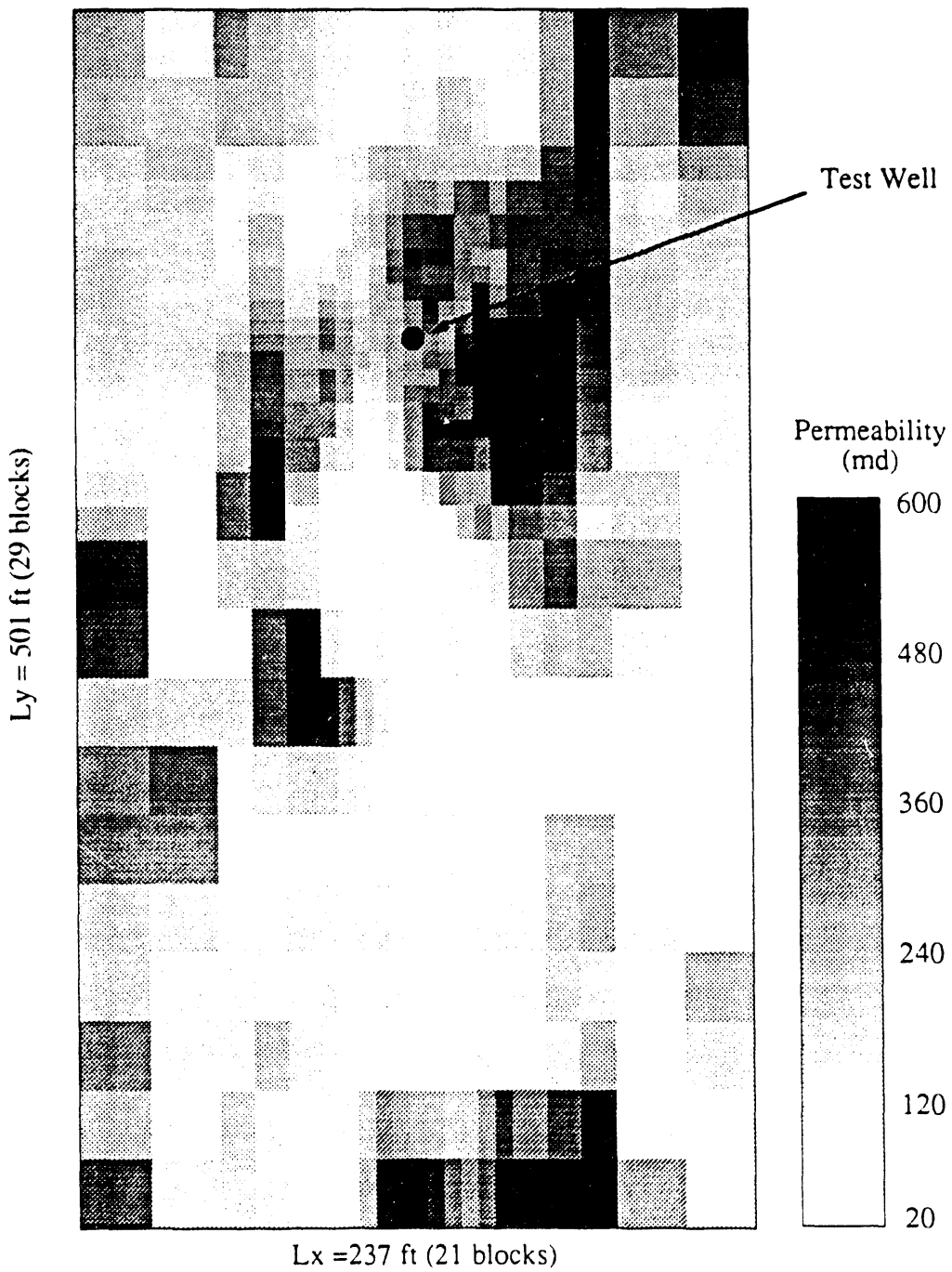

Fig. 2 Permeability field for 2D-areal simulations

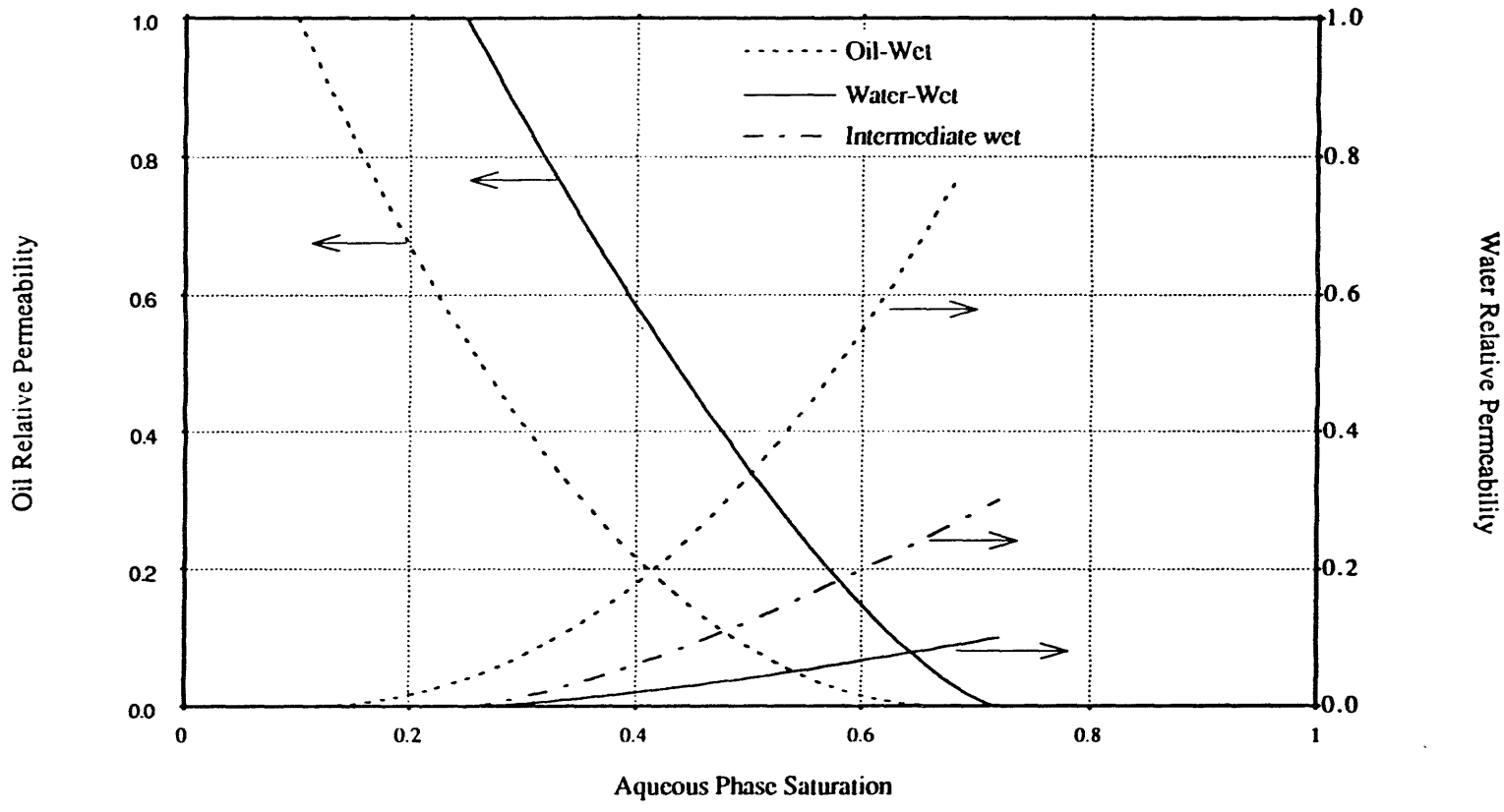

Fig. 3 Strongly and intermediate wet relative permeability curves

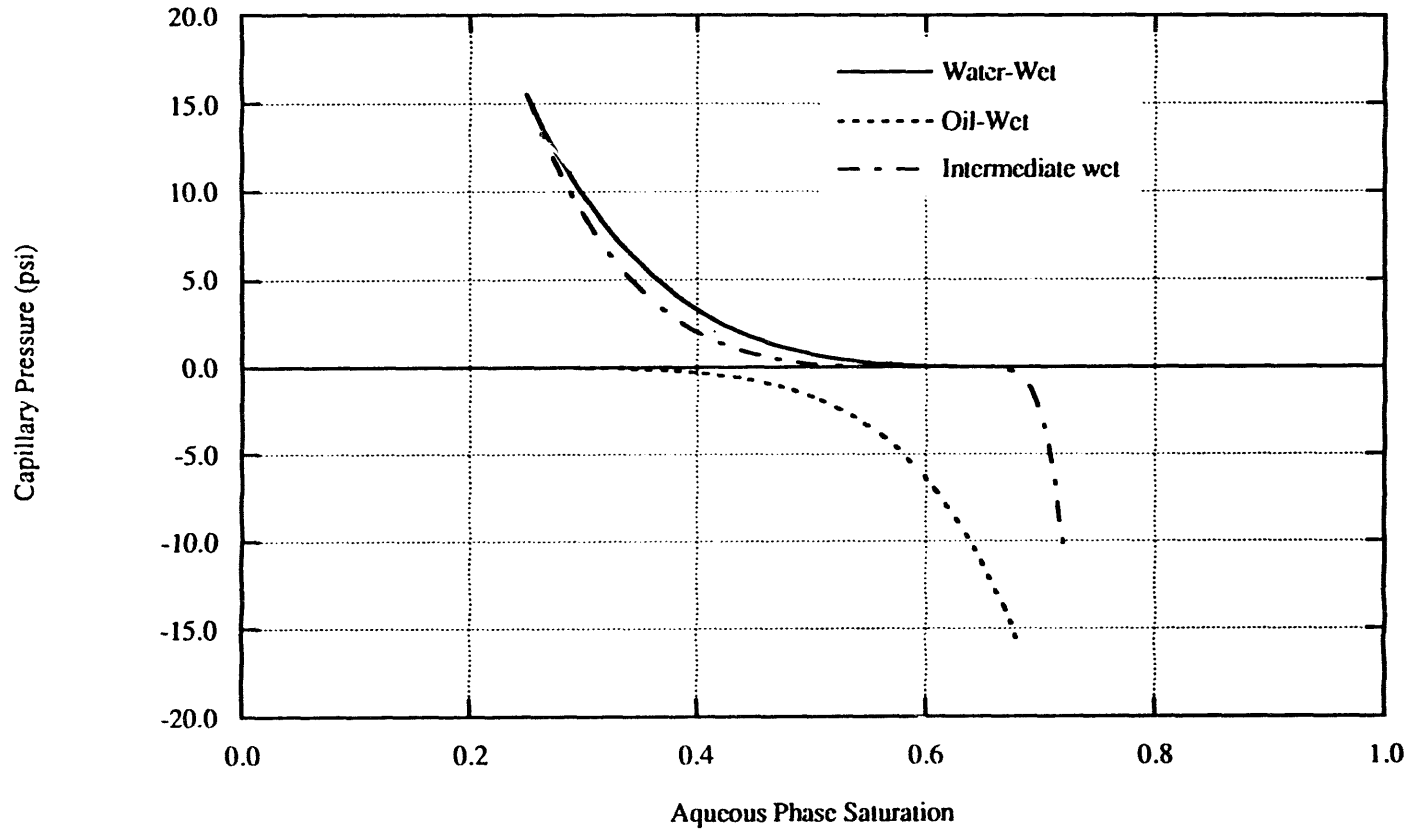

Fig. 4 Strongly and intermediate wet capillary pressure curves

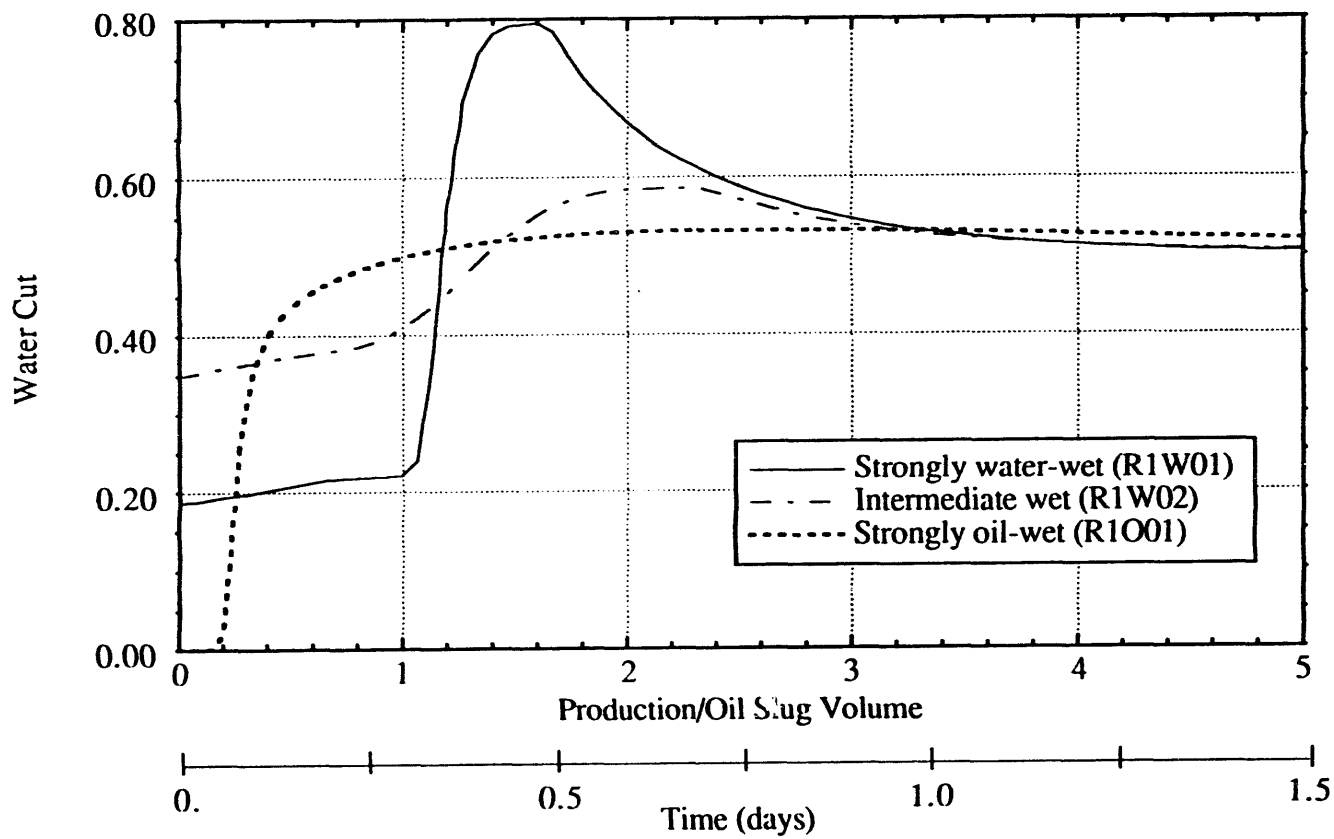

Fig. 5 Water-cut histories for radial simulations

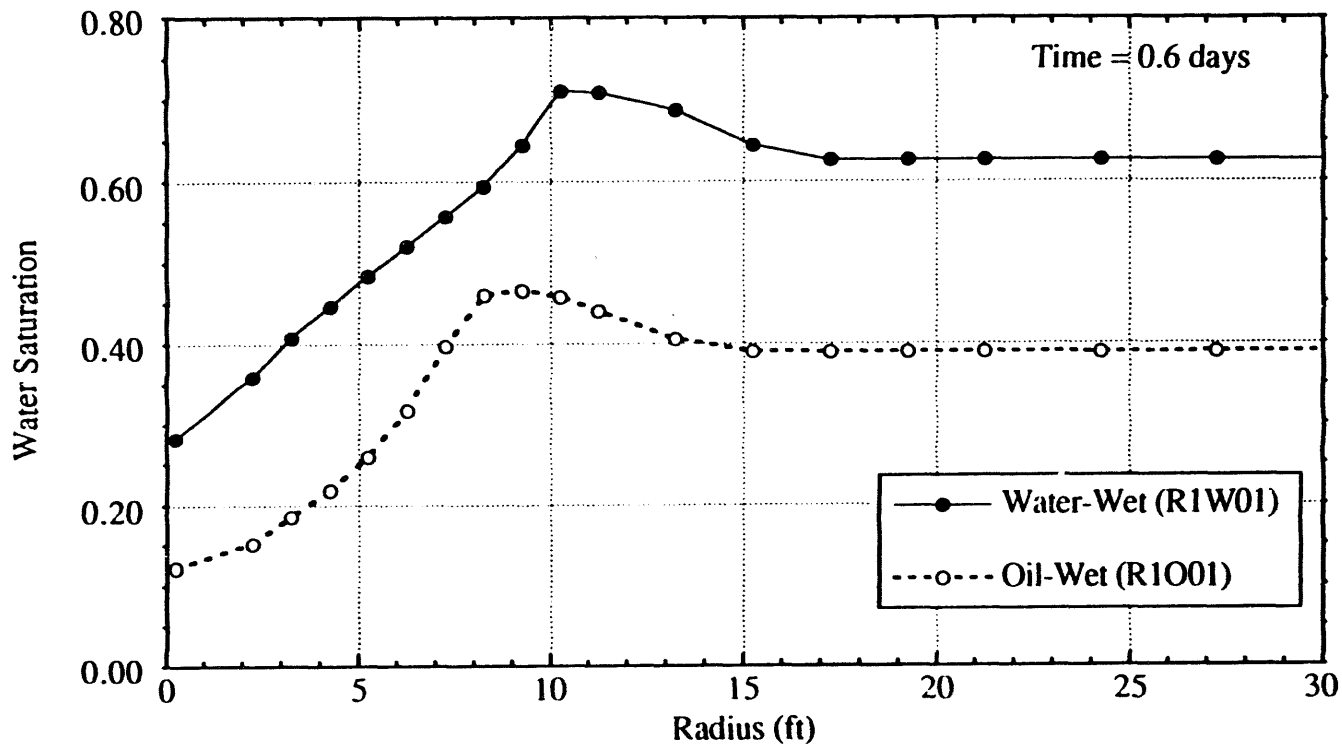

Fig. 6 Water saturation profiles at the end of injection and before shut-in

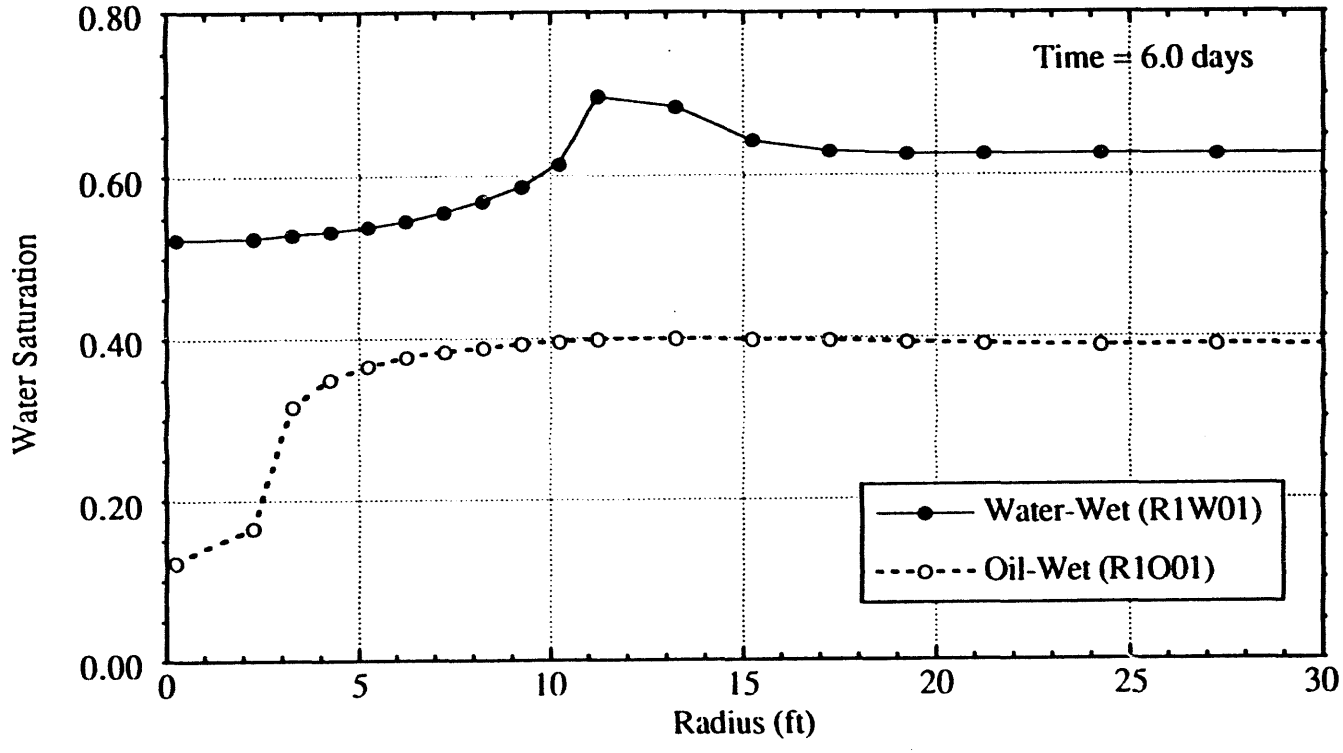

Fig. 7 Water saturation profiles at the end of the shut-in period

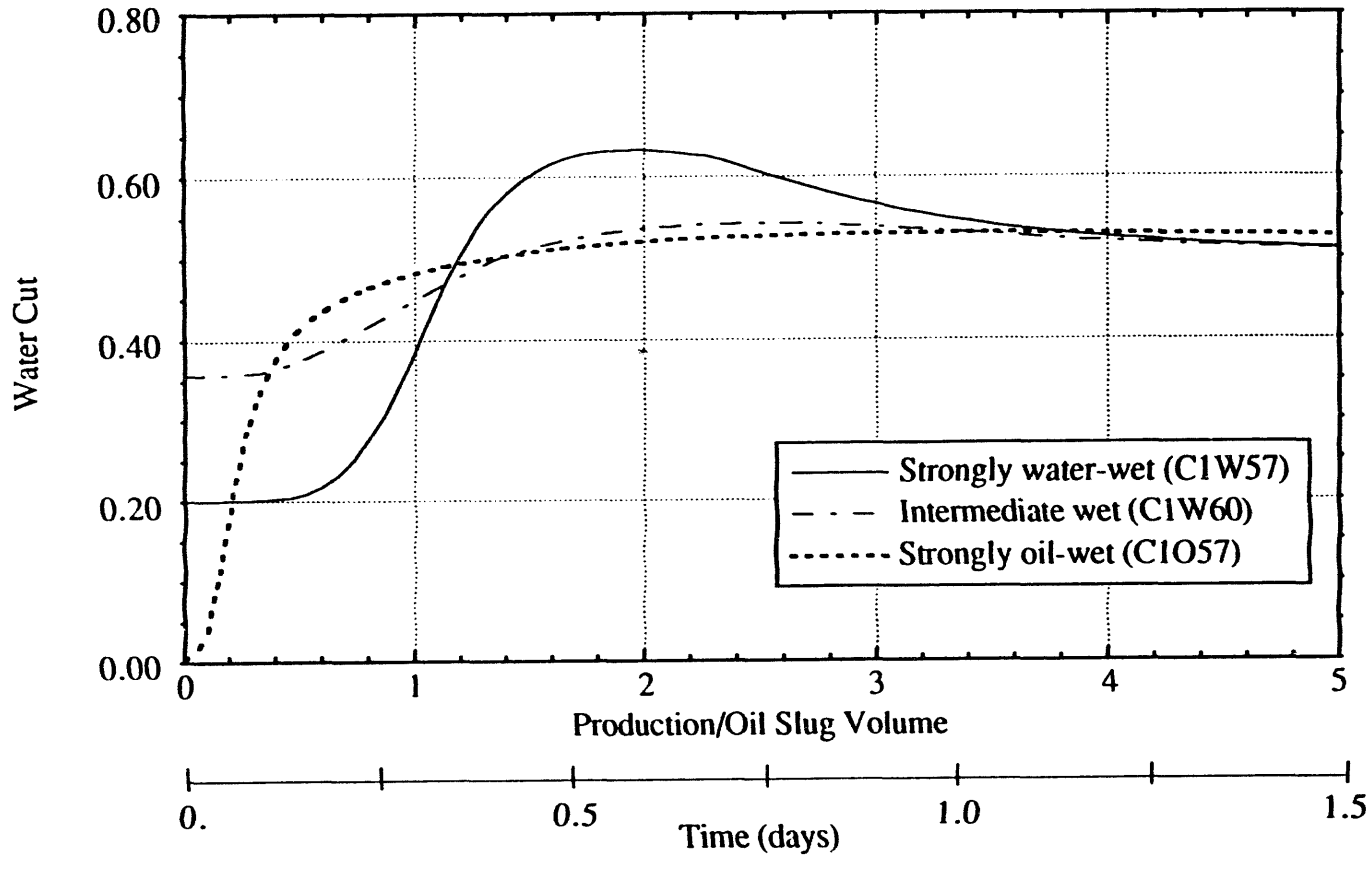

Fig. 8 **Water-cut histories for the 2D areal simulations**

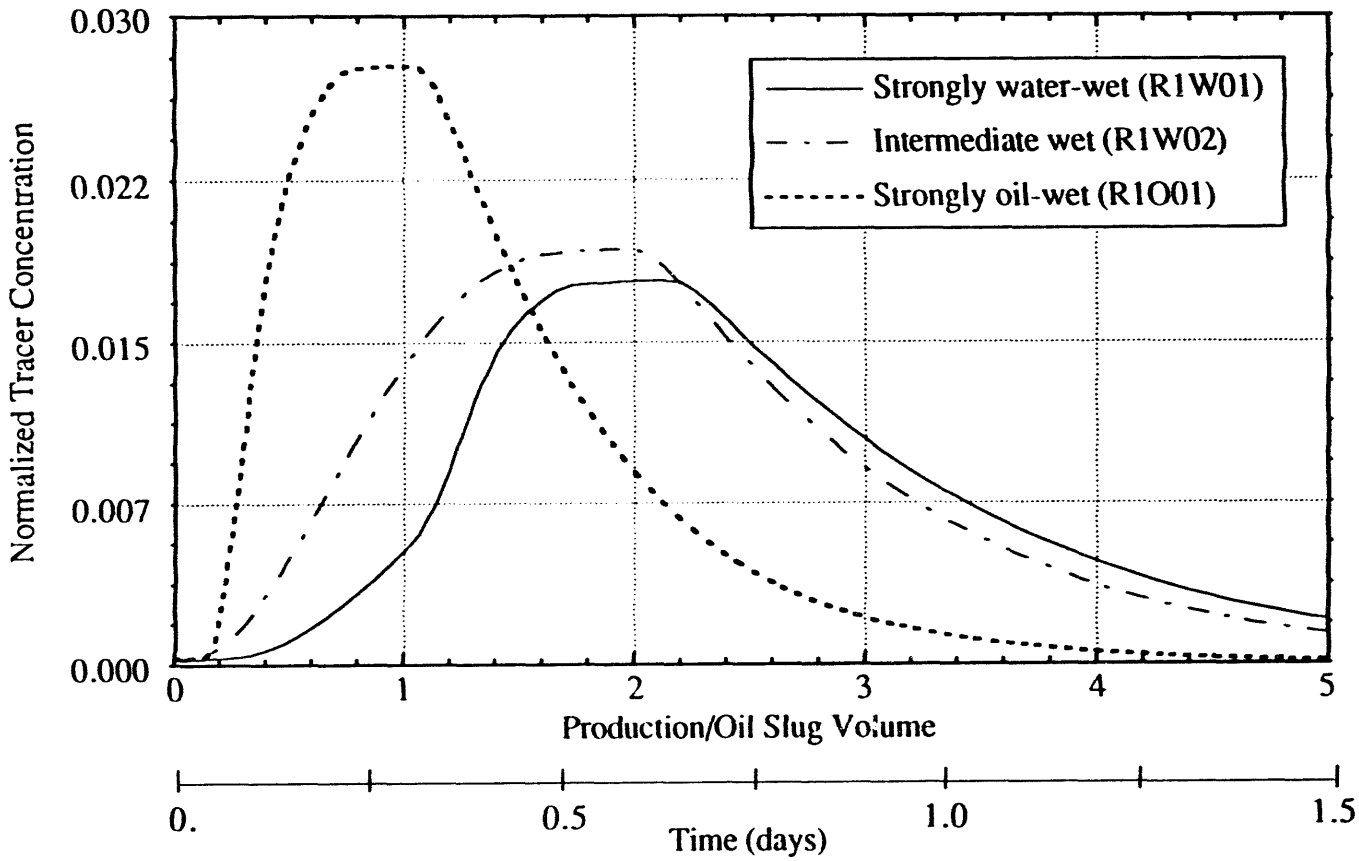

Fig. 9 **Aqueous phase ethanol histories for the radial simulations**

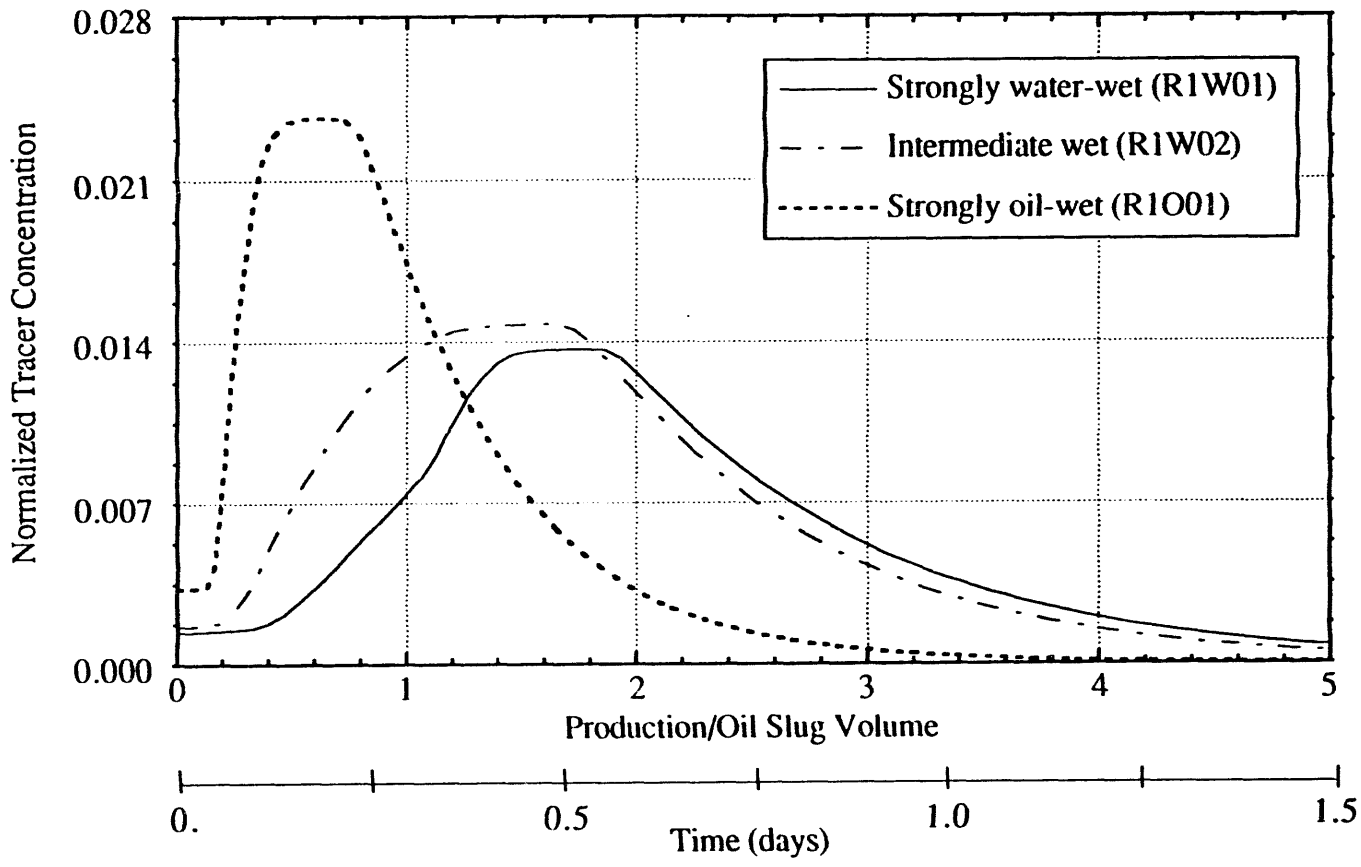

Fig. 10 **Aqueous phase n-propanol histories for the radial simulations**

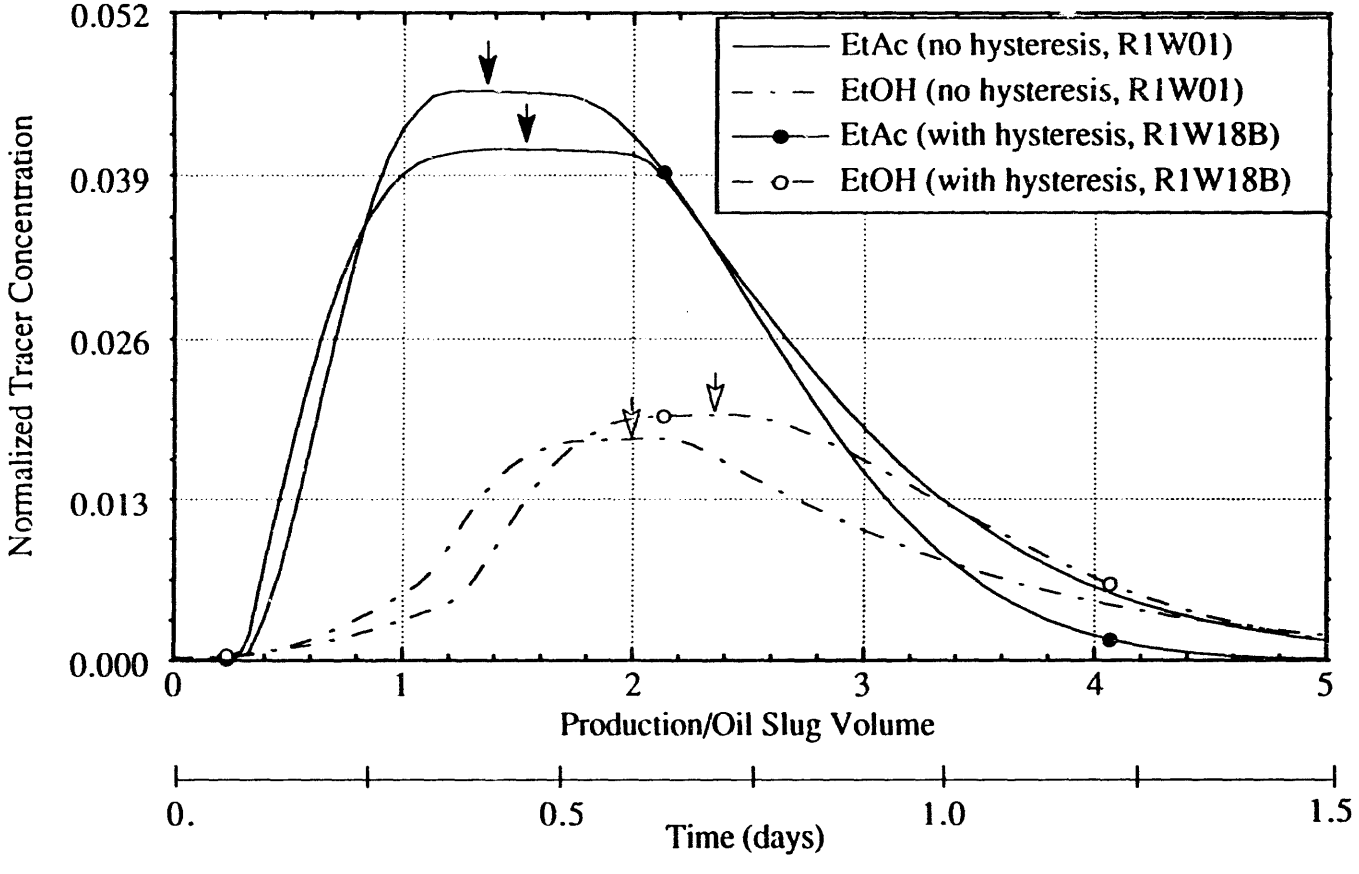

Fig. 11 **Aqueous phase tracer histories in a strongly water-wet reservoir for the radial simulations**

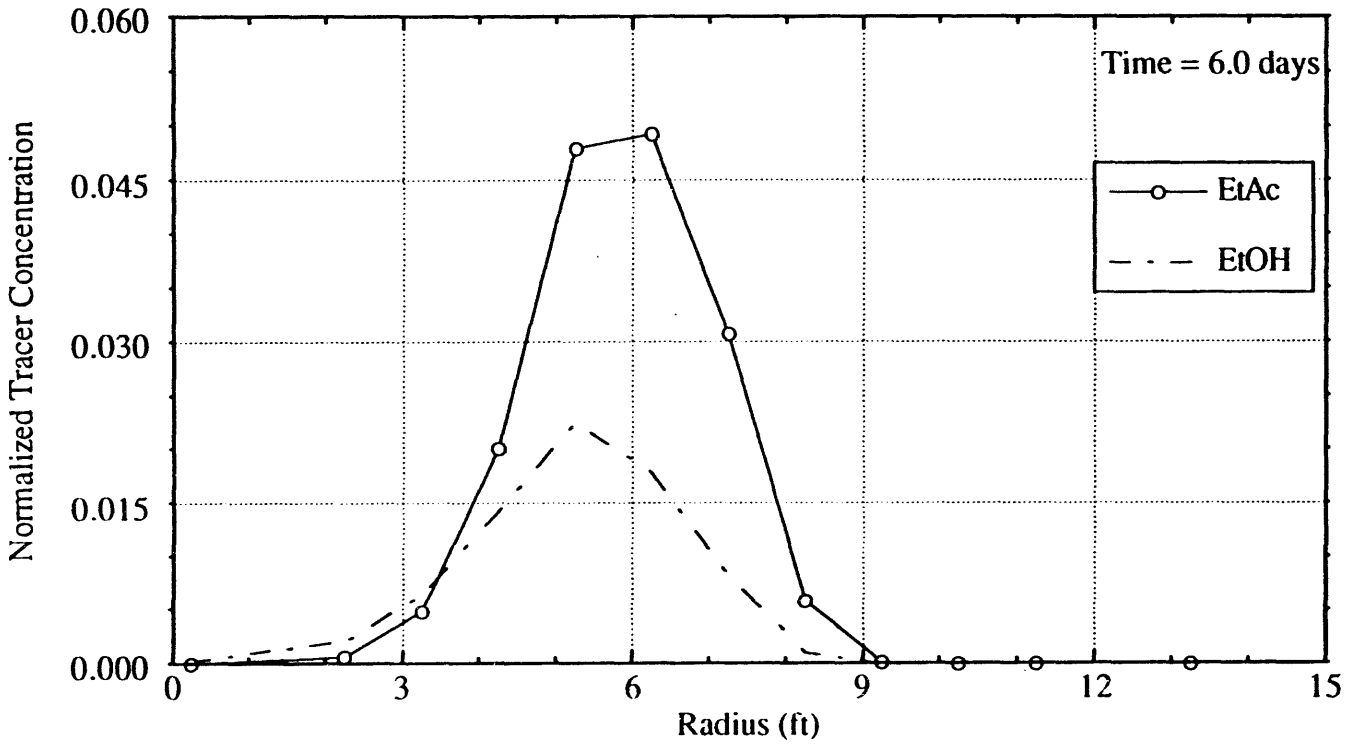

Fig. 12 **Aqueous phase tracer concentration profiles after the shut-in period in a strongly water-wet reservoir (Radial run R1W01)**

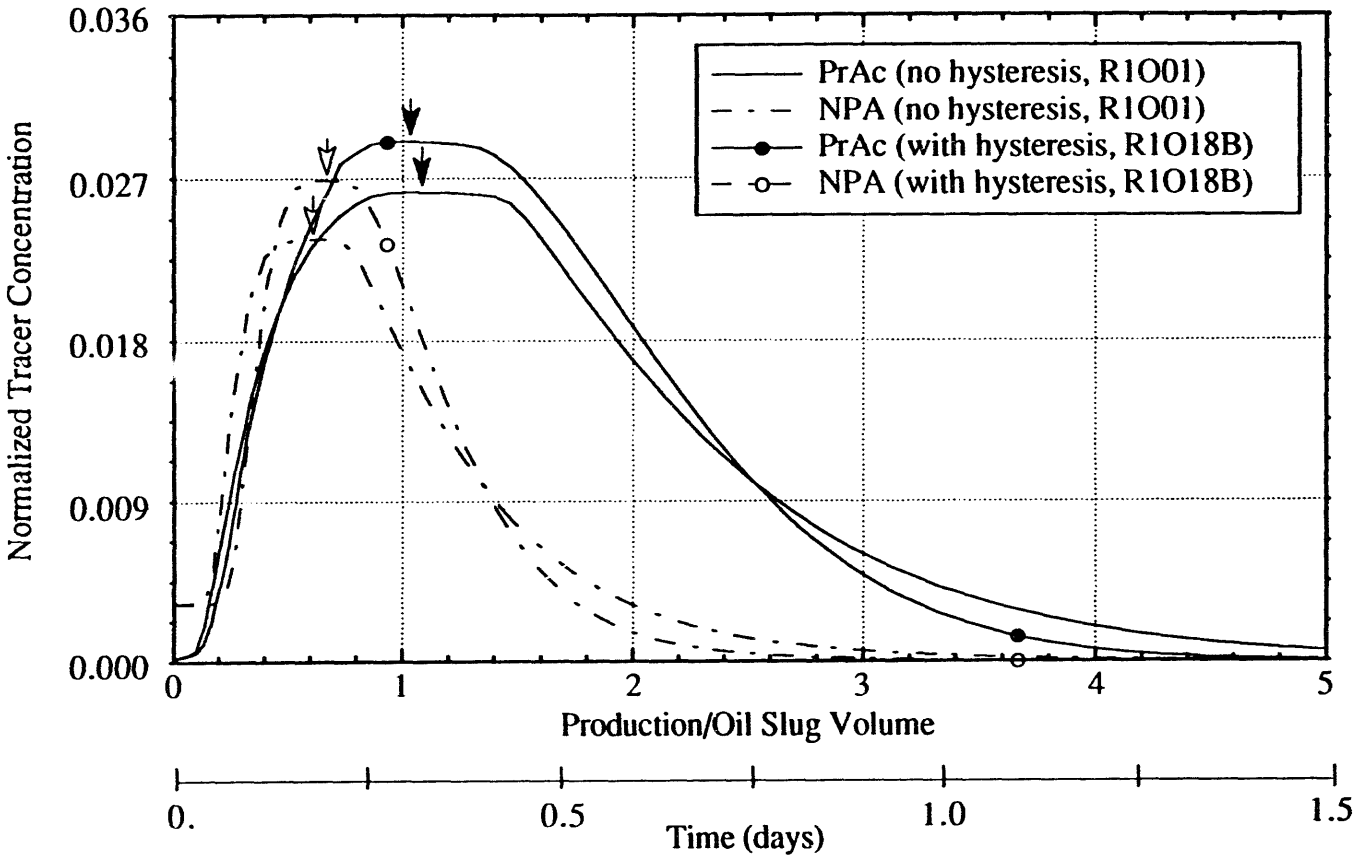

Fig. 13 **Aqueous phase tracer histories in a strongly oil-wet reservoir**

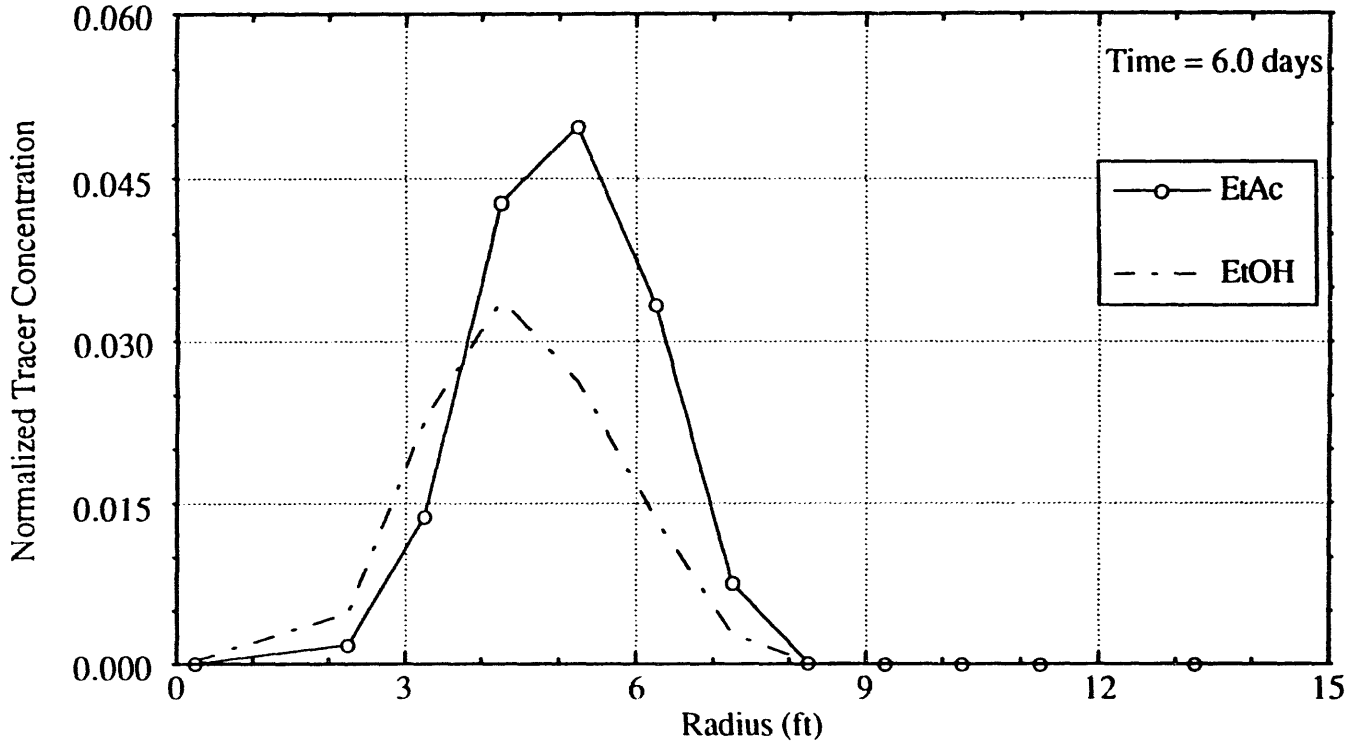

Fig. 14 **Aqueous phase tracer concentration profiles after the shut-in period in a strongly oil-wet reservoir (Radial run R1O01)**

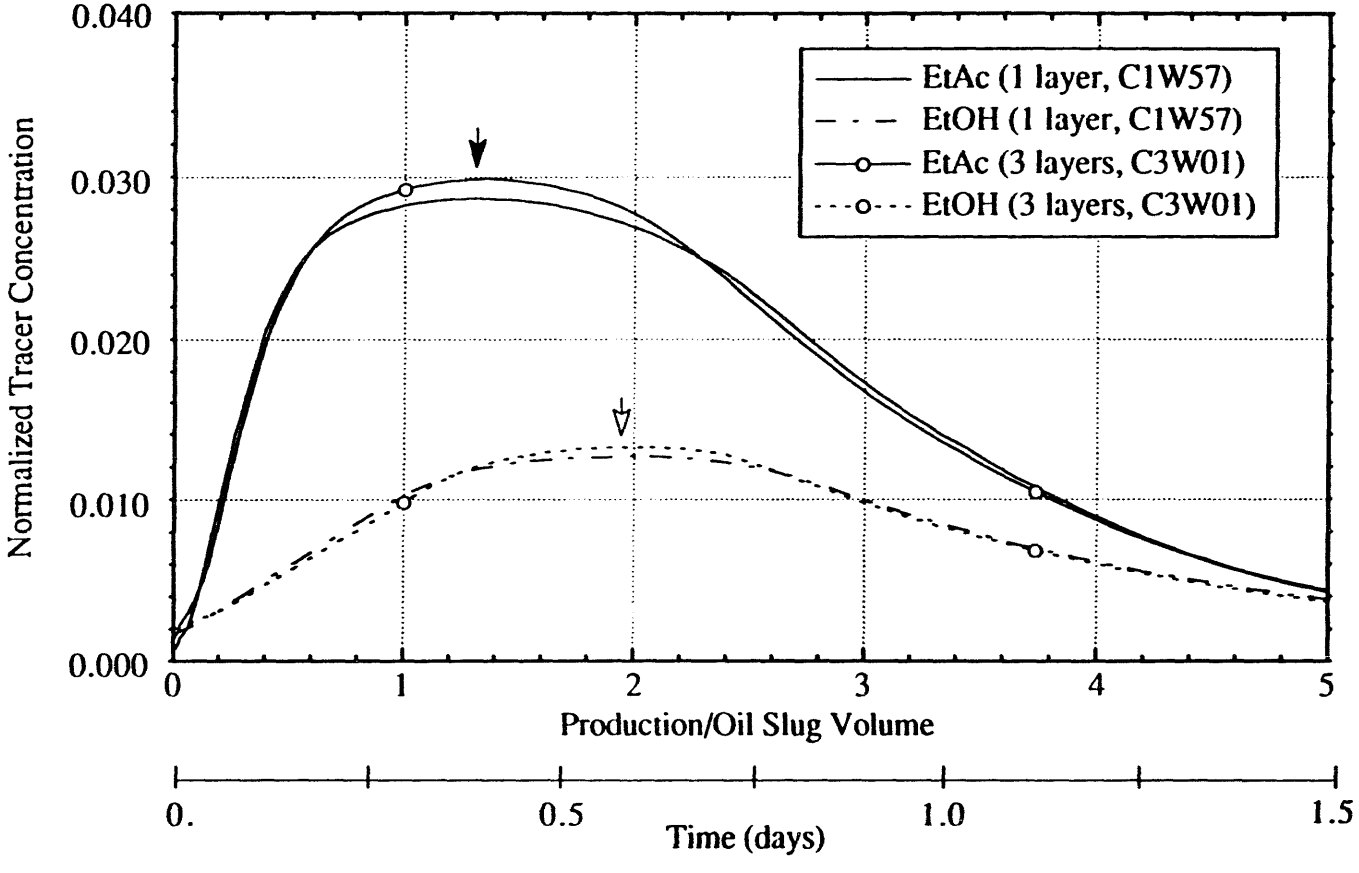

Fig. 15 **Aqueous phase tracer histories in a strongly water-wet reservoir for the 2D and 3D simulations**

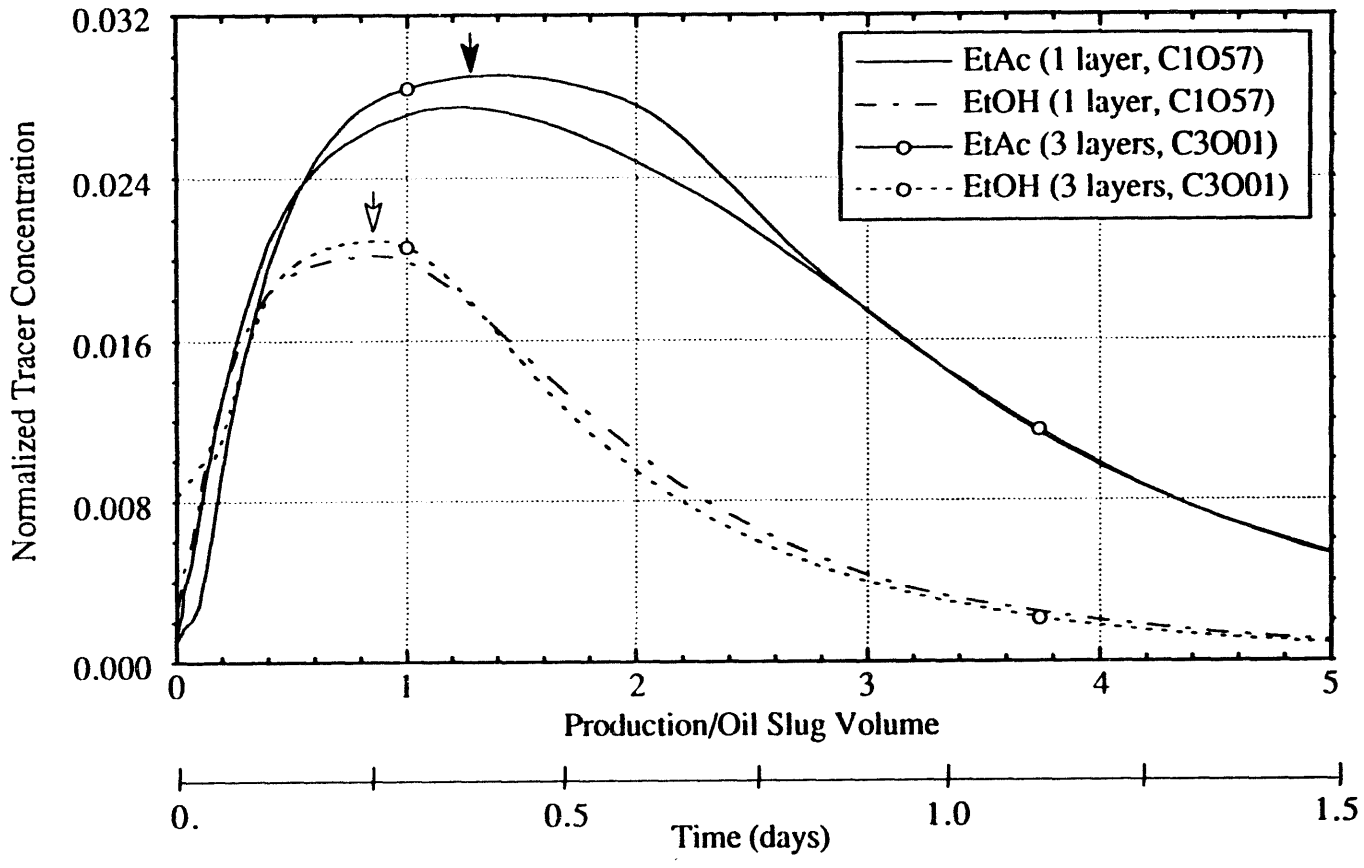

Fig. 16 **Aqueous phase tracer histories in a strongly oil-wet reservoir for the 2D and 3D simulations**

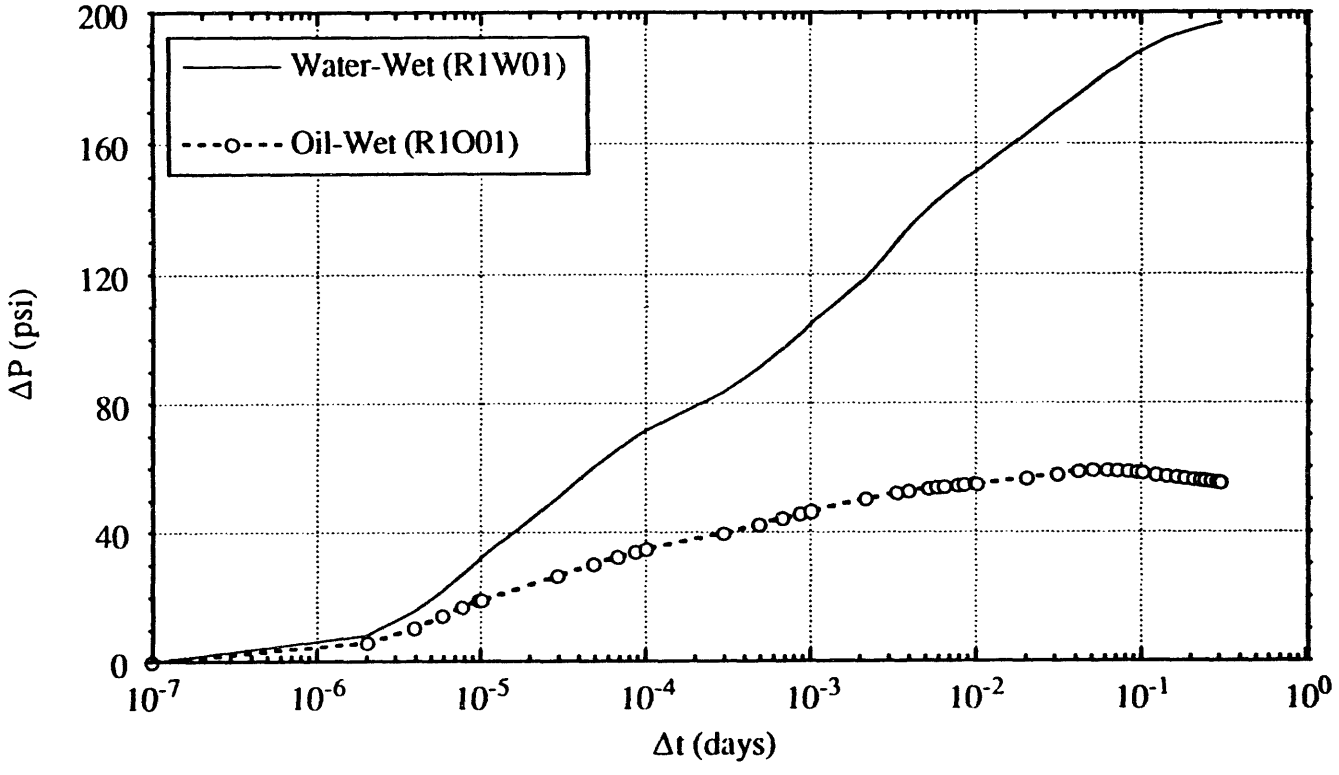

Fig. 17 Bottomhole pressure (ΔP) histories during water injection

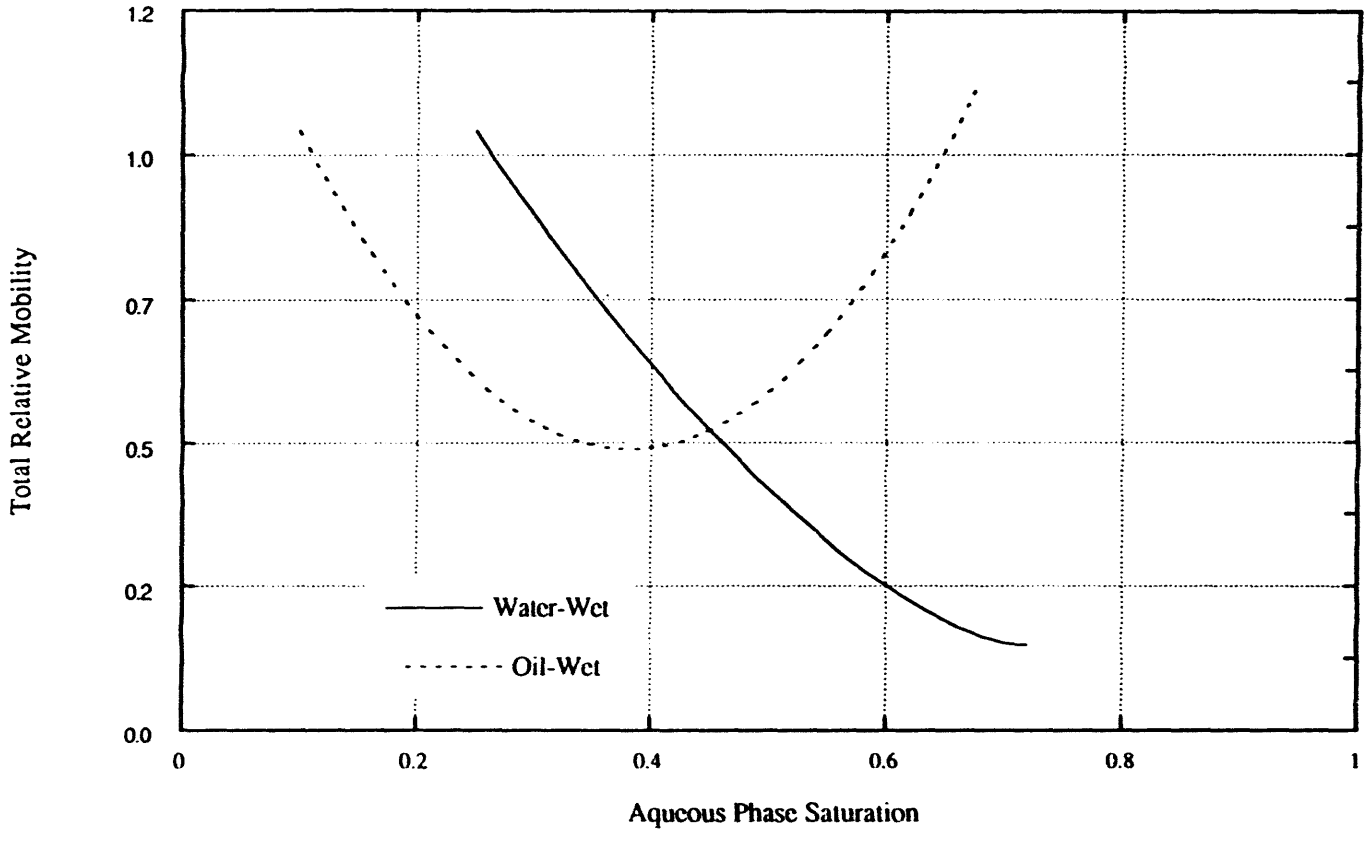

Fig. 18 Total relative mobility for strongly water- and oil-wet cases

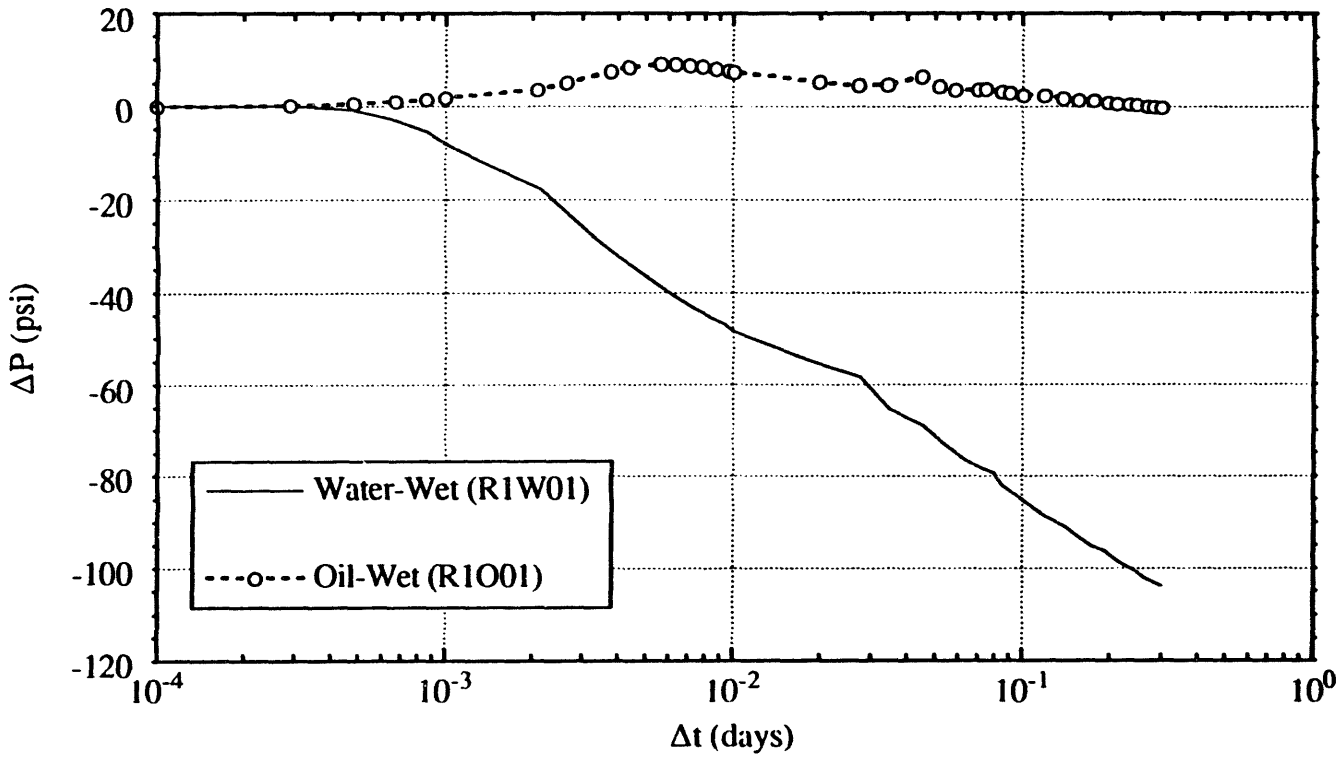

Fig. 19 Bottomhole pressure (ΔP) histories during oil injection

SECTION 2

A TYPE-CURVE APPROACH TO ANALYZING TWO-WELL TRACER TESTS

Authors: A. Datta Gupta, M.J. King, L.W. Lake, and G.A. Pope

SUMMARY

The traditional approach to analyzing field tracer data generally involves a history matching procedure that is time-consuming and frequently results in a nonunique solution. In this work we use theoretical frequency response functions to build type curves of "transfer function" and "phase spectrum" that have a dimensionless heterogeneity index as a parameter to characterize a stochastic permeability field. The "transfer function" contains information regarding the amplitude attenuating characteristics of the heterogeneous medium, and the "phase spectrum" provides information about the spacing between the frequency components of the input and output tracer pulses. In a manner analogous to type curve matching for well testing, we can analyze field tracer history by comparing the theoretical and field-observed "transfer function" and "phase relations." This analysis leads to an estimate of the heterogeneity index and pore volume. We demonstrate the technique by analyzing field tracer data from the Big Muddy field, Wyoming, and compare the use of parameters so obtained in scaling up. Results show very good agreement with the field data.

INTRODUCTION

Two-well tracer tests, injecting a tracer into a well and analyzing its breakthrough response in a second well, have been commonly used as a part of reservoir surveillance and management programs. Less common are rigorous means of analyzing the tracer response (Smith and Brown, 1984).

Analysis of field tracer response has largely been limited to qualitative evaluations of flow patterns in the reservoir (e.g., detection of preferential flow paths, well-to-well communication, fluid drift, faults, etc.). The classical streamline approach (Abbaszadeh-Dehghani and Brigham, 1984) is quantitative but is restricted to simple flow geometries with homogeneous flow properties or to noncommunicating layers. A more general approach (Allison *et al.*, 1991) is to use a numerical simulator to match the tracer production data, since arbitrary heterogeneity can be modeled and more complex fluid flow included as needed. However, such a procedure is time-consuming and can lead to non-unique reservoir parameters.

Field evidence indicates that permeability frequently varies randomly throughout the reservoir on several scales and exhibits spatial correlation. Since it is impractical, if not impossible, to describe heterogeneity in deterministic detail, in this paper we adopt a stochastic approach based on statistical characterization of reservoir heterogeneities (Gelhar and Axness, 1978).

Interpretation of tracer response for parameter estimation can be classified into two broad categories -- the time-domain approach and the frequency-domain approach. The former involves estimation of temporal and spatial moments from the observed tracer history and areal breakthrough patterns. Analysis of tracer tests in the petroleum literature has largely been limited to the time-domain approach. The frequency-domain approach, on the other hand, applies Fourier analysis to the theoretical and experimental response functions. A comparison of these methods for analysis of laboratory data has been given by Duffy and Al-Hassan (1988). The main

advantage of the frequency-domain analysis is that the impact of noise in the data is reduced. In frequency analysis, the noise content of an experiment is more or less uniformly distributed over all harmonics in the experimental frequency-response function. This is of particular importance in flow through heterogeneous media, where dispersive mixing causes attenuation of high-frequency amplitudes, resulting in so called "low pass" filtering effects. Consequently, errors are significant only in the high-frequency range, where the amplitudes of the error and the signal are of the same order (Gangwal *et al.*, 1971).

We propose the use of frequency-domain theory for convective transport to estimate a measure of heterogeneity and pore volume from field tracer response. Theoretical frequency-response functions have been obtained by mixing contributions from individual streamlines at a producer for different degrees of reservoir heterogeneities and spatial correlations. The results are used to generate theoretical "transfer functions" and "phase spectra." A type curve approach is then adopted to analyze a field tracer history by comparing the theoretical and field observed "transfer function" and "phase relations". The matching leads to an estimate of the heterogeneity parameter and pore volume without trial and error. The method presented here follows the earlier work of Duffy and Gelhar (1985, 1986), who applied frequency domain approach to analyze groundwater quality fluctuations caused by source variability.

APPROACH

Ours is a systems approach to reservoir characterization. We imagine that a tracer is introduced into an injection well (input function) and produced from a second well (output function or pulse). As shown below, an impulse response function can be derived from these two. This function is an intrinsic measure of a reservoir's response to an input. It is independent of the nature of the input and the size of the test. The function itself could be used to make predictions, but we use it to infer values of the Gelhar-Axness heterogeneity index (HI) and the pore volume (Gelhar and Axness, 1978) .

Experimental Frequency Response

We invoke the use of "linear filter theory" (Thomman, 1972) and accordingly approximate the input tracer pulse by a series of finite impulse inputs, the envelope of which forms the arbitrary input. If the individual responses to each impulse input are summed and the width of the finite impulses is made infinitesimally small, the breakthrough curve for single-phase, steady flow in a reservoir (a linear, time-invariant system) can be expressed in the form of a convolution integral,

$$c(t) = \int_{-\infty}^{\infty} h(t-\tau)\, c_0(\tau)\, d\tau \,, \tag{1}$$

where $c(t)$ and $c_0(t)$ are the output and input concentrations and $h(t)$ is the impulse response function, the response that would occur if $c_0(t)$ were a unit impulse or Dirac delta function, $\delta(t)$, input .

When expressed in the frequency domain, Eq. 1 becomes a simple product on taking its Fourier transform,

$$C(\omega) = C_0(\omega)\, H(\omega) \,, \tag{2}$$

where $C(\omega)$ and $C_0(\omega)$ are the Fourier transforms of the tracer production history $c(t)$ and injection history $c_0(t)$, respectively, and $H(\omega)$ is the Fourier transform of the impulse response function; $H(\omega)$ is called the frequency response function.

In general $H(\omega)$ is a complex quantity relating the amplitude and phase characteristics of the input and the output. It is completely characterized by the "transfer function", which contains information regarding the amplitude attenuation between input and output and the "phase spectrum," which contains information regarding the lead or lag between the frequency components comprising the input and output. The transfer function and phase spectrum are defined as follows (Duffy and Al-Hassan, 1988):

$$|H(\omega)|^2 = |C(\omega)/C_0(\omega)|^2 \tag{3a}$$

$$\Phi(\omega) = -\tan^{-1}[\,\mathrm{Im}\,H(\omega)/\mathrm{Re}\,H(\omega)]\ , \tag{3b}$$

where $\mathrm{Im}\,H(\omega)$ and $\mathrm{Re}\,H(\omega)$ are the imaginary and real parts of $H(\omega)$. Thus, from a knowledge of the injection (input) and production (output) histories of a tracer experiment, we can easily determine $H(\omega)$ by simply taking discrete Fourier transforms of the field input and output data. The experimental transfer function and phase spectrum can then be computed using Eqs. 3a and 3b.

Theoretical Frequency Response

In order to obtain the theoretical $H(\omega)$, we assume single-phase, steady flow through a two-dimensional random permeability field that has a known probability distribution and spatial correlation structure. Flow is assumed to take place between a fully perforated injector and producer. Single-phase flow equations are then solved for the velocity field from which tracer particle trajectories are obtained using the semianalytic approach.

The semianalytic approach to transit time calculation uses an underlying velocity field that is obtained numerical.y from a conventional reservoir simulator. This generalizes the streamline approach to any arbitrary configuration of wells and to heterogeneous permeability fields.

In three-dimensional flow, the geometry of streamlines in space is defined by the intersection of two families of surfaces, given by (Bear, 1988)

$$\psi = \psi(x,y,z) = \text{constant}$$

$$\chi = \chi(x,y,z) = \text{constant}\ .$$

The stream function is related to the velocity field v by

$$v = \nabla\psi \times \nabla\chi$$

For two-dimensional flow in an x-z plane, as is being considered here, planes of y=constant play the role of stream surfaces. With $\chi = y$, we obtain

$$v_x = -\frac{\partial\psi}{\partial z}$$

$$v_z = \frac{\partial\psi}{\partial x}.$$

For incompressible flow in a non-deformable permeable medium, mass continuity requires

$$\nabla . v = 0 \tag{4}$$

away from sources and sinks. In order to calculate transit times to a producer, we first obtain the velocity field numerically using a five-point discretization scheme for any arbitrary distribution of permeabilities. Now, the simplest representation of the stream function in a rectangular lattice gridblock that satisfies Eq. 4 is a bilinear function of the form

$$\psi(x,z) = \psi_0 + ax + bz + cxz. \tag{5}$$

Equation 5 is consistent with a five-point finite-difference operator for the velocity field. From Eq. 5, one obtains

$$v_x = -\frac{\partial\psi}{\partial z} = -(b + cx) \tag{6a}$$

$$v_z = \frac{\partial\psi}{\partial x} = a + cz. \tag{6b}$$

Thus, the component velocities vary linearly in the respective directions only. The constants a,b, and c for any gridblock can be obtained by linear interpolation of the numerical velocity field. For example, in the x direction,

$$\frac{\partial x}{\partial t} = v_x = v_x(0) + x/\Delta x(v_x(\Delta x) - v_x(0)),$$

which is equivalent to Eq. 6a, where

$$b = -v_x(0) \text{ and } c = -(v_x(\Delta x) - v_x(0))/\Delta x.$$

The travel time across a gridblock can be obtained by direct integration of Eq. 6. For example, in the x direction, the transit time (Δt_x) from an initial position x_0 to any location x will be given by

$$-\int dx/(b + cx) = \Delta t_x$$

$$\ln[(b + cx)/(b + cx_0)] = -c\,\Delta t_x.$$

Similarly in the orthogonal z direction,

$$\ln[(a + cz)/(a + cz_0)] = c\,\Delta t_z.$$

Since the streamlines must enter and exit through gridblock faces, the actual transit time across a gridblock will be given by the minimum over the allowed edges (Pollock, 1988). Thus,

$$\Delta t = \text{Minimum}\ (\Delta t_x\ ,\ \Delta t_z),$$

where the minimum is examined only for positive values. The transit time to any location in the domain is obtained by following the streamline backwards in time to the injector and summing up the travel times through successive grid blocks in the finite-difference model. For calculating the transit time function $\tau(\psi)$, we originate the trajectory at the producer and label the transit times as a function of the streamline. Finally, one may verify that along these trajectories, ψ is a constant. Then we have

$$(b + cx)(a + cz) = (b + cx_0)\ e^{-c\Delta t}\ (a + cz_0)\ e^{c\Delta t} = \text{constant}.$$

Hence, streamlines are hyperbolas within a gridblock with asymptotes at $x = -b/c$ and$z = -a/c$.

We assume permeability to be a log-normally distributed spatially random variable with a known covariance structure. Statistical homogeneity implies that the mean is independent of location and the covariance is a function of lag distance only. Multidimensional random fields are then generated using the Turning Band Method (TBM) (Mantoglou and Wilson, 1982; Yang, 1990). Anisotropy in correlation is introduced by a simple linear transformation of the geometry (Journel and Huijbregts, 1978) resulting in an ellipsoid correlation structure.

Along individual streamlines, convective transport of a conservative tracer can be represented by

$$\frac{\partial c}{\partial t} + \frac{\partial c}{\partial \tau} = 0 \tag{7}$$

where we have introduced the travel time coordinate τ defined by,

$$\tau = \int ds/v(s)$$

along the streamline. Note that Eq. 7 implies that tracer moves down a streamline without dissipation or interaction with the medium.

The impulse response function for Eq. 7 is given by (Duffy and Gelhar, 1986; Thomman, 1972)

$$h(\tau,t) = \delta(t - \tau) \qquad t \text{ and } \tau \geq 0$$

$$= 0. \qquad t \text{ and } \tau < 0.$$

The Fourier transform of the impulse response function yields the frequency domain solution for convection along a streamline,

$$H(\tau,\omega) = \exp\ (-\ i\omega\tau).$$

The transfer function and phase spectrum will be given by

$$|H(\tau,\omega)|^2 = 1 \tag{8a}$$

and

$$\Phi(\tau,\omega) = \omega\tau \, . \tag{8b}$$

From Eq. 8a, no amplitude attenuation occurs for pure convection along a streamline. However, in flow through heterogeneous permeable media, the overall tracer response will be the composite contribution from all streamlines, each with an appropriate delay time. Under such conditions the frequency-response function can be obtained by integrating the response from individual streamlines at the producer. The transfer function and phases can thus be obtained from the following expressions (Duffy and Gelhar, 1985,1986):

$$|H(\omega)|^2 = \left| \int_0^1 \exp(-i\omega\tau(\psi))\, d\psi \right|^2 \tag{9a}$$

$$\Phi(\omega) = \tan^{-1}\left(\int_0^1 \sin(\omega\tau(\psi))\, d\psi \Big/ \int_0^1 \cos(\omega\tau(\psi))\, d\psi \right) . \tag{9b}$$

In the above expressions, ψ represents the normalized stream function and $\tau(\psi)$ is the transit time function for the heterogeneous medium as discussed in the Appendix.

Type-Curve Matching

The basic method consists of taking Fourier transforms of the output and input tracer histories. This can be accomplished by one of several available Fast Fourier Transform (FFT) routines. The experimental transfer function and phase spectrum are then obtained using Eqs. 3a and 3b. In a manner analogous to the type curve matching procedure in well test analysis, the experimental transfer function and phase spectrum can be compared with the theoretically derived charts (type curves) in order to estimate the required heterogeneity parameter. An estimate of the pore volume can be obtained by selecting a match-point on the type curves.

RESULTS

Type Curves

For generation of type curves we used a spherical variogram to represent the spatial correlation structure of the log-permeability fields. Although, in principle, any other type of variogram could be used, the particular choice was based on its ability to match geologic data (Goggin, 1988) and also to retain consistency with the Gelhar-Axness coefficient (Gelhar and Axness, 1978). Random fields were generated for various combinations of log permeability variance ($\sigma^2_{\ln}$) and dimensionless correlation lengths (λ_D). The correlation length is made dimensionless by dividing it by the system length. Each realization was characterized by its heterogeneity index, $HI = \sigma^2_{\ln}\lambda_D$, as defined by Gelhar and Axness (1978). For random fields with correlation anisotropy, λ_D was taken to be the dimensionless correlation length in the

principal direction of flow. A k_z/k_x of 0.1 was used for generation of type curves. However, the impact of changing k_z/k_x was minimal since we assumed single-phase flow. Separate type curves were generated for correlation anisotropies ($\lambda_{xD}/\lambda_{zD}$) of 1, 10, and 20. The results that follow correspond to a $\lambda_{xD}/\lambda_{zD} = 1$.

Figure 1 shows the transit time functions corresponding to three sample realizations of permeability fields representing three values of HI. For small HI, the arrival times are more or less randomly distributed. However, with increasing HI the arrival times exhibit distinct correlated patterns, indicating preferential fluid movement or "channeling" through streaks of large permeability. Such "channels" are characterized by "flat regions" in the transit time function, in which considerable change in streamfunction is observed over a relatively short interval of time. Also, the variance of the arrival times increases with HI because of near-stagnant regions.

Figures 2A and 2B show transfer functions and phase spectra corresponding to these three cases. The transfer function contains information regarding the amplitude attenuating characteristics of the medium. Clearly as the HI is increased, the transfer function shows more and more high-frequency amplitude filtering. Thus, the reservoir acts as a so-called "low pass filter." The phase spectrum, on the other hand, contains information about the breakthrough characteristics of the tracer response. It exhibits almost a linear growth with frequency. Both curves will be used in subsequent calculations to estimate heterogeneity parameters from field tracer response.

Multiple Realizations

In order to verify the consistency of the results, we examined the transfer function and phase characteristics of multiple realizations with the same HI. We discuss two examples here.

Figure 3A shows the transit time function for two realizations of the permeability field where only the random seed was varied. The variance of log permeability, $\sigma^2_{\ln}$ and the dimensionless correlation length, λ_D, for these cases were 0.05 and 0.4, respectively, resulting in a HI of 0.02. Transit time functions for two other realizations with the same HI of 0.02 are shown in Fig. 3B. However, different combinations of $\sigma^2_{\ln}$ and λ_D viz. (0.1, 0.2) and (0.2, 0.1) were used to generate these fields.

Figures 4A and 4B plot the transfer function and phase spectra corresponding to all four cases. The closeness of the curves indicates that HI is a general summary of the effects of heterogeneity on the tracer response. Of course, for this particular case, the closeness is partly because the HI's used are small. The phase spectra show a close agreement also. With increasing HI, the variability increases somewhat and an average over multiple realizations is taken to obtain theoretical frequency response.

Radioactive Decay

If the tracer undergoes radioactive decay, the frequency-response function for convection along a streamline will be given by (Duffy and Gelhar, 1985)

$$H(\tau,\omega) = \exp(-(i\omega + \kappa)\tau) \quad , \tag{10}$$

where κ is a first-order rate constant describing the decay. Figure 5 shows the effects of the decay on the transfer function for a HI = 0.1. Whereas the amplitude exhibits attenuation, the phase characteristics remain unchanged because of radioactive decay.

Residual Phase Saturation

The presence of a residual phase will primarily affect the breakthrough characteristics of a tracer response. Under such circumstances, the transfer function will remain virtually unchanged, but the phase spectrum will indicate early breakthrough because of the presence of an immobile phase. This is indicated in Fig. 6. The slope of the phase spectrum indicates the average residence time of the tracer. Hence, one way to estimate the residual phase saturation would be to match the transfer function first and then exploit the difference in slope between the observed phase response and the expected phase response in the absence of any residual phase. However, in general any definitive information regarding residual saturation would require two tracers, one of which partitions with the immobile phase.

Data Analysis

The theoretical frequency response curves calculated using Eqs. 9a and 9b and shown, for example, in Figs. 4A and 4B, can be considered "analog" responses. Here, the frequency axis is not limited to any particular upper range and in theory, we should be able to resolve infinitely high frequencies. However, in the analysis of field ("digital") data, the degree of resolution will be limited by the sampling interval. For a sampling interval of Δt days, the maximum meaningful frequency will be the Nyquist frequency given by (Karl, 1989)

$$f_c = 1/(2\Delta t) \quad \text{or} \quad \omega_c = 2\pi f_c = \pi/\Delta t \ . \tag{11}$$

This is an important quantity that will be used in the subsequent analysis.

Sampling in the time domain introduces periodicity in the Discrete Fourier Transform (DFT) spectrum (Karl, 1989). If the spectrum is wider than $\pi/\Delta t$, an overlap superimposes portions of the true spectrum causing distortion, otherwise known as aliasing. Although aliasing can be minimized by increased time domain sampling, this may be cost-prohibitive, or field data may not exist at sufficiently close intervals. In practice, however, the tail of the DFT spectrum may be masked by noise, in which case only meaningless information exists in the vicinity of the Nyquist frequency anyway. In order to avoid such complications, since we are primarily interested in the large-scale fluctuations resulting from correlated streaks of permeability, we will restrict the matching procedure to the low frequency region.

Another important consideration in the analysis of field data is to compute the DFT spectrum at sufficient number of frequency points to facilitate the type curve matching procedure. This is accomplished by appending zeros to the tracer history data. This procedure, known as "zero padding", is normally a good practice in computing spectra of discrete data by the DFT. Adding zeros to the tracer data in the time domain corresponds to interpolation in the frequency domain and results in a well-defined transfer function, as illustrated in Fig. 7. Similar improvement is also observed in the phase spectrum.

FIELD APPLICATION

In this section, we illustrate the type curve matching procedure through application to a field example, the Big Muddy low-tension pilot project. A complete description of the Big Muddy pilot project can be found elsewhere (Saad *et al.*, 1989). The test pattern selected in this study is a one-acre five-spot made up of five new wells drilled inside a five-acre area defined by four existing waterflood wells (Fig. 8). The pattern has been waterflooded since 1953 and at the time of the

initiation of the pilot project in 1978, the oil cut was less than 1%. Four different tracers were injected: tritium was injected in Well J14, ammonium thiocyanate into Well J31, and methanol and ethanol were injected in Wells W79 and S27, respectively. The field production history of tritium in the center producer Well J30, shown in Fig. 9, has been analyzed here.

The entire low-tension pilot project, including the tracer histories, was previously simulated by Saad *et al.* (1989). A reasonable agreement with the tracer history was obtained with a finite-difference simulator using a three- or a four-layer reservoir description in conjunction with a longitudinal dispersivity of 16 ft. In contrast, we attribute the tracer dispersion only to reservoir heterogeneities in this study, and thus no physical dispersion has been included in our calculations.

Type-Curve Inference

Figures 10A and 10B show the transfer function and phase spectrum corresponding to the tritium production history in Well J30. As customary, the DFT analysis has first been carried out assuming $\Delta t = 1$ day, which results in $\omega_c = \pi$ radians/day. Hence, the frequency axis must be rescaled by dividing by the appropriate sampling interval, which in this case was 60 days. Also, in order to make the frequency axis dimensionless (as in the type curves), we must multiply it by T, the time required to inject one pore volume. In fact, T will be estimated by selecting an appropriate match point during the type curve analysis.

As in well test analysis (Earlougher, 1977), the type curve matching involves sliding the transfer function derived from field data on the type curves horizontally until an appropriate match is obtained (Fig. 11). We estimate HI = 0.3 from this. Also, selecting a match point on the frequency axis, we must have

$$\omega_d = \omega_m/\Delta t\, T \quad \Rightarrow \quad T = \omega_d/\omega_m\, \Delta t \ , \tag{12}$$

where ω_d and ω_m are the frequency values for the match point read from the type curve and the estimated transfer function, respectively. For this example case, $\omega_d = 2.0$, $\omega_m = 0.18$, and $\Delta t =$ 60 days, resulting in T = 667 days. The actual field value for one pore volume injection was estimated to be 625 days (Saad *et al.*, 1989).

So far in our analysis we have not used the phase spectrum. Ideally, both the transfer function and the phase spectrum should be matched simultaneously in order to uniquely define the frequency response. The slope of the phase spectrum contains information regarding the mean residence time of the tracer, which is affected by the presence of any immobile phase and the flow geometry, in addition to heterogeneity. For the Big Muddy example, the deviation of the phase spectrum (Fig. 12) can be attributed mainly to the presence of a significant residual oil saturation (estimated to be about 32% in the field (Saad *et al.*, 1989)).

Prediction of Field Tracer Response

We now validate our approach by predicting the tracer history using the parameters estimated from the type curve analysis. First, individual streamtube response is obtained by computing tracer history in cross sections with random permeability fields generated using the parameters estimated from the type curve matching. The overall tracer history is obtained by summing the individual streamtube responses depending upon the flow geometry.

For the Big Muddy field, a Dykstra-Parsons coefficient (V_{DP}) of 0.5-0.6 ($\sigma^2_{\ln} \approx 0.80$) was reported based on the core data. Field evidence indicated the existence of a large permeability

layer towards the top of the formation. For stochastic characterization of the reservoir, we first generated random fields with $\sigma^2_{ln} = 0.8$ and $\lambda_D = 0.30$, having a spherical covariance structure. This corresponded to a $\lambda_x = 55$ ft and a $\lambda_z = 15$ ft based on the aspect ratio, L/H. Next, all of the available geologic information, including the high- permeability layer near the top of the formation, were honored by conditioning the random field (Yang, 1990). On inclusion of the high-permeability layer, σ^2_{ln} became close to 1.0, resulting in a HI of 0.3, the estimated value from type curve matching. Tracer histories from two such realizations of random fields are shown in Fig. 13. We consider these tracer histories as individual streamtube response.

Next, in order to include the effects of areal geometry on the field tracer response, we compute the breakthrough pattern of streamtubes for a five-spot pattern. This is shown in Fig. 14 for areally homogeneous as well as heterogeneous cases. The areally heterogeneous case has been included only to illustrate the effects of areal heterogeneity in our predictions. An arbitrary V_{DP} of 0.45 was used to generate an areally heterogeneous field by a stochastic moving average method (Mishra *et al.*, 1988). The field tracer history is obtained by combining the streamtube responses as follows: (Lake, 1989)

$$c(t_D) = \Sigma c_{st}(t_D/\tau_a(\psi_i))\, \Delta\psi_i / \Sigma\, \Delta\psi_i \quad , \tag{13}$$

where $\tau_a(\psi_i)$ = breakthrough time (PV) for streamtube $\Delta\psi_i$
$c_{st}(t_D)$ = streamtube concentration response.

The predicted field tracer histories corresponding to the two realizations of random fields are shown in Figs. 15A and 15B along with the field data. Overall, the agreement is quite good considering that no history matching was involved. Also, predictions appear to improve if areal heterogeneity is incorporated in the analysis.

DISCUSSION

Prediction of fluid flow through permeable media requires integration of effects from many different length scales. When the mean residence time of a tracer in the permeable medium is not long enough to sample all the heterogeneities, the tracer continues to experience the effects of longer-range fluctuations in permeability with increasing time or travel distance. Such a phenomenon, known as the "scale effect," manifests itself as an apparent dispersivity that continues to grow as the sampling interval is increased (Arya *et al.*, 1988).

The analysis presented in this report assumes a linear transport equation and uses a stochastic characterization of reservoir heterogeneity with parameters estimated from the tracer response. Since the tracer response will only contain "characteristic signatures" of heterogeneities on a scale smaller than the well spacing, it is important to incorporate information regarding reservoir continuity, such as deterministic layers, by conditioning the random field. As such, the stochastic characterization serves to fill up the void. Such an approach to reservoir characterization will exhibit a behavior consistent with field observations (Arya *et al.*, 1988), i.e., intermediate between a diffusive spreading in which mean square displacement grows linearly with time and a purely convective spreading (layered media) in which the mean square displacement grows as t^2.

An important distinctive feature of our work compared to previous works (Abbaszadeh-Dehghani and Brigham, 1984; Allison *et al.*, 1991), apart from stochastic characterization of heterogeneity, is the fact that we restrict our entire analysis to the frequency domain. This reduces

the possibility of identifying "noise" (false peaks) in the tracer concentration history as layers. To illustrate this, in Fig. 16 we show the concentration history corresponding to two permeability fields having the same HI = 0.2 but different reservoir dimensions. Table 1 gives the derived layer properties using the history matching approach of Abbaszadeh-Dehghani and Brigham (1984). The transfer functions and phase spectra for these two cases are shown in Figs 17A and 17B. Whereas history matching of tracer response has resulted in different layer properties, we obtain almost identical results for both the cases in the frequency domain. The differences here, which are ignored in our analysis, are mainly in the high-frequency region .

Table 1

Computed Layer Properties by History Matching
(Abbaszadeh-Dehghani and Brigham, 1984)

SYSTEM SIZE	50X50	SYSTEM SIZE	100X100
LAYER #	kh/Σkh	LAYER #	kh/Σkh
1	0.436	1	0.305
2	0.327	2	0.221
3	0.237	3	0.202
		4	0.160
		5	0.112

CONCLUSIONS

1. Frequency-domain solutions have been obtained for single-phase tracer transport in stochastically heterogeneous permeable media. The tracer response is analyzed in the frequency domain because this reduces the impact of noise in the data.

2. Type curves have been generated as a function of the dimensionless heterogeneity index defined by Gelhar and Axness. The tracer motion was computed using a new transit time algorithm that is semianalytic and thus very fast. This method uses a finite-difference solution for the pressure equation followed by an analytic solution for the streamline flow of the tracers in an arbitrarily heterogeneous medium.

3. A simple and efficient method for analyzing two-well tracer data is given based upon these type curves. This method has the advantage that it does not involve history matching or trial and error. Both the heterogeneity index and the tracer pore volume can be easily and quickly estimated by this procedure.

4. Unlike the traditional approach whereby a deterministic "layer-cake" reservoir description is derived by history matching, we adopt a stochastic approach that allows for quantification of the uncertainty in predictions.

5. The proposed method has been successfully applied to analyze and predict the tracer history of a pilot test in the Big Muddy field, Wyoming, for the purpose of illustrating its practical application to real field data.

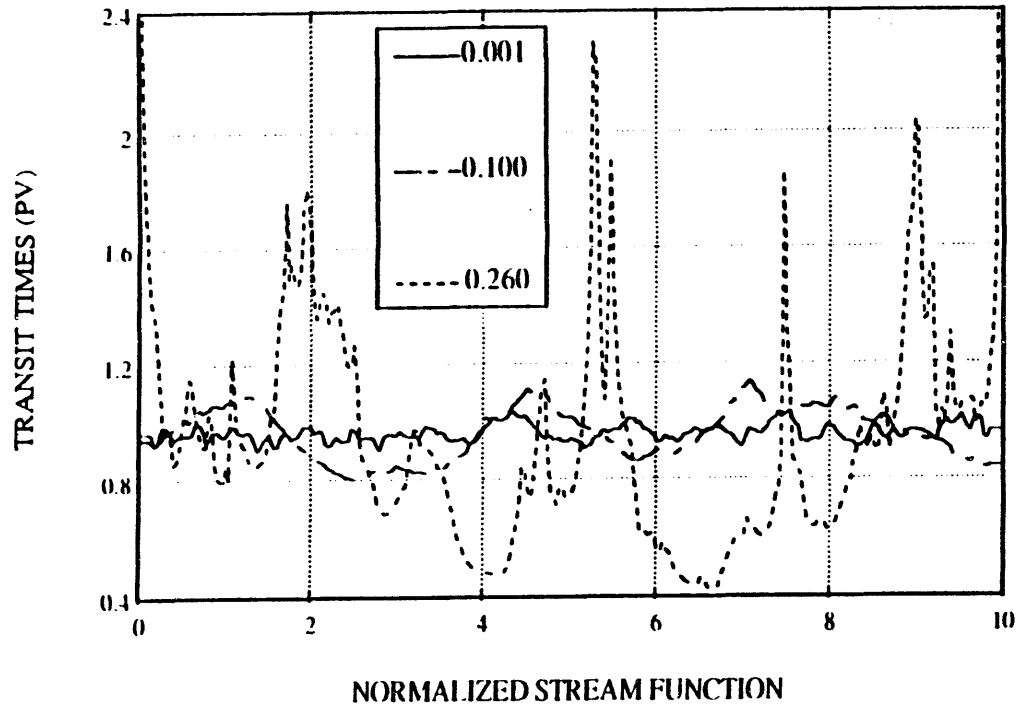

Fig. 1 Transit Time Function for Three Different Heterogeneity Indices.

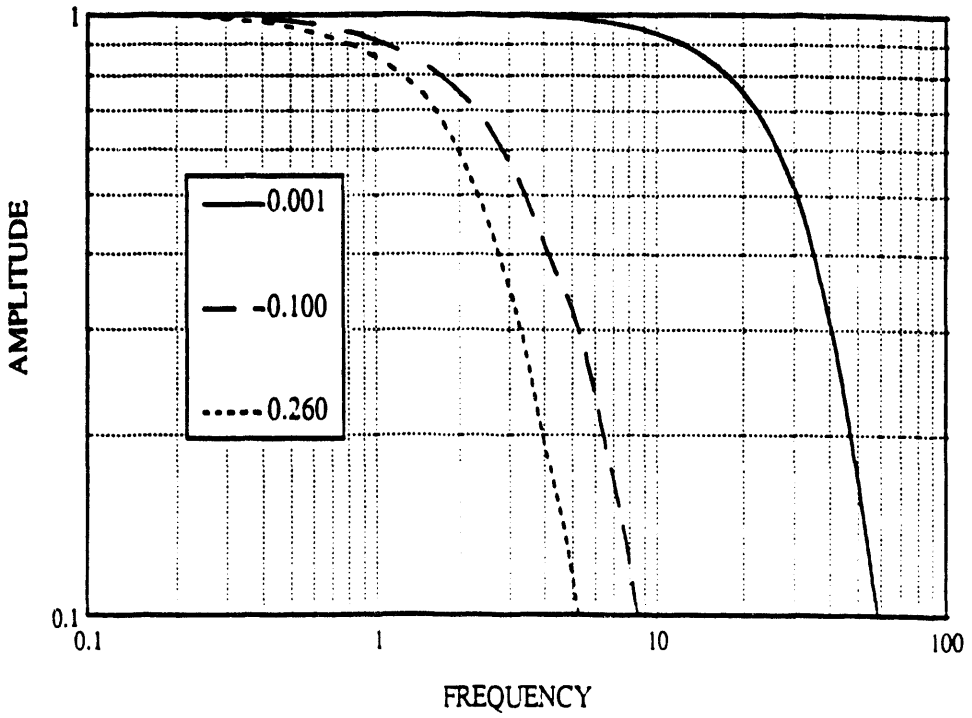

Fig. 2a Transfer Functions Corresponding to Three Heterogeneity Indices.

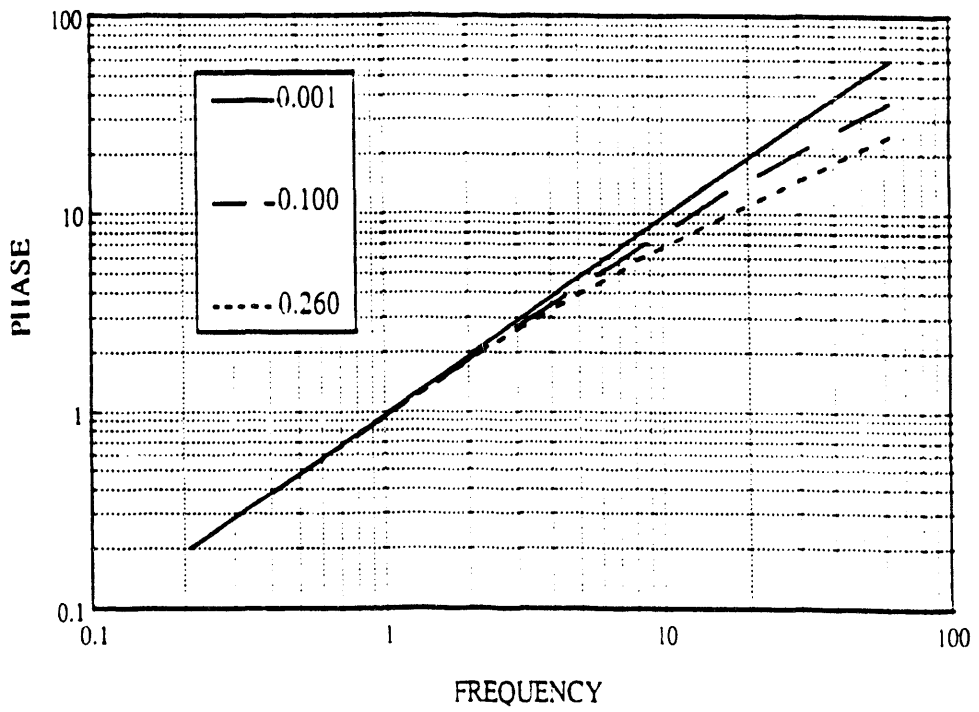

Fig. 2b Phase Spectra Corresponding to Three Heterogeneity Indices.

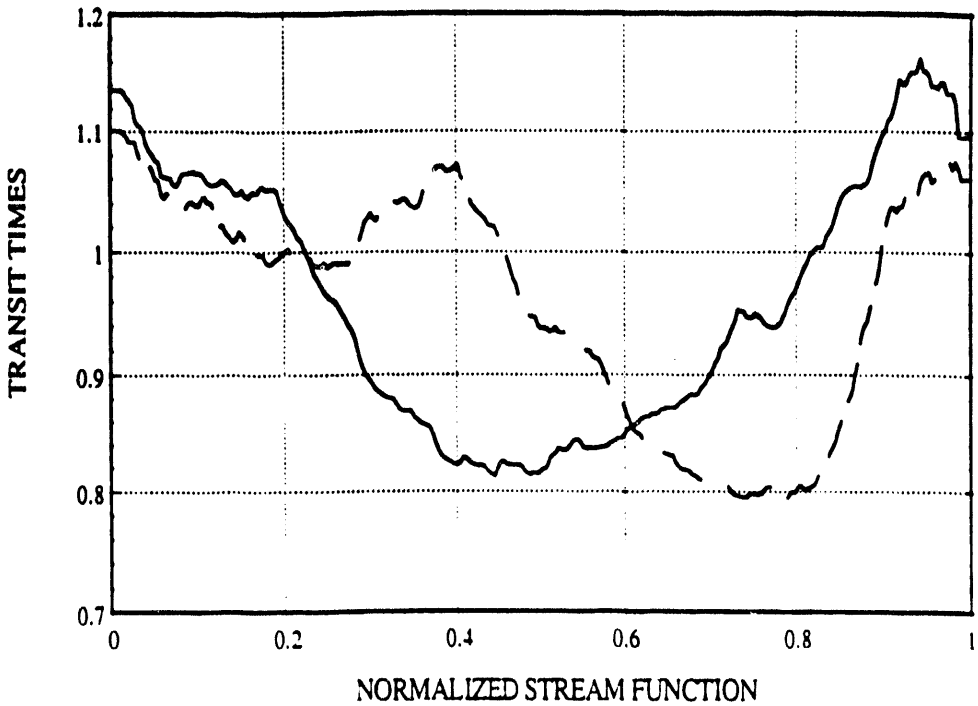

Fig. 3a Transit Time Functions for Two Realizations With Heterogeneity Index of 0.02. Only Random Seed was Varied.

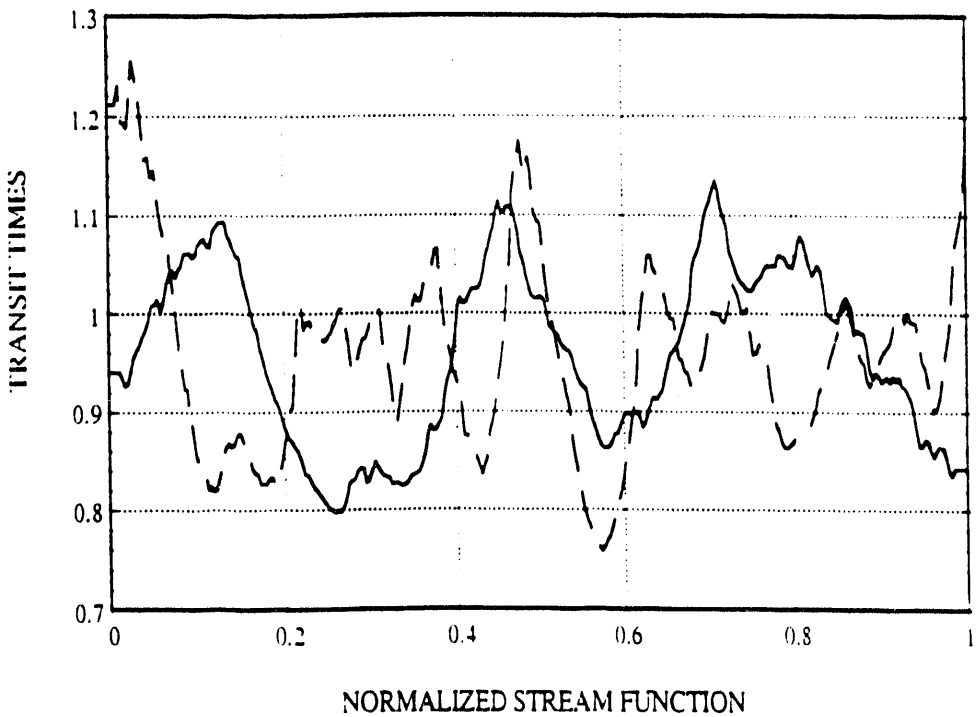

Fig. 3b Transit Time Function for Two Realizations with Heterogeneity Index of 0.02 having Different Combination of Permeability Variance and Correlation Length.

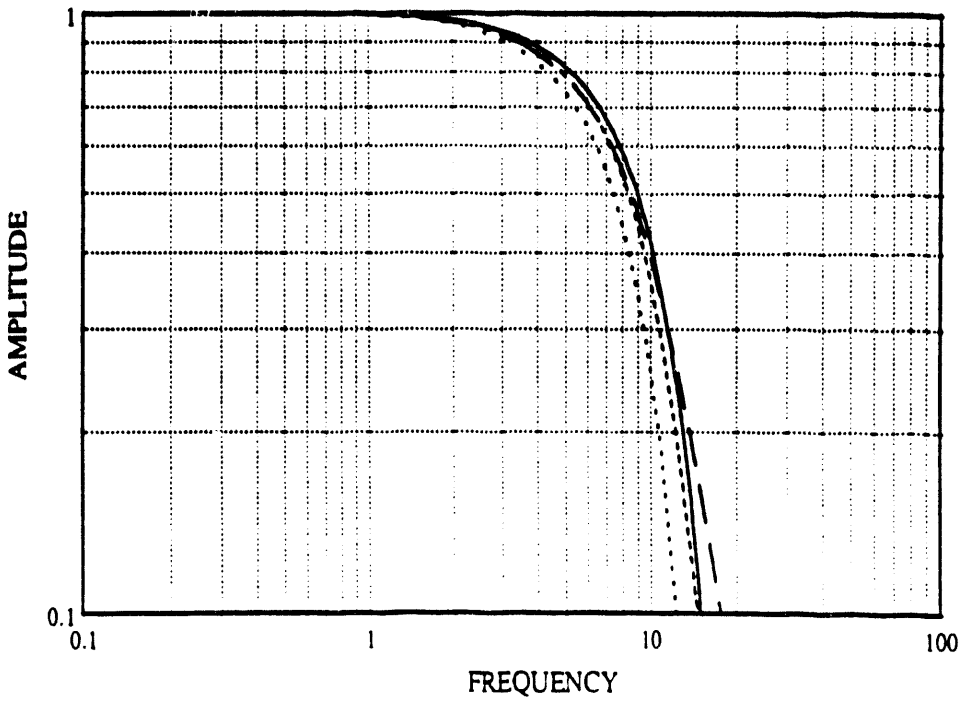

Fig. 4a Transfer Function for Four Realizations with Heterogeneity Index of 0.02.

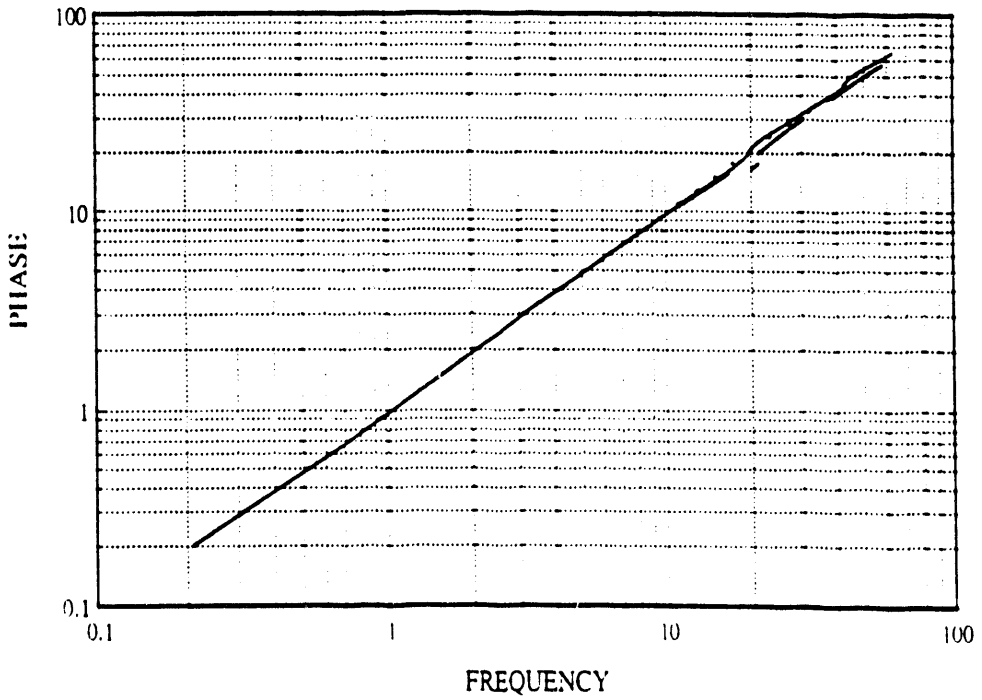

Fig. 4b Phase Spectrum for Four Realizations with Heterogeneity Index of 0.02.

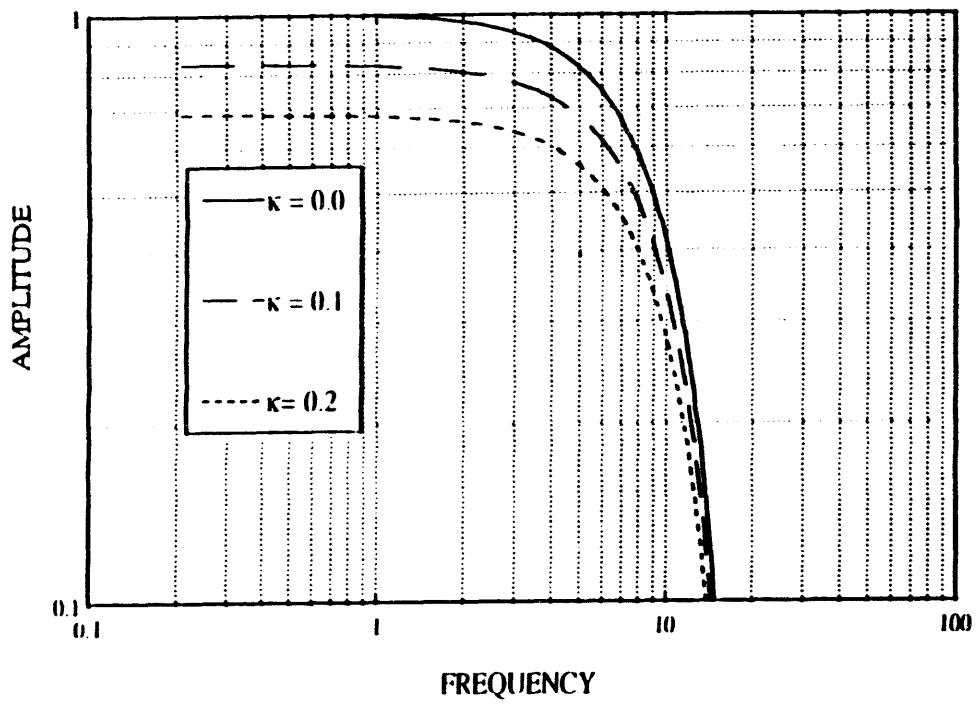

Fig. 5 Effect of Radioactive Decay of Tracer on the Transfer Function.

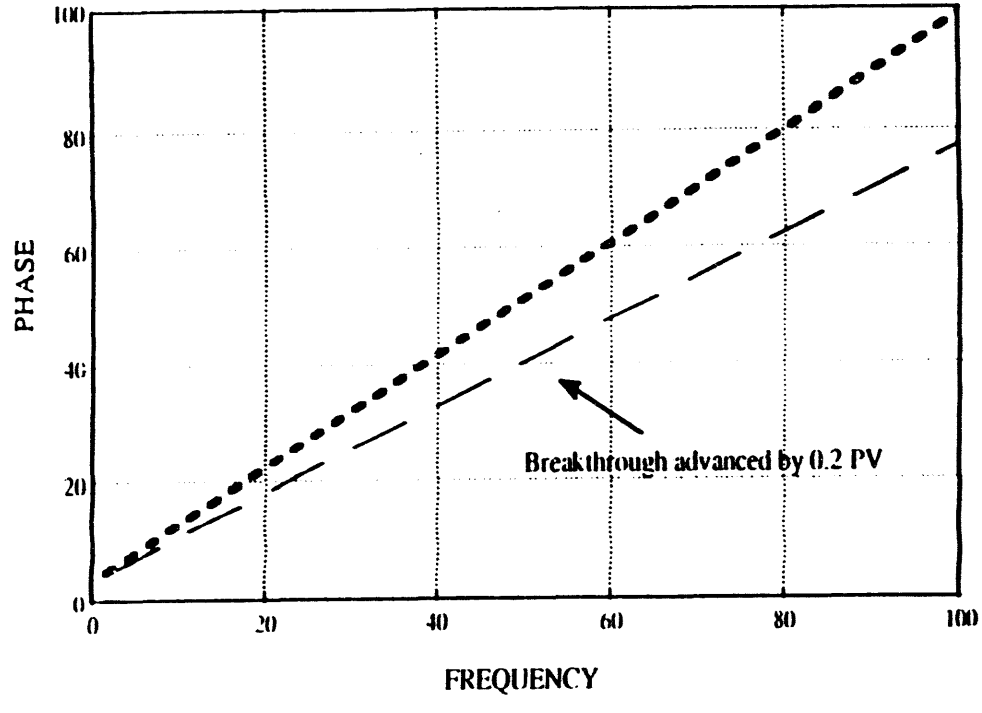

Fig. 6 Effect of Early Breakthrough of Tracer on the Phase Spectra.

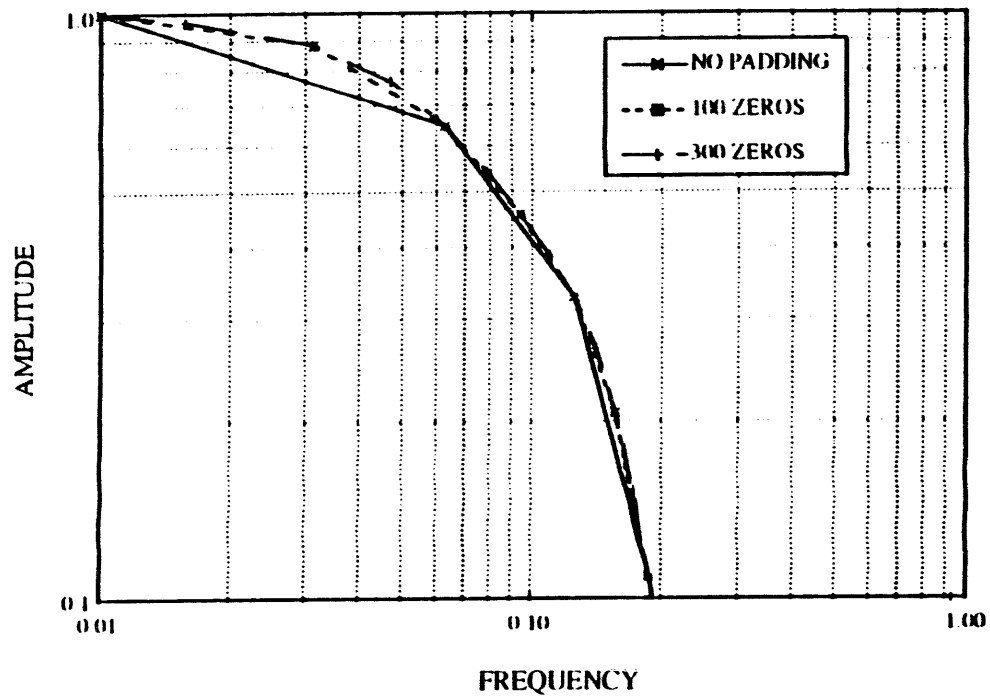

Fig. 7 Effect of Zero Padding of Data on the Transfer Function Calculations.

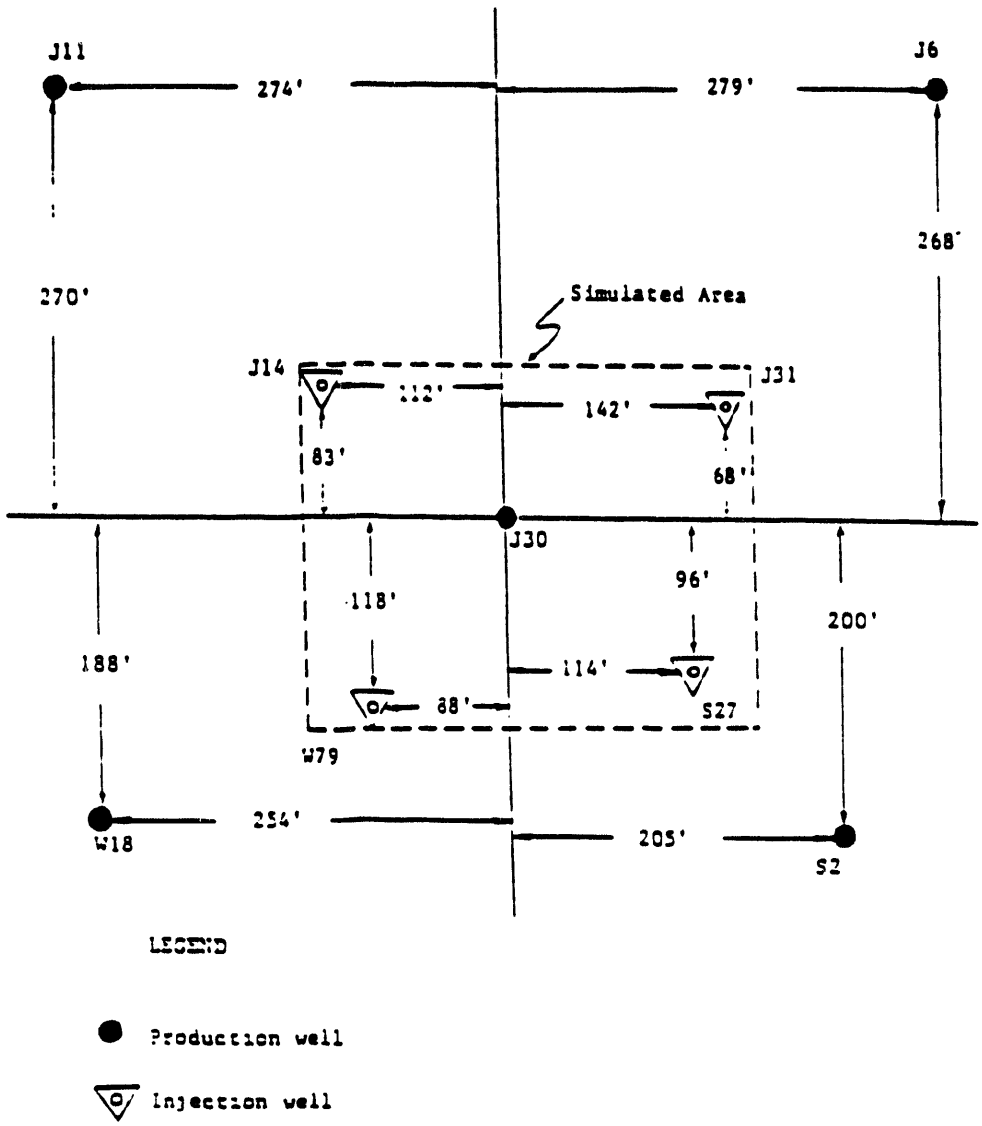

Fig. 8 Big Muddy Pilot Test Area.

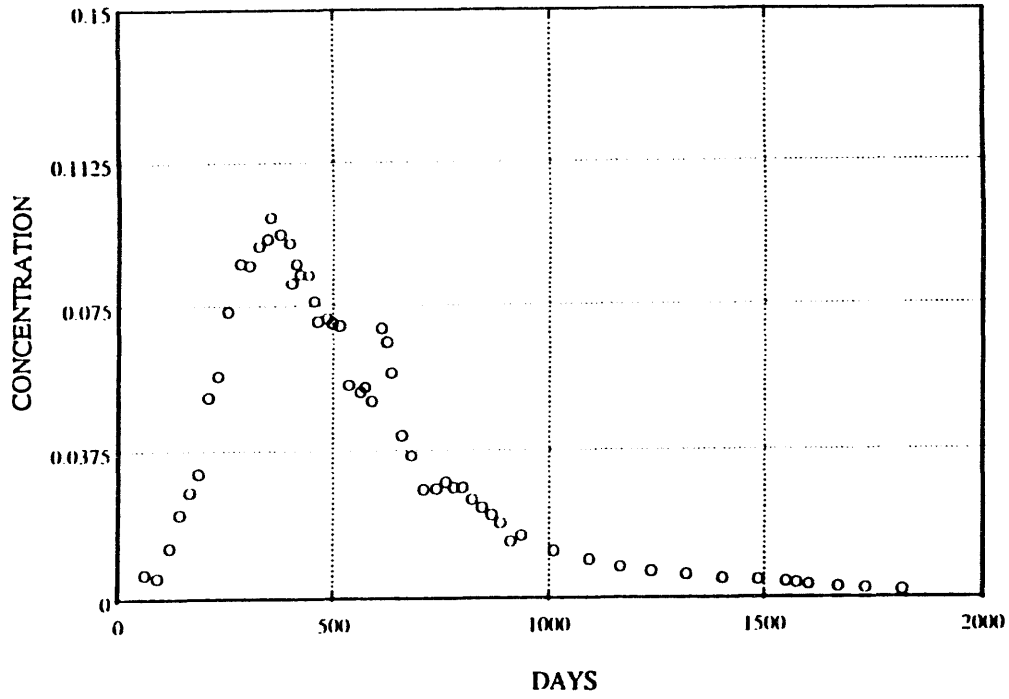

Fig. 9 Tritium Production History at Well J30, Big Muddy Field.

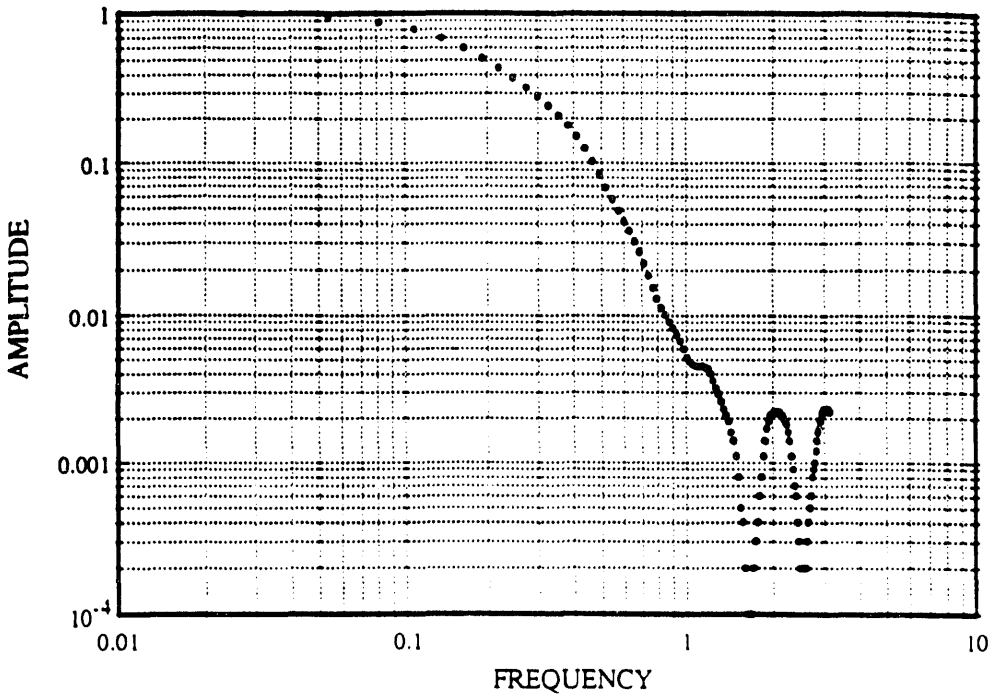

Fig. 10a Transfer Function for the Tritium History.

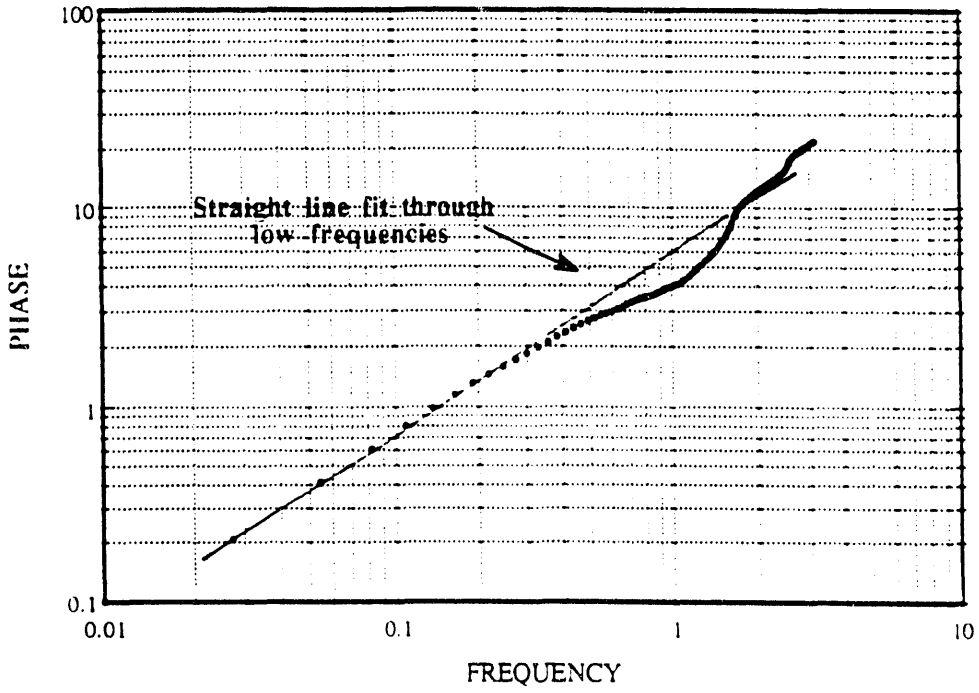

Fig. 10b Phase Spectrum for the Tritium History.

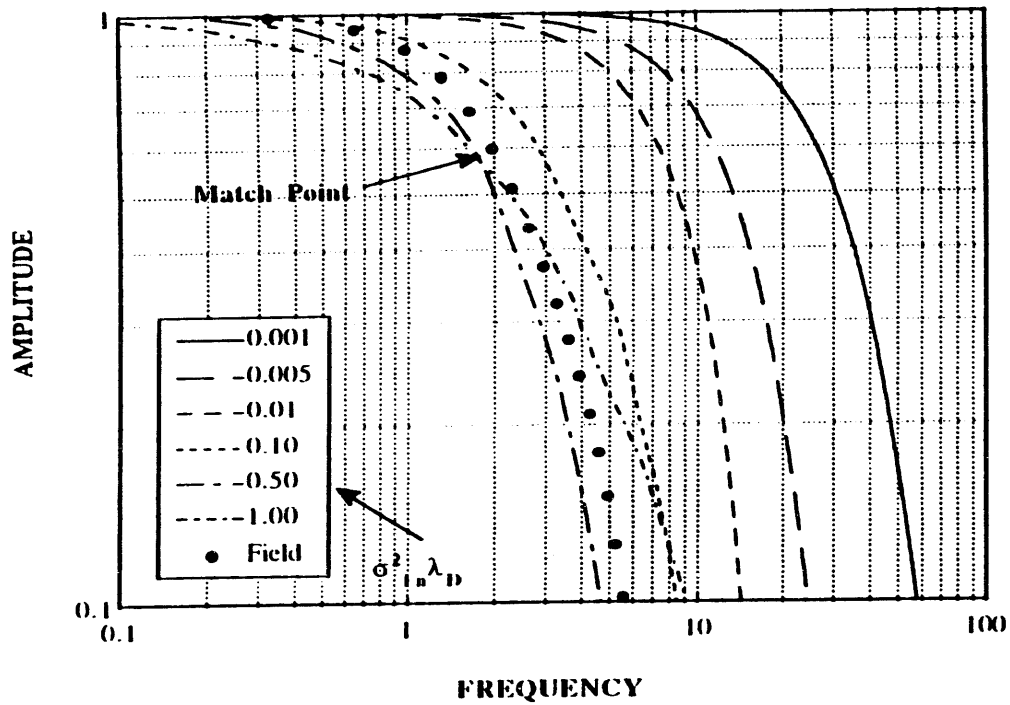

Fig. 11 Matching of Transfer Function.

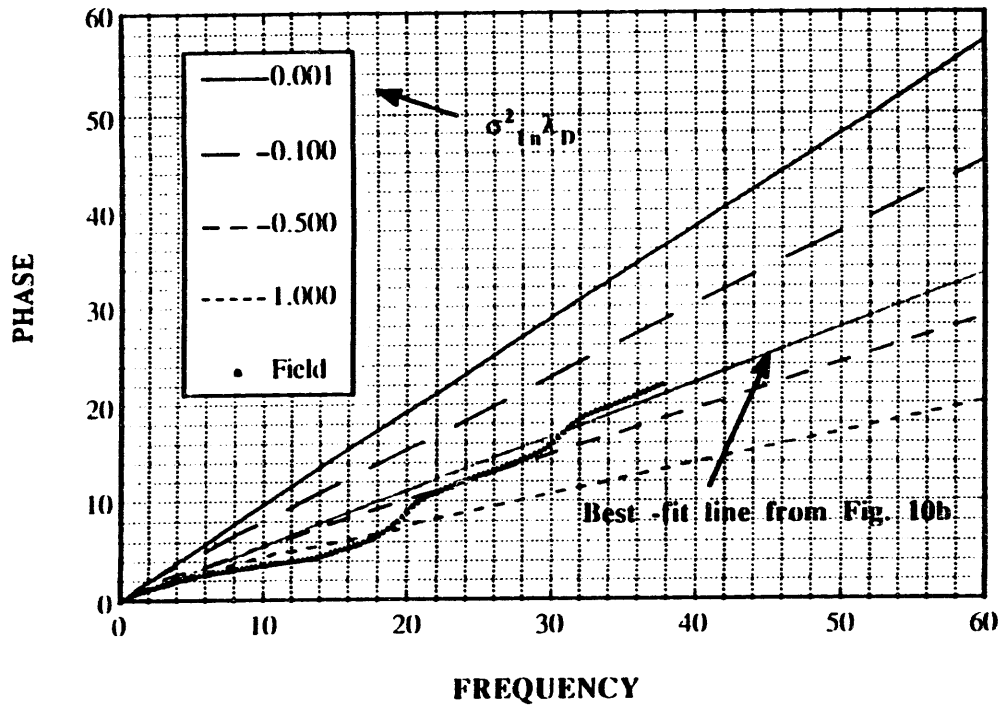

Fig. 12 Matching of Phase Spectrum.

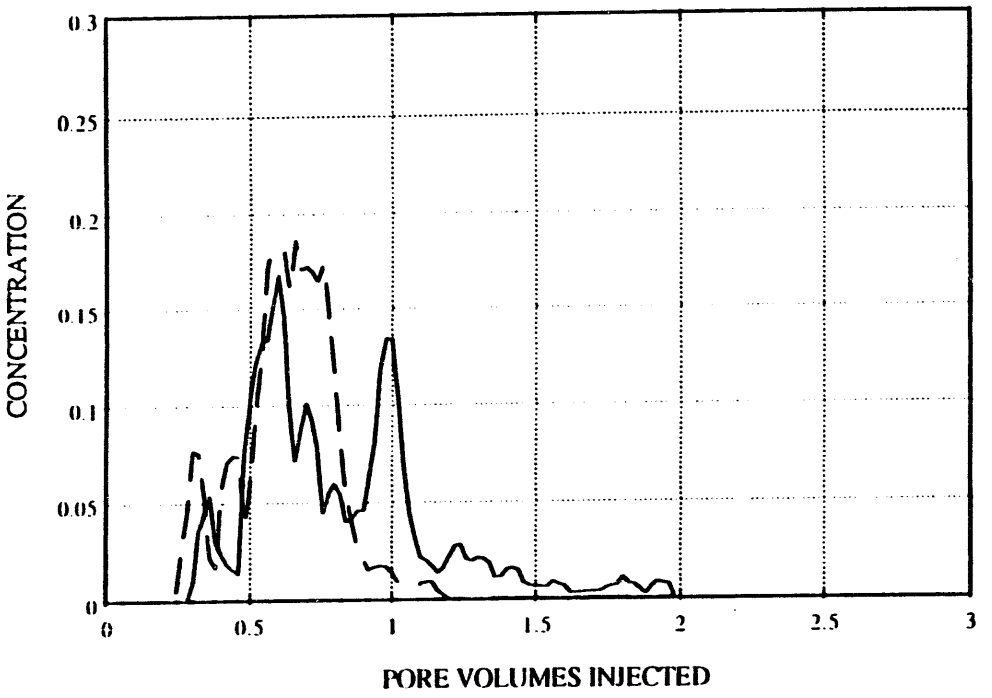

Fig. 13 Tracer Histories for two Realizations of Random Permeability Field.

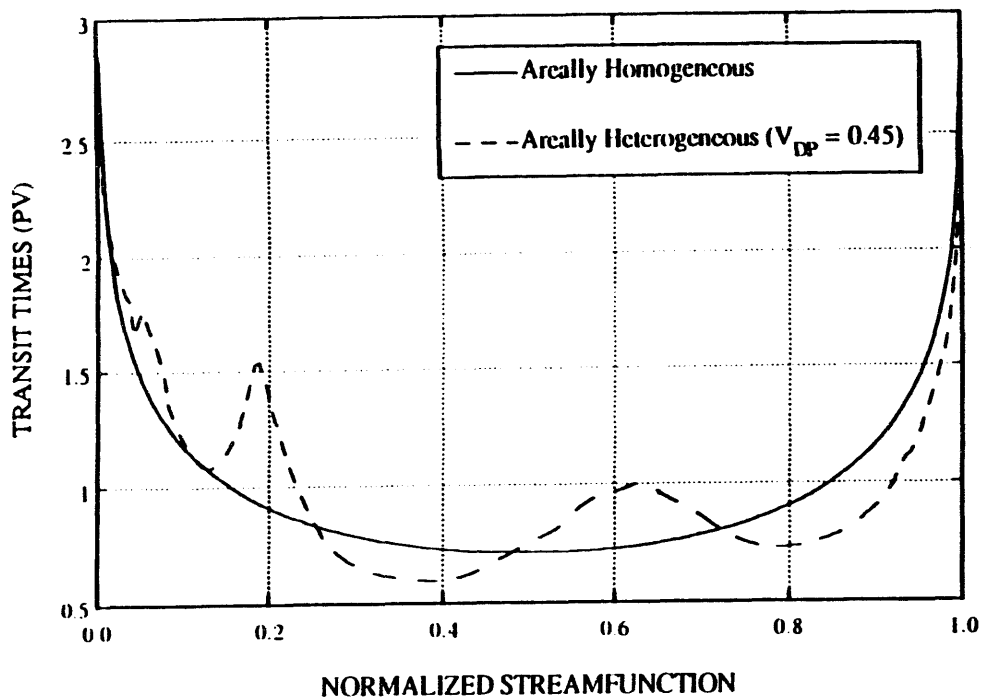

Fig. 14 Transit Time Function for a Quarter Five Spot Pattern.

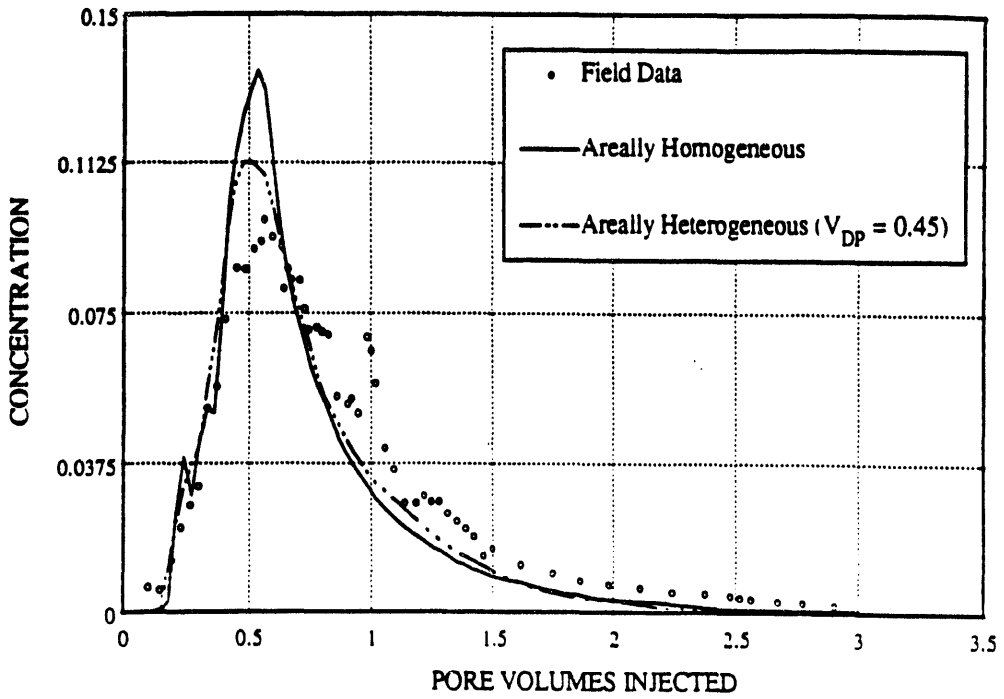

Fig. 15a Prediction of Field Tracer History Based on Estimated Parameters (Realization 1).

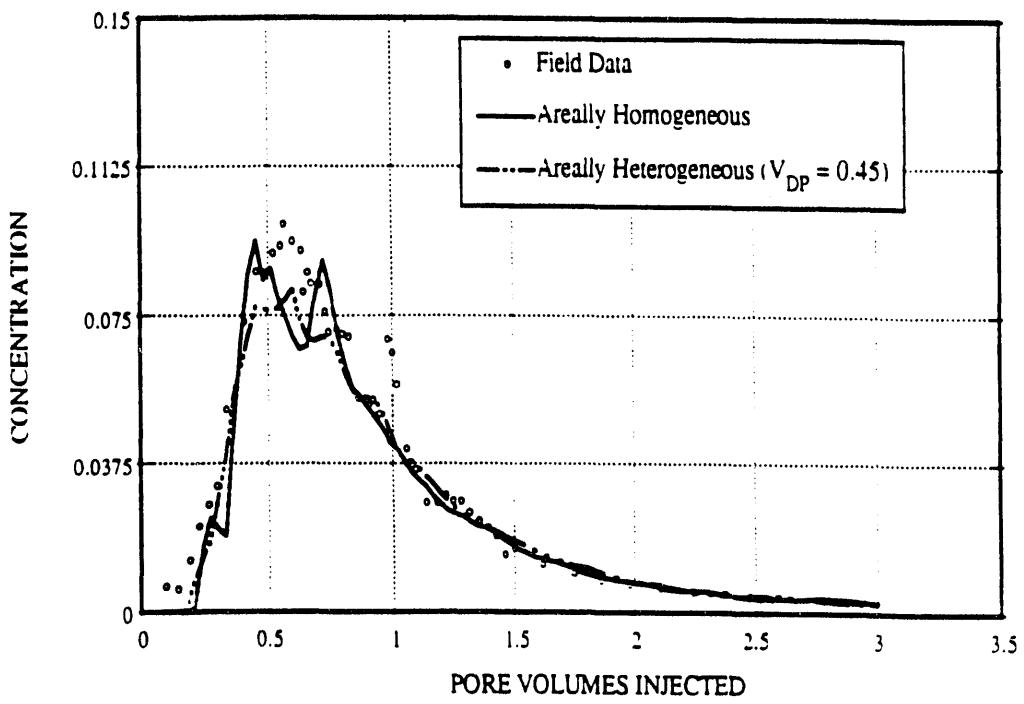

Fig. 15b Prediction of Field Tracer History Based on Estimated Parameters (Realization 2).

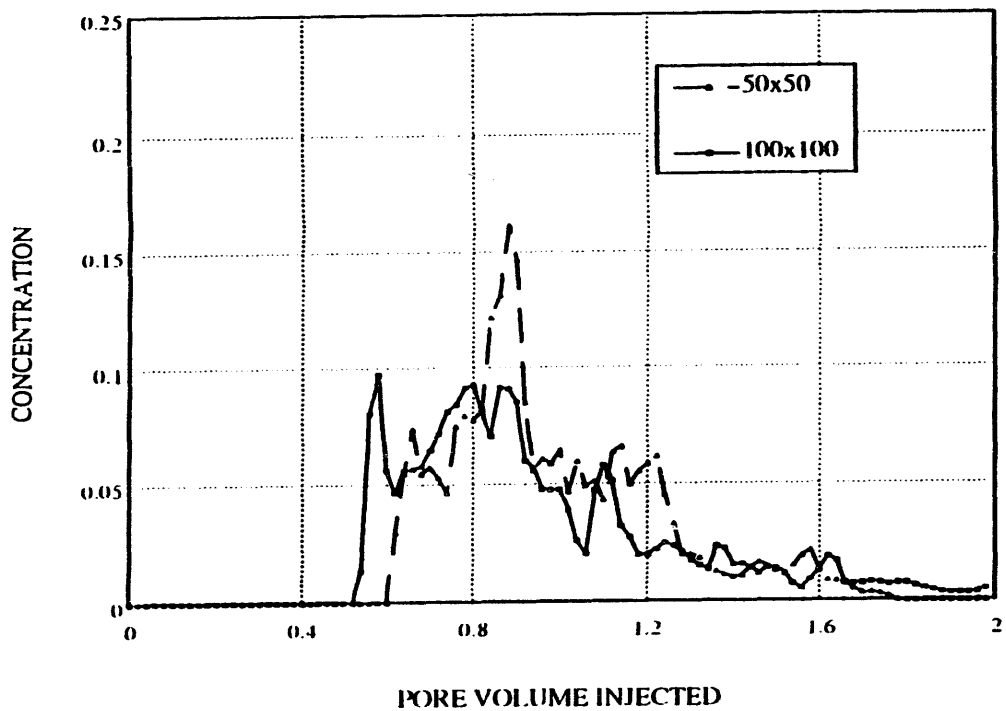

Fig. 16 Concentration Histories for Different System Sizes with Heterogeneity Index of 0.20.

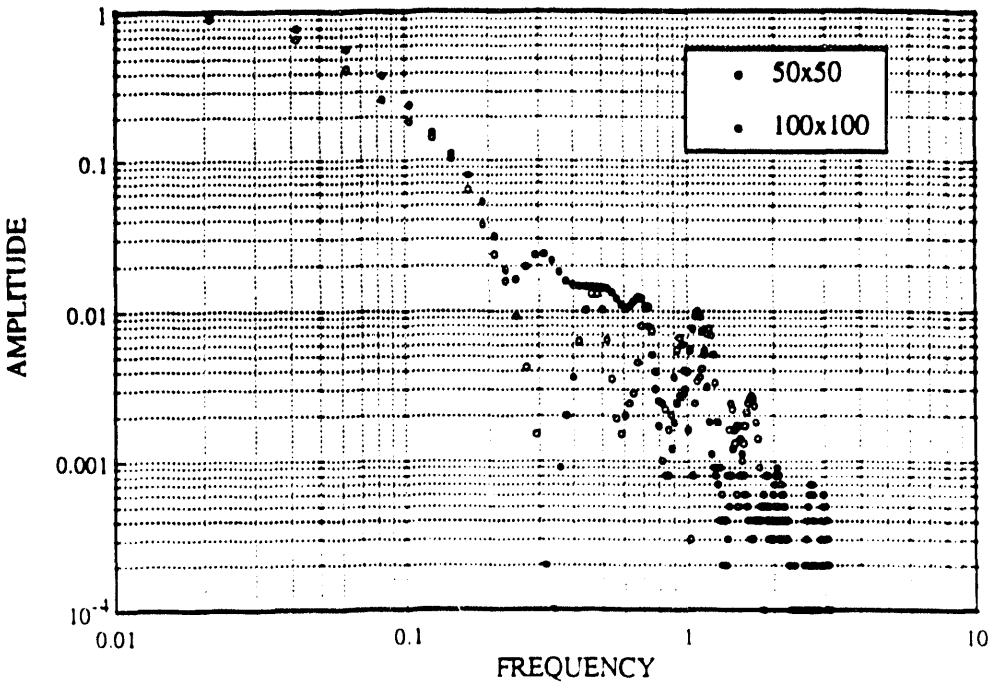

Fig. 17a Transfer Functions for Different System Sizes with Heterogeneity Index of 0.20.

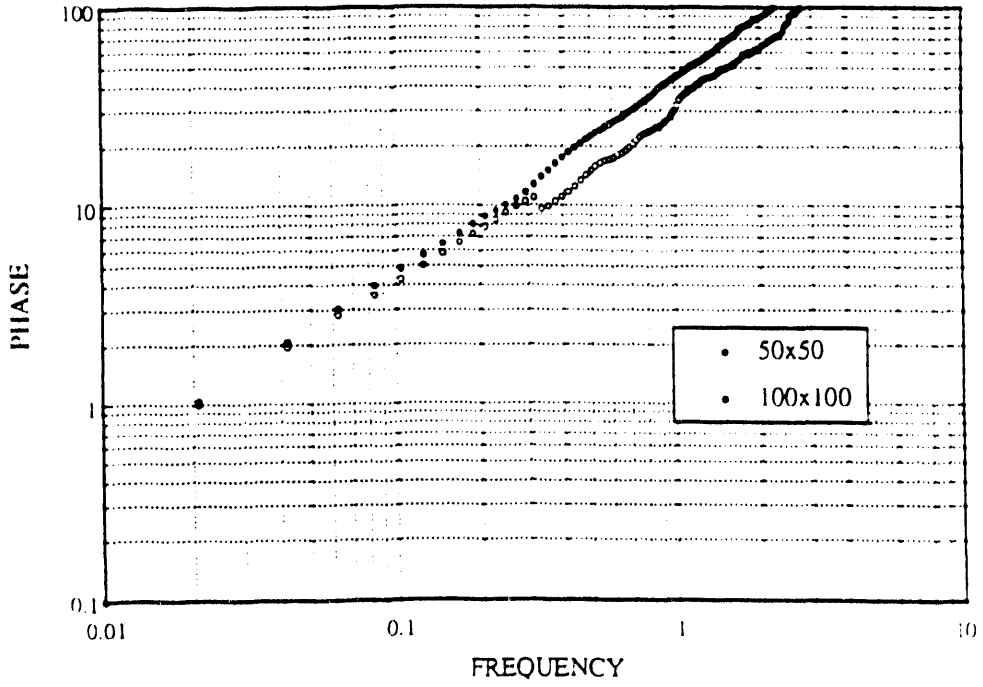

Fig. 17b Phase Spectra for Different System Sizes with Heterogeneity Index of 0.20.

SECTION 3

HETEROGENEITY AND MIXING IN FLOW THROUGH RESERVOIRS

Authors: A. Datta Gupta, L.W. Lake, and G.A. Pope

SUMMARY

The objective of this work is to quantify the channeling and dispersive behavior of tracer flow through heterogeneous permeable media. The growth rate of channels, which constitute the deterministic and long wavelength response, in particular, has been studied as a function of the permeable media properties. We use a simple one-dimensional stochastic model to characterize the transition from channeling to dispersion. Finally, we show that a heuristic model of channeling can represent the tracer response from permeability fields that exhibit long-range correlation.

OBJECTIVE AND APPROACH

Dispersion through heterogeneous permeable media, in general, exhibits a behavior intermediate between a diffusive spreading (dispersive), where the mean square displacement grows as t^1, and a convective spreading (channeling), where the mean square displacement grows as t^2 (Koch and Brady, 1988; Arya *et al.*, 1988). We focus here primarily on the contributions of large-scale fluctuations (channels) induced by long-range permeability correlations and examine their growth as a function of the permeable media properties (Waggoner *et al.*, 1991). We restrict results to unit mobility ratio miscible displacements in the absence of physical dispersion and gravity (tracer flow).

Approach

We first derive a functionality at a producing well that describes the behavior of an ensemble of particles allowed to flow, from a common inlet, through a series of movements as determined by the permeability distribution. The sequence of such movements will result in several continuous paths that have a distribution of lengths, if viewed at a fixed time, or a distribution of arrival times, if viewed at a fixed position. We adopt the latter viewpoint here.

We assume permeability to be a random variable with a lognormal distribution and a known spatial correlation structure. Statistical homogeneity implies that the mean is independent of location and the covariance is a function of lag distance only. Flow takes place between fully open injectors and producers in a two-dimensional cross-section.

For single phase steady flow in a non-deformable medium, mass continuity requires:

$$\nabla \cdot v = 0 \text{ and } v(x,z) = -k(x,z)/\mu \, \nabla P \tag{1}$$

The velocity field, $v(x,z)$, is obtained numerically. Particle trajectories are then derived using a semianalytic approach (Datta Gupta *et al.*, 1992). With the trajectories known, we compute arrival times $\tau(\psi)$ of the tracer particles at the producer as a function of normalized streamfunction, ψ. The variance of transit times at the producer will be given by

$$\sigma_\tau^2 = 1/N \sum_{i=1}^{N} (\tau(\psi_i) - \langle\tau\rangle)^2 \tag{2}$$

where N is the number of streamlines sampled and $\langle\tau\rangle$ is the mean.

For linear flow in a homogeneous medium the arrival times will be identical for all the streamlines, and hence σ_τ^2 will be identically zero. The variance in Equation (2) contains contributions from all frequencies; however, as we shall see, it can be separated into a long-range or deterministic component (channeling) and a random component (dispersion). One way of accomplishing this is through spectral decomposition whereby σ_τ^2 can be attributed to discrete frequencies.

The power spectrum of the arrival times is given by:

$$G(\omega) = 1/\pi \int_{-\infty}^{\infty} \Phi_{\tau\tau}(s)\, e^{-i\omega s}\, ds \tag{3}$$

where $\Phi_{\tau\tau}$ is the autocovariance of the transit times. Inverting Equation (3) gives

$$\Phi_{\tau\tau}(s) = \int_{-\infty}^{\infty} G(\omega)\, e^{i\omega s}\, d\omega \tag{4}$$

from which it follows that

$$\sigma_\tau^2 = \Phi_{\tau\tau}(0) = \int_{-\infty}^{\infty} G(\omega)\, d\omega\,. \tag{5}$$

Thus, the power spectrum is the variance of the amplitudes of the Fourier components necessary to reconstruct a sample of a given arrival time distribution. We can now focus on the low-frequency Fourier modes that correspond to the large-scale fluctuations or channels.

ANALYSIS AND RESULTS

We have used a spherical variogram for the generation of random permeability fields. This particular choice was based on its flexibility and ability to match measured permeability data (Goggin, 1988). Also, we have assumed an isotropic correlation structure for permeabilities and $k_x = k_z$.

Figure 1 shows the $\tau(\psi)$ function corresponding to a Dykstra-Parsons coefficient (Dykstra and Parsons, 1950) $V_{DP} = 0.6$ (or a log-permeability variance, $\sigma_{\ln}^2 = 0.84$) and a dimensionless range $\lambda_D = 0.02$. The range, the distance over which permeabilities are spatially correlated, is made dimensionless by dividing by the injector-producer distance.

At small ranges, arrival times are more or less randomly distributed. On increasing the range ten-fold to $\lambda_D = 0.2$, the transit times now exhibit a distinct correlated pattern, indicating preferential fluid movement or channeling (Fig. 1). Channels are the flat regions in the $\tau(\psi)$ function over which a large change in streamfunction occurs in a short interval of time.

From Channeling to Dispersion

The variance of arrival times at a specific location x for a one-dimensional medium with random velocity fluctuations is given by (Simmons, 1982):

$$\sigma_\tau^2(x) = 2/u^4 \int_0^x (x-y)\, R(y)\, dy \tag{6}$$

where R(y) is the covariance of the velocity field and u is the mean velocity. If we assume an exponential form of the velocity covariance (consistent with a first-order Markov model as discussed later), the following expression can be derived:

$$\omega^2/\varepsilon^2 = 2/\alpha^2[\alpha - (1 - e^{-\alpha})] \tag{7}$$

where $\alpha = x_D/\lambda_D$, ω = coefficient of variation of the transit time and ε = coefficient of variation of the velocity field.

In Equation (7) the long-range case is characterized by $\omega = \varepsilon$ i.e. a constant ω or an invariant velocity statistics with respect to x (Simmons, 1982). This condition is satisfied by a layer-cake reservoir description with log-normal permeability distributions (Dykstra and Parsons, 1950). Figure 2 shows the transition from a strictly layered to a strictly dispersive system as a function of α. At the producer $x_D = 1$ and the medium is strictly layered for $\lambda_D > 10$ and strictly dispersive for $\lambda_D < 0.1$. We have superimposed some of our semianalytic results on the same figure.

If the covariance of the velocity field is represented by a power-law expression i.e. $R(y) \sim 1/y^\beta$, Equation (6) gives $\sigma_\tau^2 \sim x^{2-\beta}$ and we obtain anomalous diffusion in the range $0 < \beta < 1$, as observed by Koch and Brady (1988) and Glimm *et al.* (1990).

In general, all displacements have some character of both dispersion and channeling, and in the following section we attempt to separate the two.

Separating Channeling from Dispersion

The variance of the arrival times at the producer is the overall response of the heterogeneous medium. If we postulate that σ_τ^2 at the producer is caused by both dispersion and channeling, the latter will constitute the deterministic component of the total variance. Thus, we can quantify the extent of channeling if we can isolate the deterministic component of σ_τ^2.

Figure 3 shows the variance spectrum of the transit times corresponding to three different λ_D's. The spectrum gives the distribution of variance over different frequency components. For a completely uncorrelated medium, the spectrum will be flat, indicating that σ_τ^2 is evenly distributed

across all frequencies. However, with increased correlation, more variance is concentrated toward low frequencies, leading to large-scale fluctuations or channeling. This behavior of the variance spectrum is typical of a first-order Markov process for which the stochastic component of the variance (σ_ε^2) is related to σ_τ^2 as follows (Priestley, 1981):

$$\sigma_\varepsilon^2/\sigma_\tau^2 = 1 - \rho^2 \tag{8}$$

In the above expression, ρ is lag-one autocorrelation of transit times that is obtained by fitting the transit time spectrum to the spectrum of a first-order Markov model (Priestley, 1981). Figure 4 shows a sample fit of the transit time spectrum. The fit is quite good, especially at the important low frequencies.

We can now quantify channeling by isolating the deterministic component of σ_τ^2. Figure 5 shows the results ($1 - \sigma_\varepsilon^2/\sigma_\tau^2$) for various V_{DP} and λ_D. Even when correlation in the permeability field is small ($\lambda_D = 0.1$), a significant portion of the flow is dominated by channels.

Comparison with a Heuristic Model

For small λ_D, the permeable medium acts like a diffusive system that causes a Gaussian distribution of arrival times at a producer. With increased correlation, channeling becomes predominant and the tracer particles do not undergo enough random steps to exhibit Fickian behavior. The arrival time distribution at the producer now appears as a truncated Gaussian distribution.

While it is possible to separate channeling from dispersion, there is no heuristic model available that can make use of this. We will use a heuristic model proposed by Koval (1963) to reproduce σ_τ^2 in the following; however, since the Koval model was originally intended to model channeling (or viscous fingering), we should expect some scale dependence of the heterogeneity parameter H_k, as discussed below, when the flow is in the dispersive regime.

The Koval model incorporates the effects of channeling through a modification of the transport term in the conservation equation,

$$\frac{\partial c}{\partial t_D} = -\frac{\partial F}{\partial x_D} \tag{9a}$$

where

$$F = H_k c/(1 + c(H_k - 1)) \tag{9b}$$

In Equation 9b, H_k is an empirical factor, called the Koval heterogeneity factor. For a unit mobility ratio miscible displacement in a heterogeneous medium, $H_k = 1/t_{Dbt}$ where t_{Dbt} is the dimensionless breakthrough time.

Figure 6 compares the Koval model with our semianalytic computations for a $\lambda_D = 0.3$. The agreement is good over a large range of permeability variance. The steep section of the plot, which characterizes the arrival of "fast" particles travelling along preferential channels, is modeled particularly well by the Koval model. Finally, as shown in Fig. 7, the heterogeneity factor, H_k, appears to correlate well with a dimensionless heterogeneity index, $\sigma_{\ln}^2\lambda_D$ as defined by Gelhar and

Axness (1983).

SUMMARY AND CONCLUSIONS

Channeling is reflected by 'persistence' in the transit time function $\tau(\psi)$. The variance spectrum of transit times behaves like a first-order Markov process that allows us to quantify channeling by isolating the deterministic and the stochastic components of the transit time variance. A simple one-dimensional stochastic model has been used to characterize the transition from channeling to diffusion in systems with finite correlation lengths. Finally, we show that a heuristic model (Koval) of channeling effectively reproduces the truncated Gaussian behavior exhibited by arrival time distribution in the presence of long-range correlation of permeabilities.

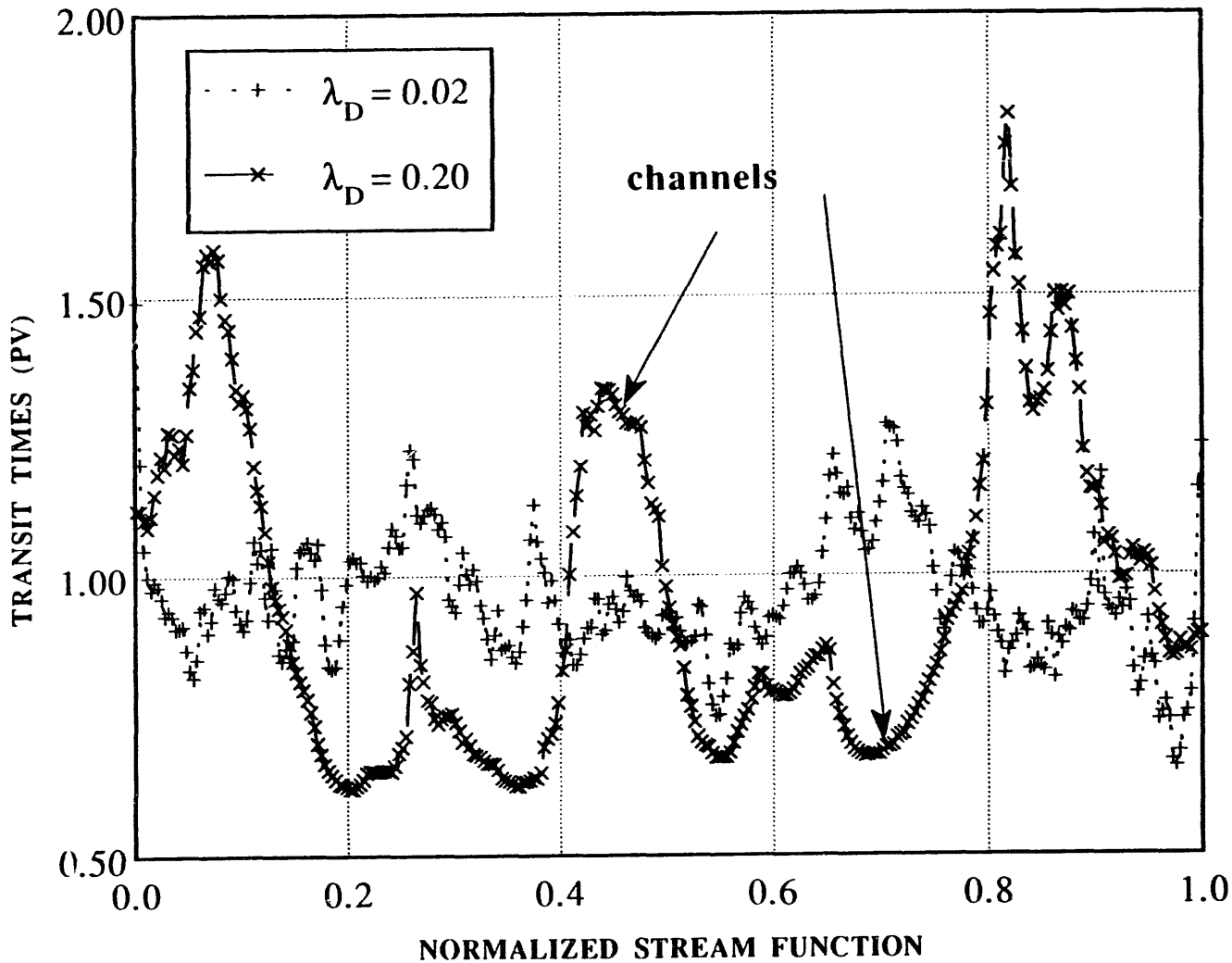

Fig. 1. Transit time function for two dimensionless ranges of permeabilities (V_{DP} = 0.6).

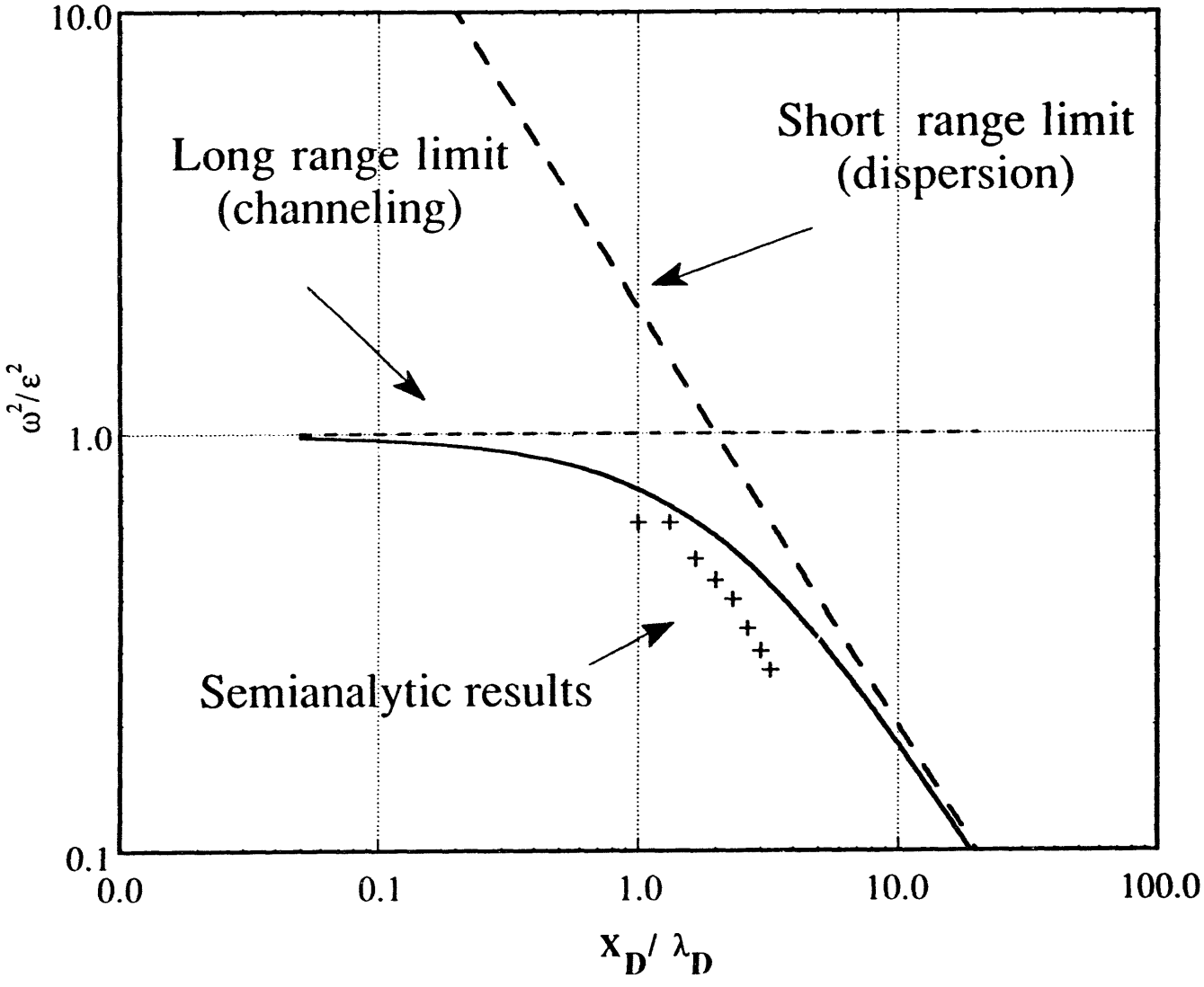

Fig. 2. Transition from channeling to dispersion.

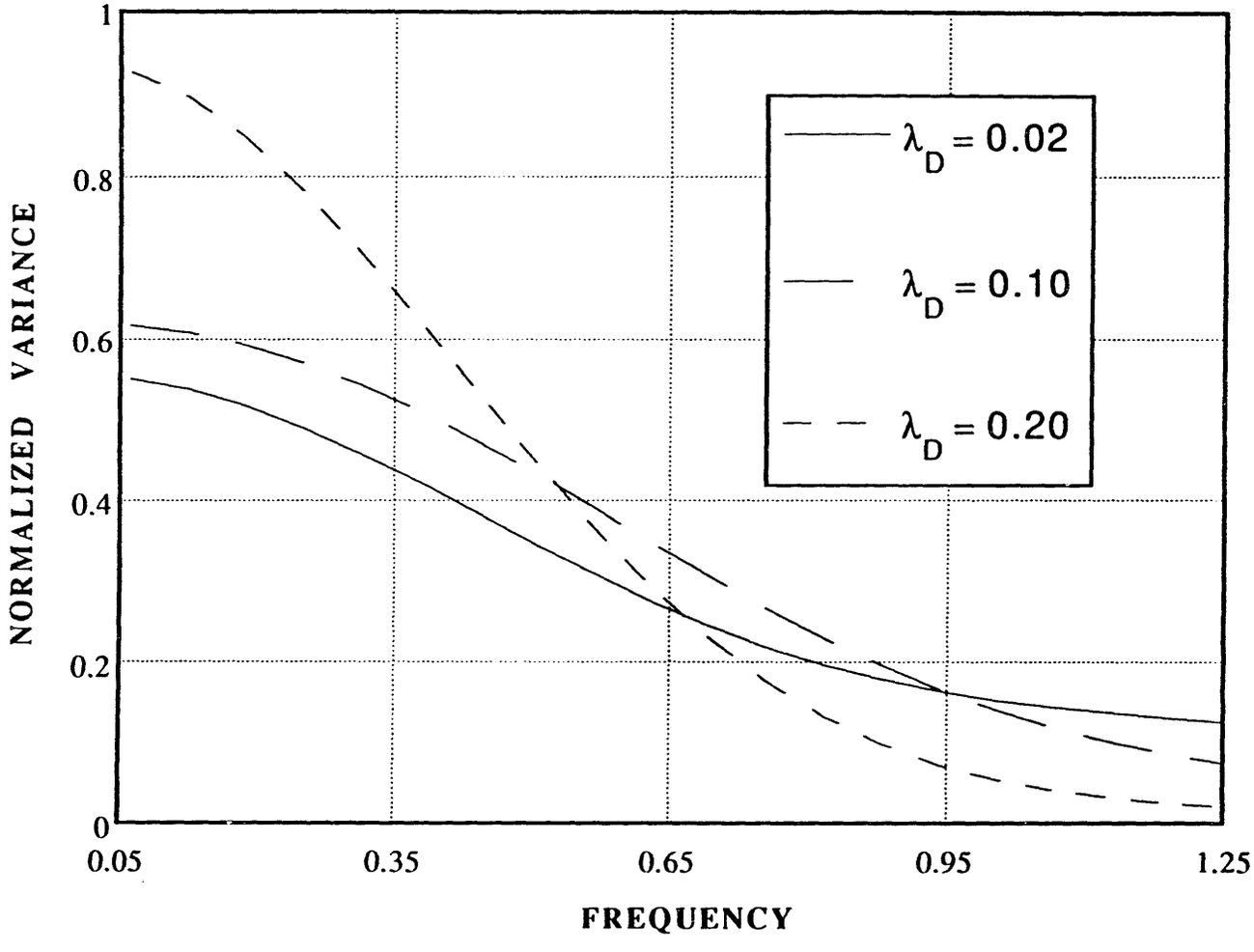

Fig. 3. Transit time spectra for different dimensionless ranges (V_{DP} = 0.6). Parzen window used for discrete data.

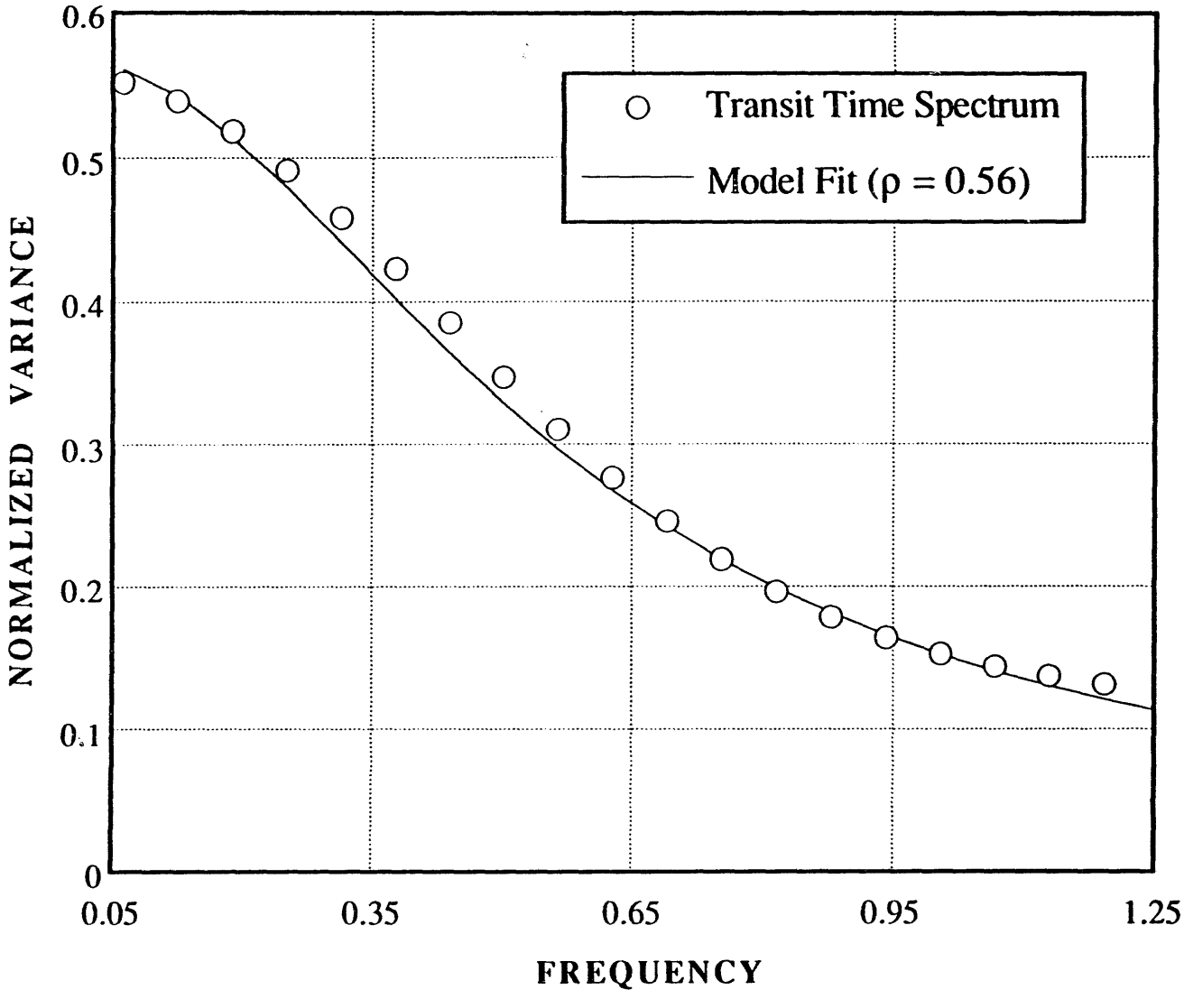

Fig. 4. Example fit of transit time spectrum to a first-order Markov model.

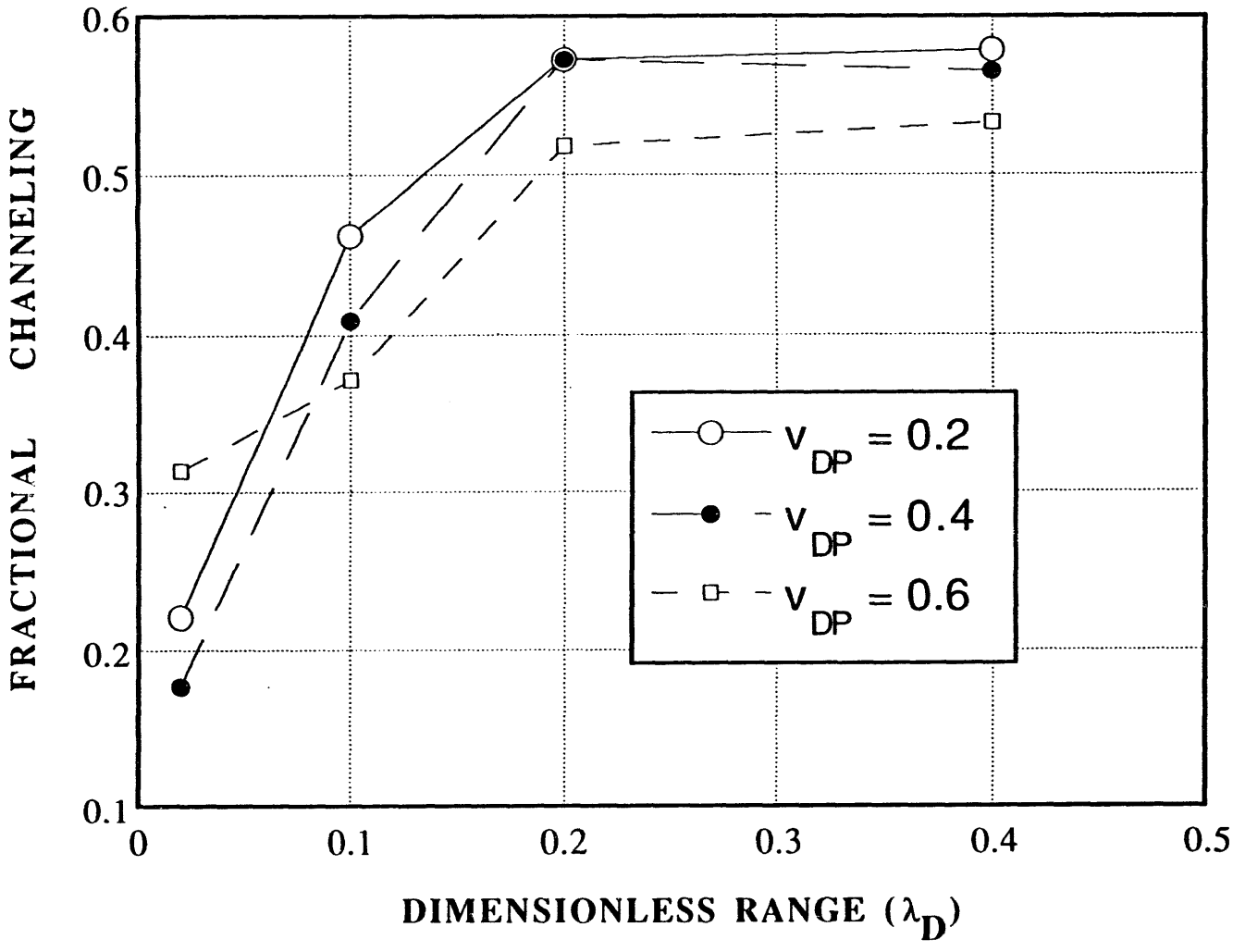

Fig. 5. Fractional channeling vs. dimensionless range.

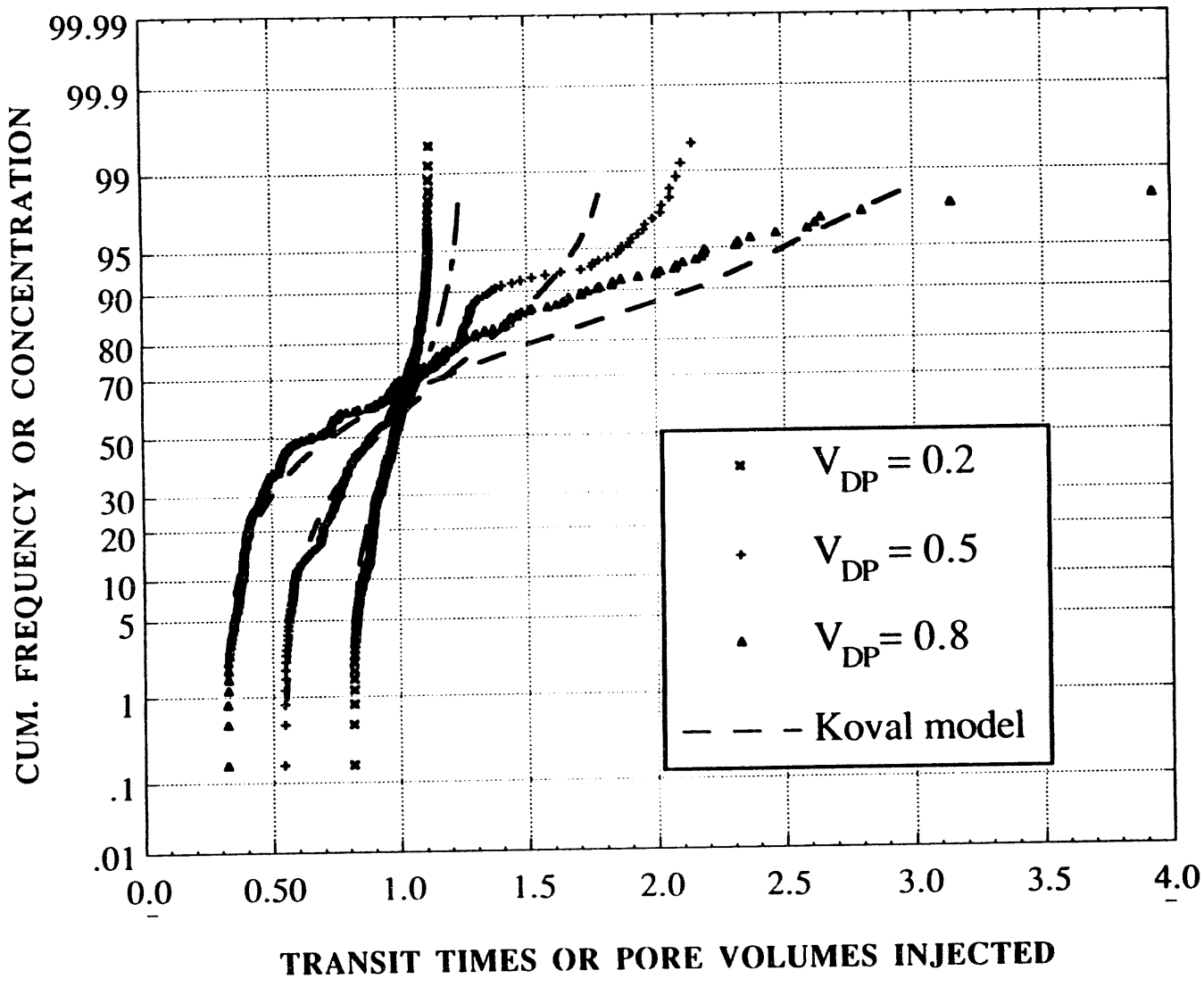

Fig. 6. Semianalytic computation vs. the Koval model for $\lambda_D = 0.30$ and various V_{DP}.

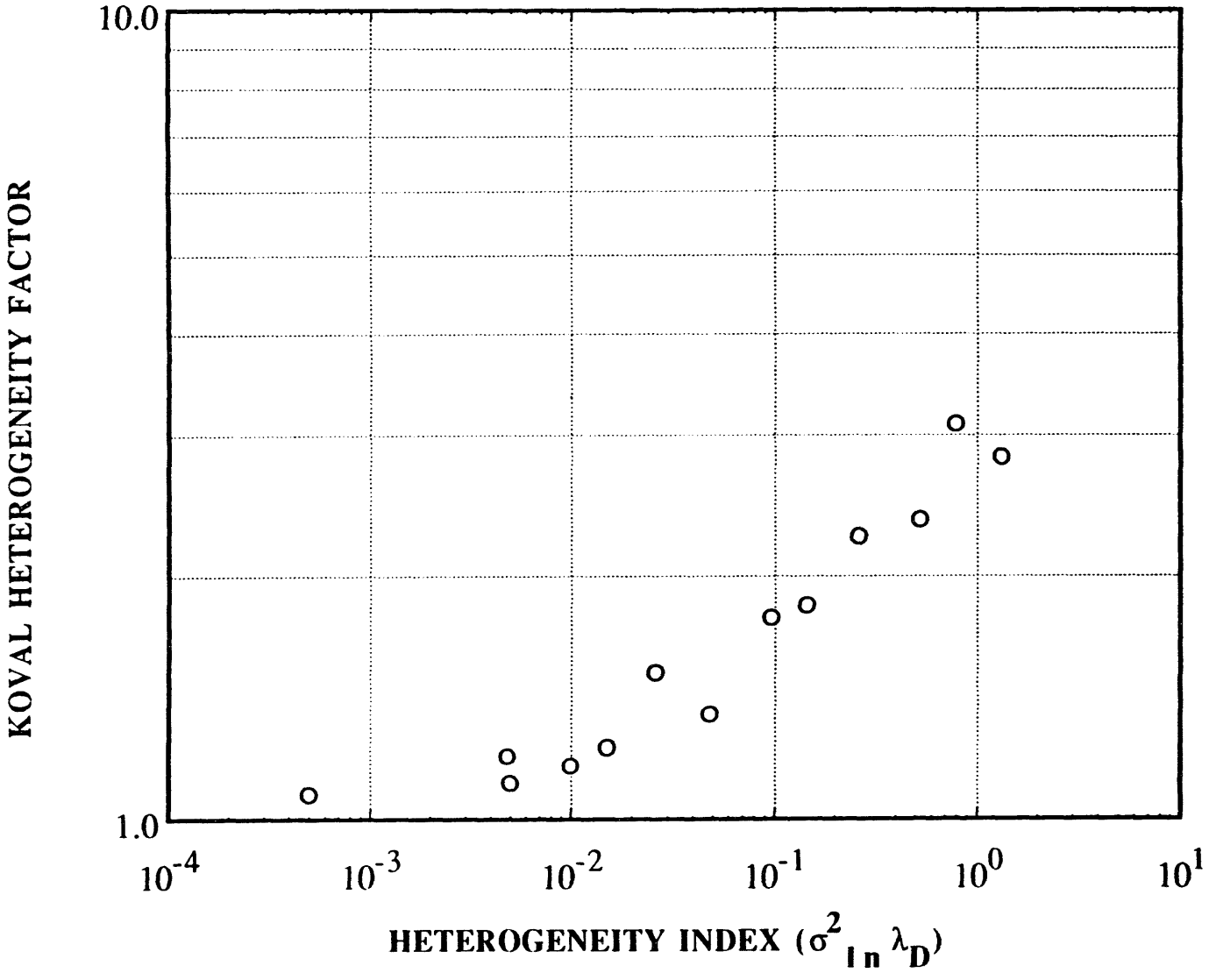

Fig. 7. Koval Heterogeneity Factor (H_k) vs. $\sigma^2_{\ln \lambda_D}$.

SECTION 4

SIMULATION OF TRACER FLOW UNDER FIELD CONDITIONS

Authors: V. Maroongroge, G.A. Pope, and K. Sepehrnoori

SUMMARY

The reservoir under study is the 26R reservoir, which is one of the reservoirs at the Elk Hills Naval Petroleum Reserve No. 1. The 26R reservoir is a northwest-southeast trending elongated Stevens sandstone reservoir. Figure 1 shows a map of the 26R reservoir along with other Stevens zone reservoirs in the Elk Hills field. Figure 2 shows more details of the 26R reservoir and the test wells for this project from Program Proposal 26R Reservoir Tracer Testing Project (September 12, 1991). This reservoir has been under a gas injection pressure maintenance program since 1978. When the gas injection program started, pressure communication was observed at the injector (Well No.366U-26R) and producers in another reservoir (Western 31S reservoir) located across the northeast boundary of the 26R reservoir. A tracer test is being conducted in the field with the newly developed perfluorocarbon tracers to investigate fluid communication between layers inside the 26R reservoir and to test the possibility of fluid communication with other surrounding reservoirs. The tracer test program consists of five stages and different PFT's will be used at different stages. Another proven gas tracer (SF_6) will be injected together with the PFT's. The following lists the objectives of each stage and explains how the test will be carried out. The planned tracer test project is supplied to us by Brookhaven National Laboratory (Senum, 1991).

Stage No.1: Injecting tracer No.1 into Well No.366U-26R, which intersects the fault, to determine fluid communication along the fault and across the northeast boundary of the 26R reservoir. This stage started in mid-December 1991.

Stage No.2: Injecting tracer No.2 into Well No.364-26R on the west side of the fault to determine fluid communication between layers on the west side of the fault within the 26R reservoir.

Stage No.3: Injecting tracer No.3 into all the injectors located on the west side of the fault to determine fluid communication across the fault.

Stage No.4: Injecting tracer No.4 into Well No.328-25R on the east side of the fault to determine fluid communication between layers on the east side of the fault.

Stage No.5: Injecting tracer No.5 into all the injectors located on the east side of the fault to determine fluid communication across the fault.

The following are the preliminary results to illustrate the impact of partitioning between the gas and oil and dispersive mixing in the reservoir on the breakthrough times and peak produced concentrations of the perfluorocarbon tracers at the 26R reservoir conditions.

RESULTS

Simulations of perfluorocarbon tracers (PFT's) under the conditions of the 26R reservoir at Elk Hills Naval Petroleum Reserve No. 1 were conducted using the fluid description from Well No.378A-26R. The hydrocarbon components were lumped into seven pseudocomponents using an expert system for UTCOMP developed at The University of Texas by Khan (1991). The mole fraction of methane was adjusted to give an oil saturation of 25% and a gas saturation of 45% at 2,400 psia and 200°F. The initial water saturation was taken as constant at 30%. Because gas injection has been occurring at the crest of the 26R reservoir for some time, single-phase flow of gas was assumed. Average reservoir properties were taken from the 26R simulation report by Scientific Software-Intercomp (SSI) (Rial, 1990).

A total of seven different tracers were simulated. The first tracer is a hypothetical tracer with a zero partition coefficient. The partition coefficients for the PFT's were obtained from experimental data except for SF_6, which was obtained from the Peng-Robinson equation of state since no data were available for it. We simulated the tracer flow in this reservoir using two simple reservoir descriptions, a 2D vertical cross section and a 2D areal. The permeabilities of the 2D vertical cross-sectional model of the reservoir with 17 different layers were based on the SSI report. Table 1 shows reservoir and fluid descriptions used for the 2D vertical cross-sectional simulation. Results of this simulation are shown in Fig. 3. The breakthrough times are as early as 100 days, although the initial produced tracer concentrations at these breakthrough times are possibly below the detection limit. The peak arrival times range from 300 to 400 days.

Next we simulated a 2D areal model that takes into account the following: areal sweep, the position of tracer injection well and observation wells, dilution from other injectors, and the injection and production rates. Using production rates from the observation wells and a steady-state streamline model, each injector was assigned rate by counting the number of streamlines from the producer back to the injector. Using this procedure, an accurate injection rate of an injector relative to others was important. Lacking field data, an equal injection rate was assumed for all injectors. Table 2 shows reservoir and well data for the 2D areal simulation. The same fluid description was used for both 2D vertical cross-sectional and 2D areal simulations.

Figure 4 shows the streamlines and the area to be simulated inside a rectangle. The assumptions are that the boundary between the W31S and the 26R reservoirs is open and there is no fault within the 26R reservoir. Figures 5 to 13 show the simulated produced tracer concentrations at the observation wells located around the tracer injection well. The earliest breakthrough time is about 600 days. The actual breakthrough time may be earlier than the simulated one for the following reasons. First, the tracer injection well (Well No.366U) is located at the crest of the structure, and we use the whole perforation interval of this well as the thickness of the reservoir, since the depth to the gas-oil contact is not available. If the thickness of the gas cap is smaller than 300 ft, the injected gas will rise to the top because of gravity and will sweep only a small portion of the whole thickness. The breakthrough time will be earlier and the produced tracer concentration will be higher. Second, heterogeneities such as preferential flow paths or channels are not included.

From Figs. 5 to 13, one can see that the highest produced tracer concentration is at Well No.386A. The dilution factor at this well is about 5000 times lower than the injected value. This mean that the injected tracer concentration should be on the order of 10^6 or 10^7 picoliter/liter of injected gas. Although the boundary is open, most of the wells located in the W31S reservoir show a small amount of tracer produced because of dilution by other injectors. Assuming that tracer injection concentration is 10^6 picoliter/liter of injected gas and the minimum detectable limit is 10^{-15} liter/liter, these wells will show only small amounts of tracers. A careful interpretation of the

field results and more data are needed for the description of this complicated reservoir.

CONCLUSIONS AND FUTURE WORK

A tracer option has been added to UTCOMP that includes tracer dispersion, partitioning, radioactive decay, adsorption, and capacitance. The tracer option in UTCOMP has been validated and used to study the flow of different types of gas tracers in slim-tube experiments and in a preliminary study of a field tracer test. Both 2D vertical cross-sectional and a 2D areal simulations have been done as part of this preliminary study. The next step will be to combine these to get a 3D result. Both more data and more modeling will be required to yield a quantitative interpretation of this tracer project in this complicated reservoir. The newly implemented tracer option in UTCOMP will allow future work in this area.

Table 1. Reservoir and Fluid Descriptions for 2D Vertical Cross-Sectional Simulation of Tracer Flow at Conditions of 26R Reservoir

<u>Reservoir Data</u>	
Dimensions (ft)	
Length	500
Width	300
Thickness	500
NX x NY x NZ	50 x 1 x 17
Porosity (fraction)	0.20
Residual Oil Saturation (fraction)	0.35
Reservoir Temperature (^{o}F)	200
Initial Reservoir Pressure (psia)	2400
Longitudinal Dispersivity (ft)	25
Transverse Dispersivity (ft)	2.5

Table 1. Reservoir and Fluid Descriptions for 2D Vertical Cross-Sectional Simulation of Tracer Flow at Conditions of 26R Reservoir (Cont'd)

Layer	Thickness (ft)	Horizontal Permeability (md)	Vertical Permeability (md)	Water Saturation (fraction)	Gas Saturation (fraction)
1.A	29.41	166	16.6	0.27	0.47
2.B	29.41	136	13.6	0.18	0.53
3.B1	29.41	176	17.6	0.16	0.54
4.D	29.41	255	25.5	0.16	0.54
5.E1	29.41	382	38.2	0.15	0.55
6.E2	29.41	512	51.2	0.19	0.52
7.E3-E4	29.41	466	46.6	0.22	0.50
8.F	29.41	405	40.5	0.09	0.58
9.H	29.41	120	12.0	0.13	0.56
10.I	29.41	165	16.5	0.15	0.55
11.J	29.41	51	5.1	0.11	0.57
12.K	29.41	87	8.7	0.22	0.50
13.L	29.41	196	19.6	0.08	0.59
14.M	29.41	126	12.6	0.12	0.56
15.N	29.41	134	13.4	0.21	0.51
16.O	29.41	24	2.4	0.19	0.52
17.P	29.41	4	0.4	0.26	0.47

Well Data

Injection Rate (MSCF/D)	2164
Tracer Injection Interval (days)	0.04167
Total Number of Tracers Used	7

Table 1. Reservoir and Fluid Descriptions for 2D Vertical Cross-Sectional Simulation of Tracer Flow at Conditions of 26R Reservoir (Cont'd)

Fluid Descriptions

Initial Hydrocarbon Composition (mole fraction)

CO_2	0.002226
C1	0.7228
C2-3	0.055944
C4-6	0.045402
C7-13	0.09849
C14-23	0.052458
C24+	0.02268

Component Critical Properties

Component	P_{ci} (psia)	T_{ci} (°R)	V_{ci} (cu ft/lb-mole)	ω_i	Wt_i (lbm/lb-mole)	Parachor
CO_2	1069.87	547.56	1.506	0.2250	44.01	49.00
C1	667.20	343.08	1.586	0.008	16.04	71.00
C2-3	655.26	616.19	2.876	0.1290	36.78	133.94
C4-6	488.65	835.81	4.979	0.2417	70.15	230.85
C7-13	333.91	1057.62	8.668	0.5782	129.38	368.15
C14-23	251.11	1287.40	15.531	0.8660	241.50	675.64
C24+	240.42	1599.33	28.562	1.2116	441.28	989.33

Table 2. Reservoir and Well Data for 2D Areal Simulation of Tracer Flow at Conditions of 26R Reservoir

Area (ft x ft)	4660 x 3600
Thickness (ft)	300
NX x NY x NZ	22 x 17 x 1
Porosity (fraction)	0.20
Permeability (md)	100
Constant Water Saturation (fraction)	0.30
Initial Gas Saturation (fraction)	0.45
Oil Saturation (fraction)	0.25
Residual Oil Saturation (fraction)	0.3
Reservoir Temperature (^{o}F)	200
Initial Reservoir Pressure (psia)	2400
Longitudinal Dispersivity (ft)	100
Tracer Injection Interval (days)	1
Number of Injectors	5
Number of Producers	9
Well Number	Rate(lb-moles/day)
366U-26R	9819
356-26R	17822
377-26R	7647
344A-26R	4645
388-26R	12997
347-26R	-8015
378A-26R	-5475
336-26R	-14453
363-26R	-5475
362-26R	-3053
382-26R	-2908
384-26R	-1561
386A-26R	-6515
358-26R	-5475

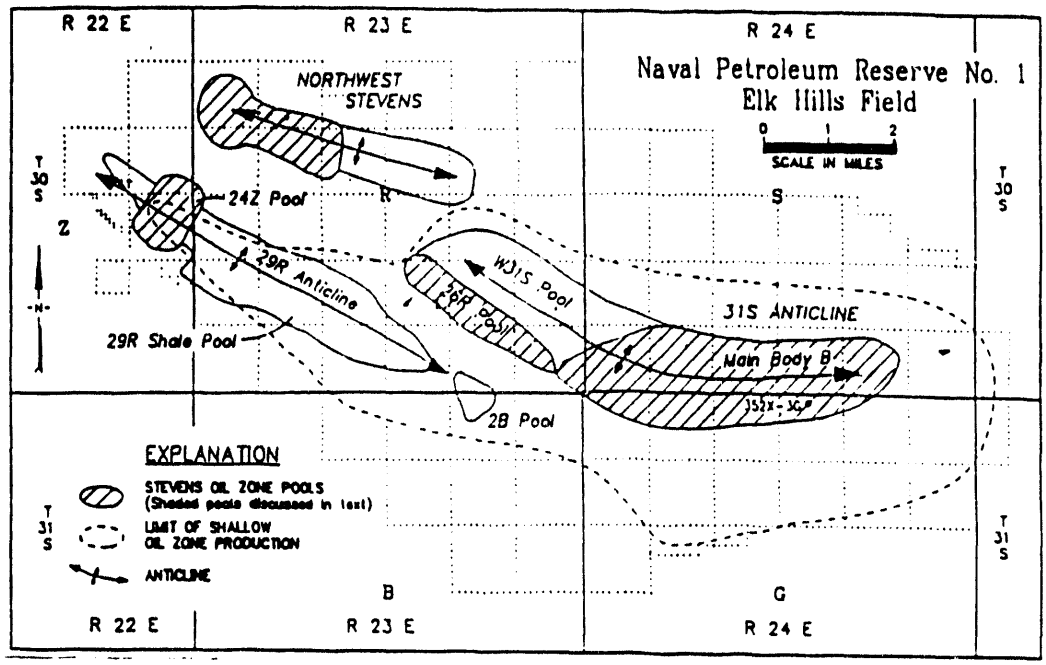

Fig. 1 Map of the Naval Petroleum Reserve No. 1 and the Elk Hills Field showing the distribution of shallow oil zone production and Stevens Zone reservoir (Ezekwe *et al.*, 1991).

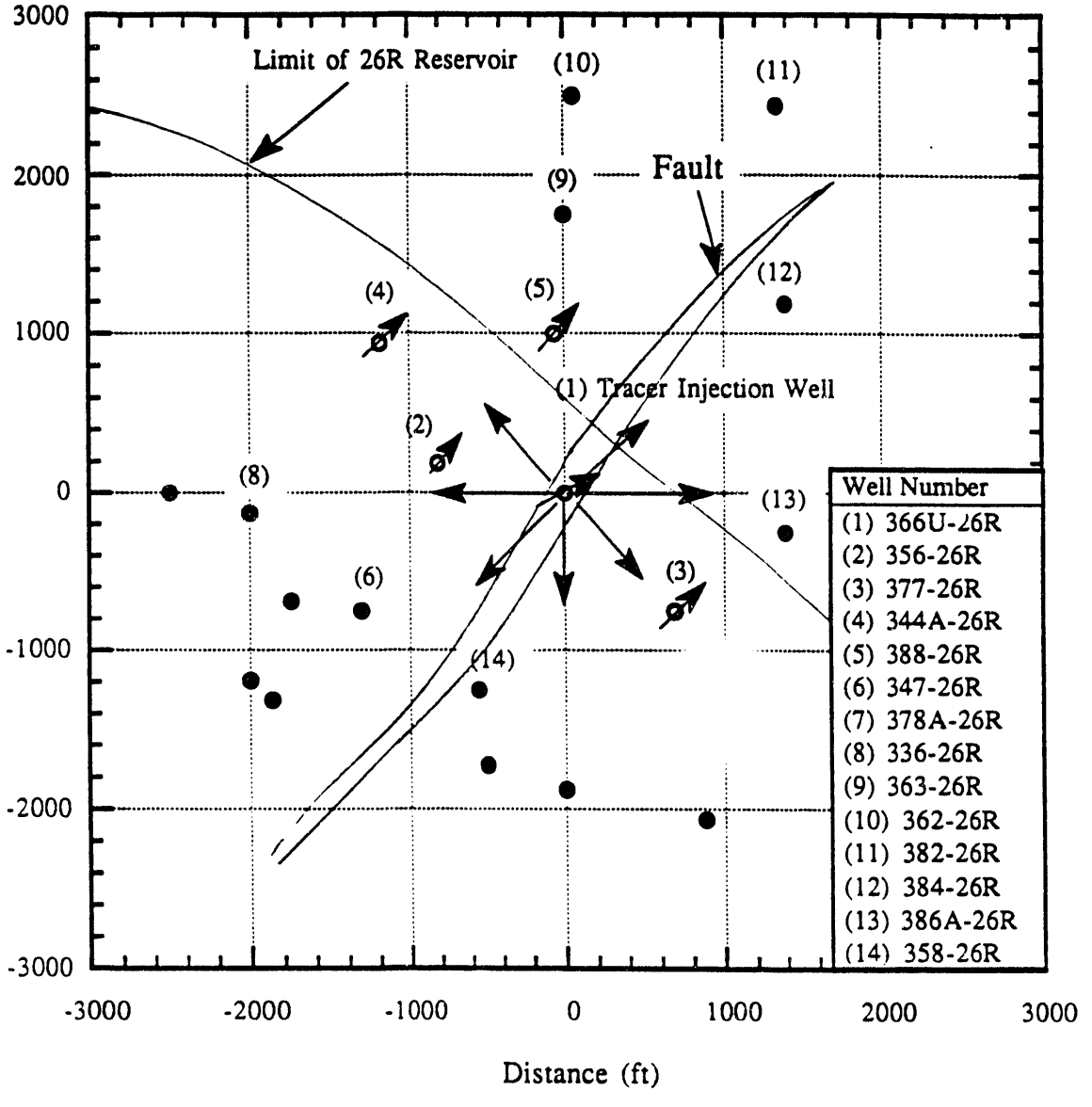

Fig. 2 Map of 26R tracer test project showing well locations.

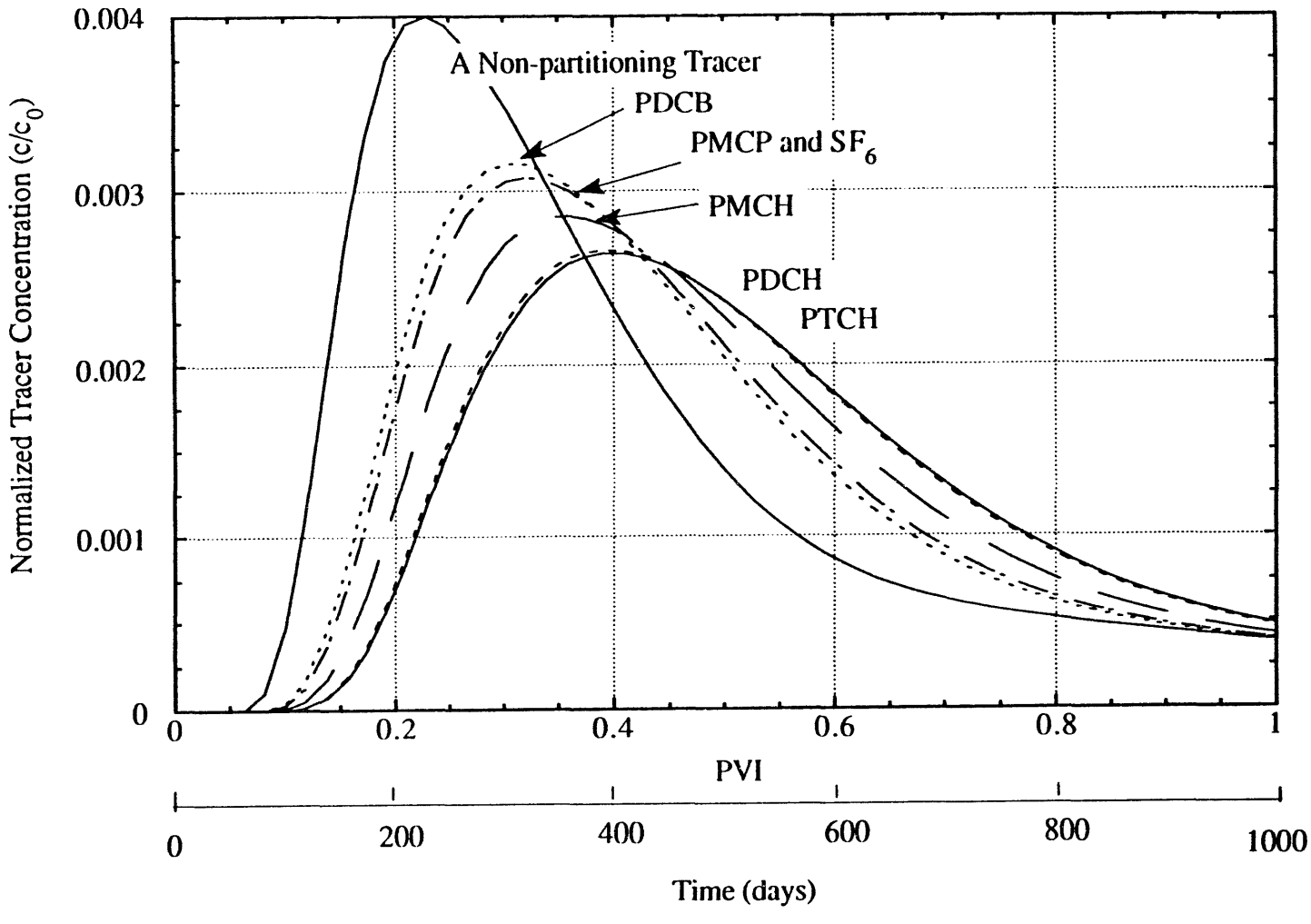

Fig. 3 Simulated tracer concentrations for 26R reservoir 2-D vertical cross-sectional model.

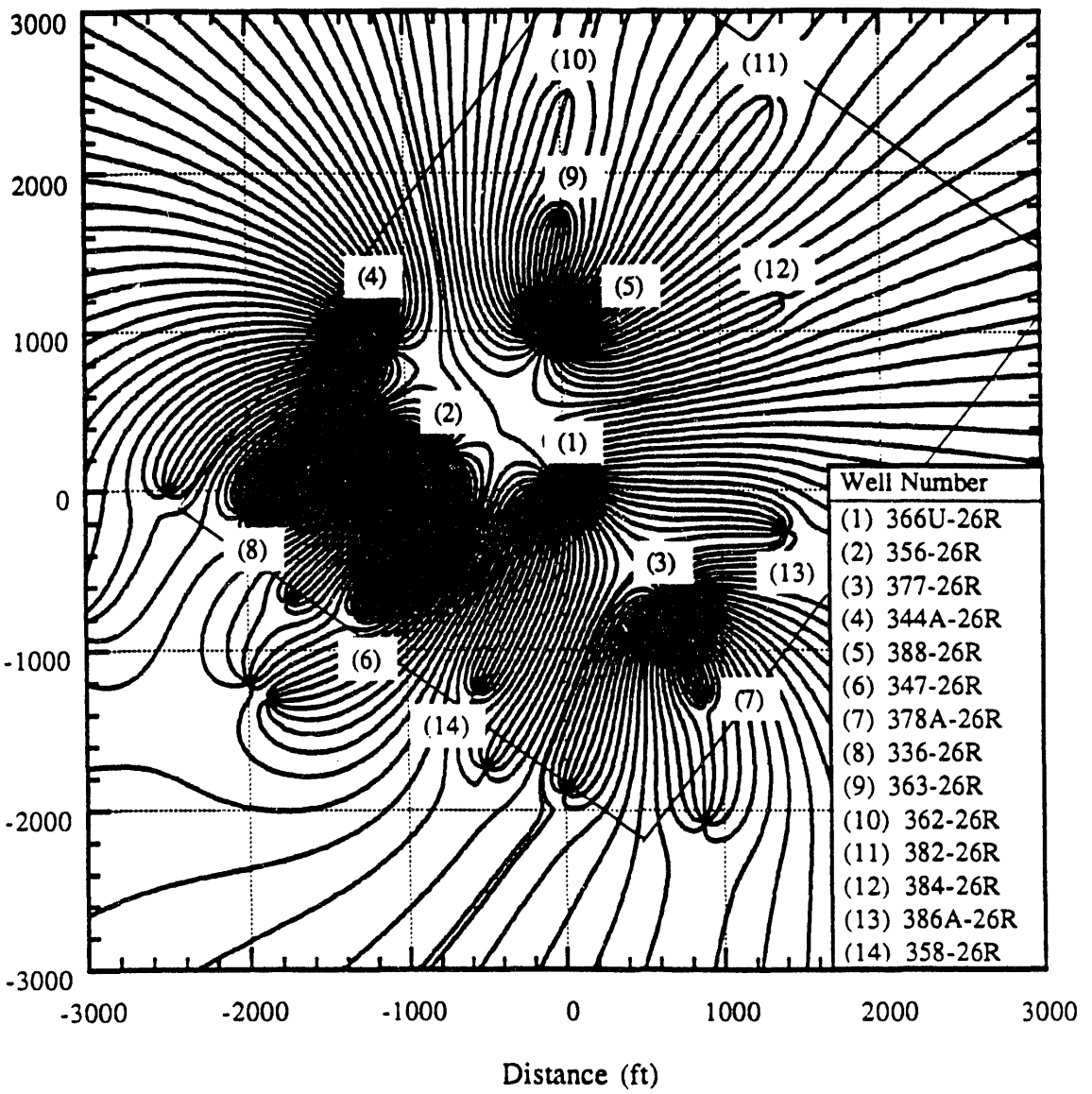

Fig. 4 Results from streamline model used to determine the boundary of area to be simulated.

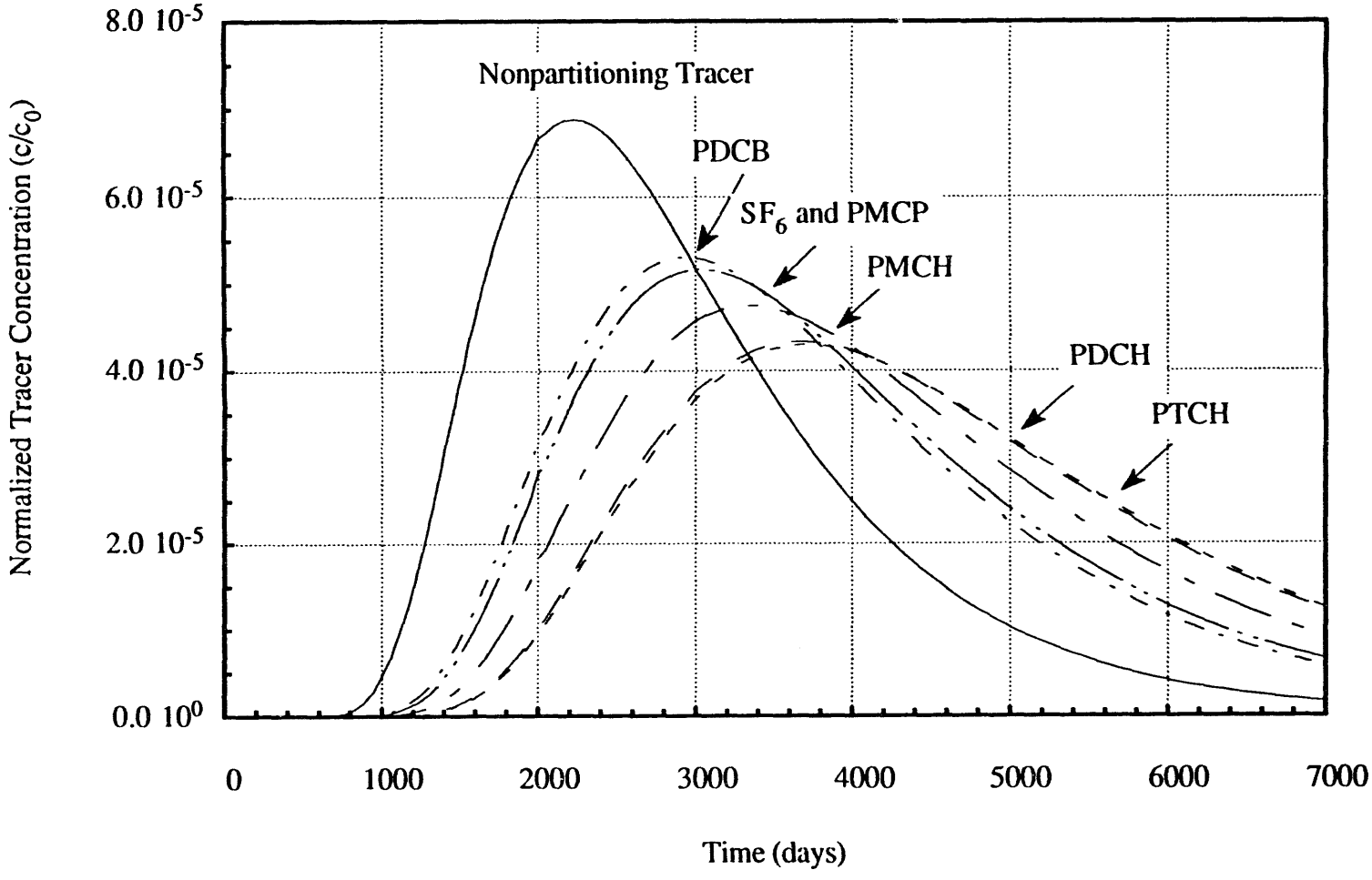

Fig. 5 Simulated tracer concentration history at Well No.347-26R.

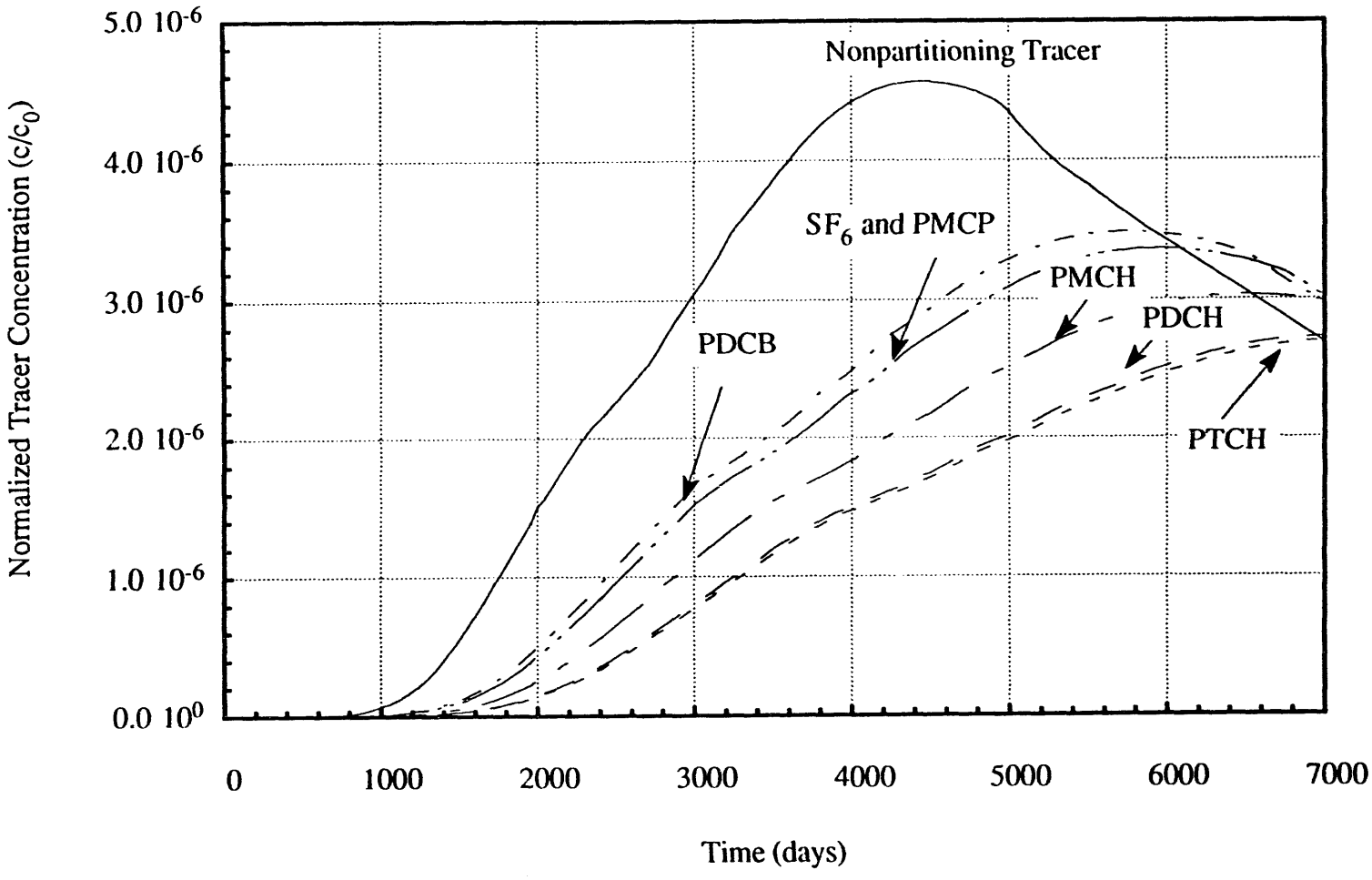

Fig. 6 Simulated tracer concentration history at Well No.378A-26R.

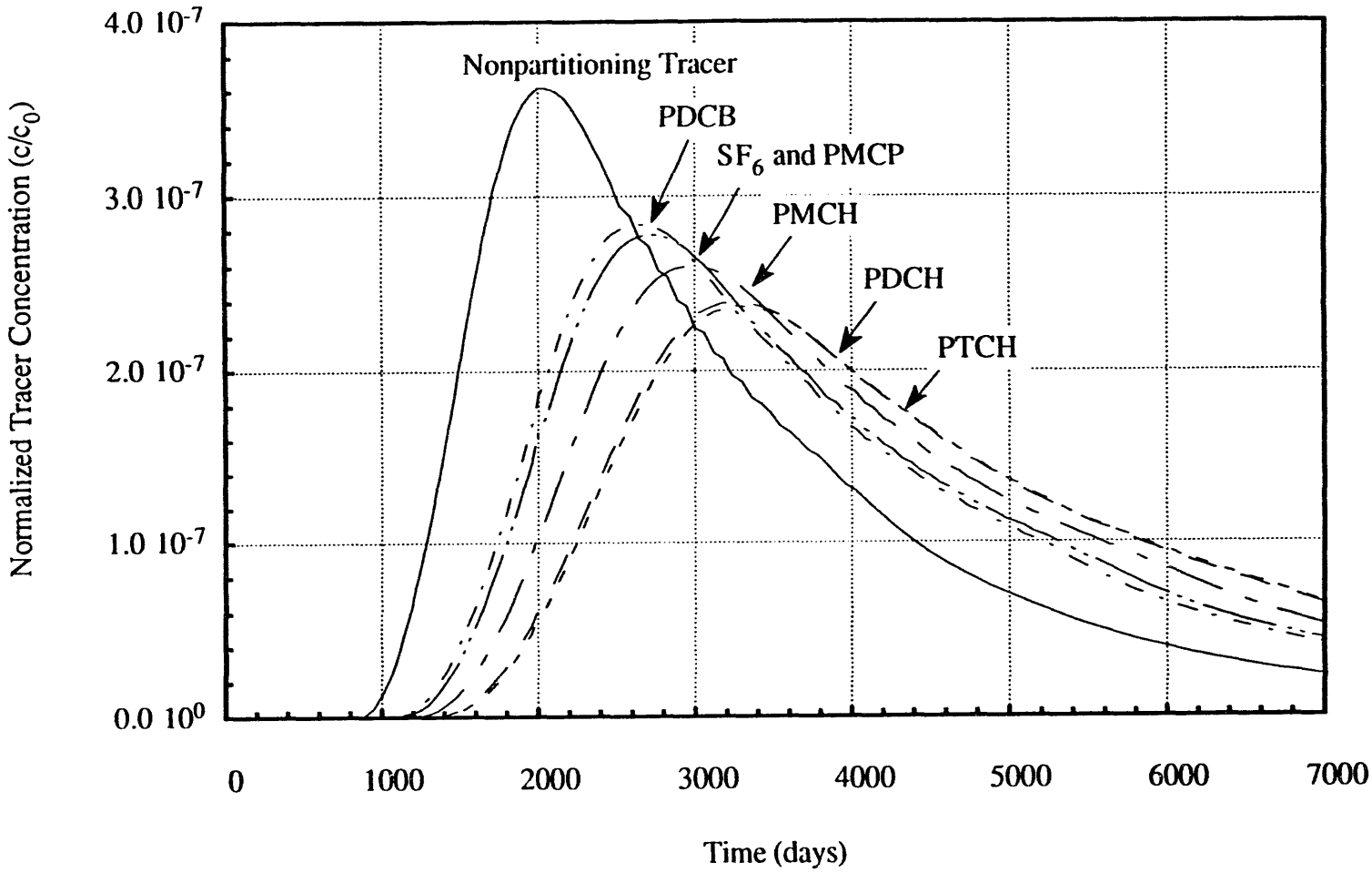

Fig. 7 Simulated tracer concentration history at Well No.336-26R.

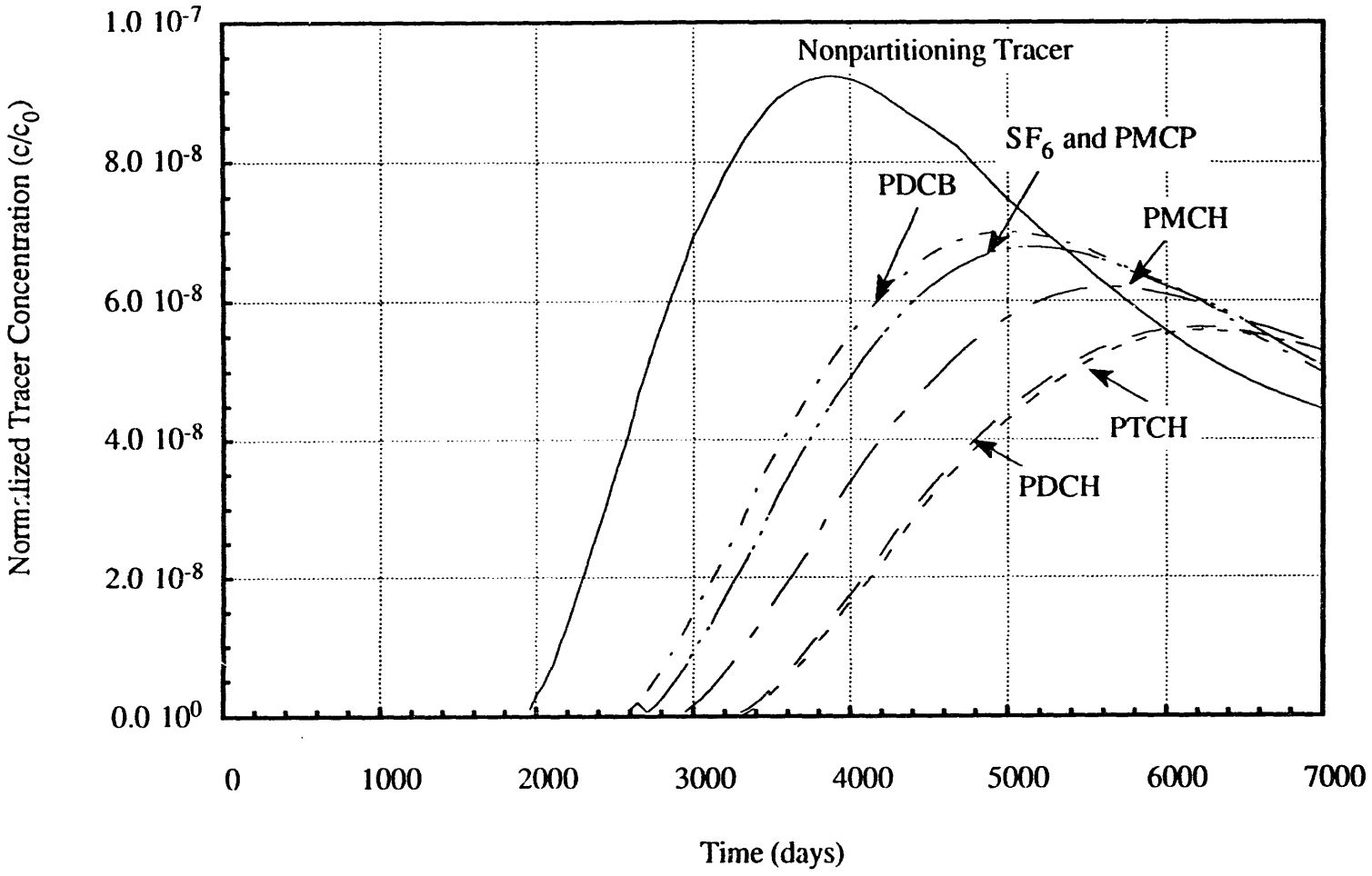

Fig. 8 Simulated tracer concentration history at Well No.363-26R.

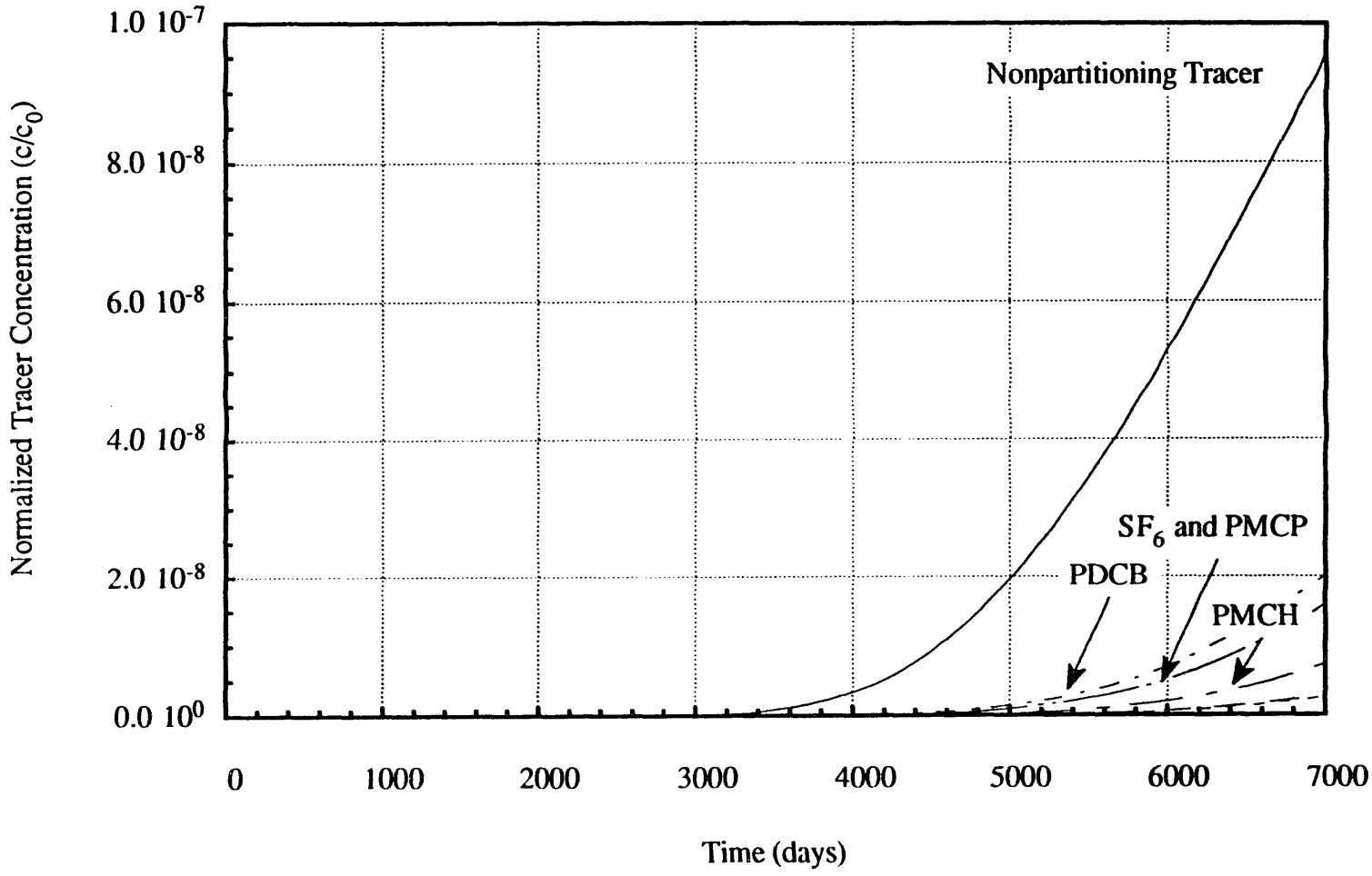

Fig. 9 Simulated tracer concentration history at Well No.362-26R.

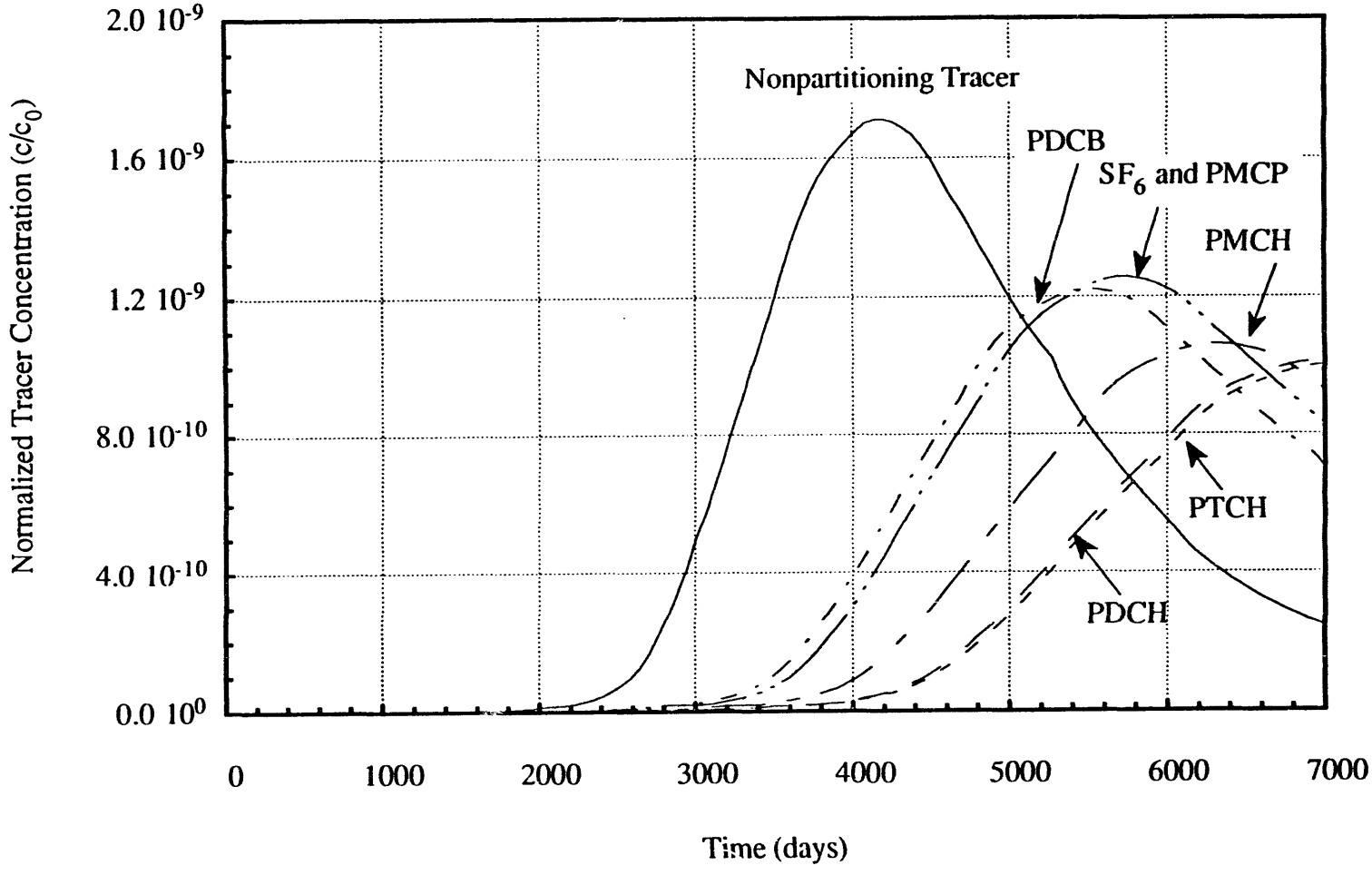

Fig. 10 Simulated tracer concentration history at Well No.382-26R.

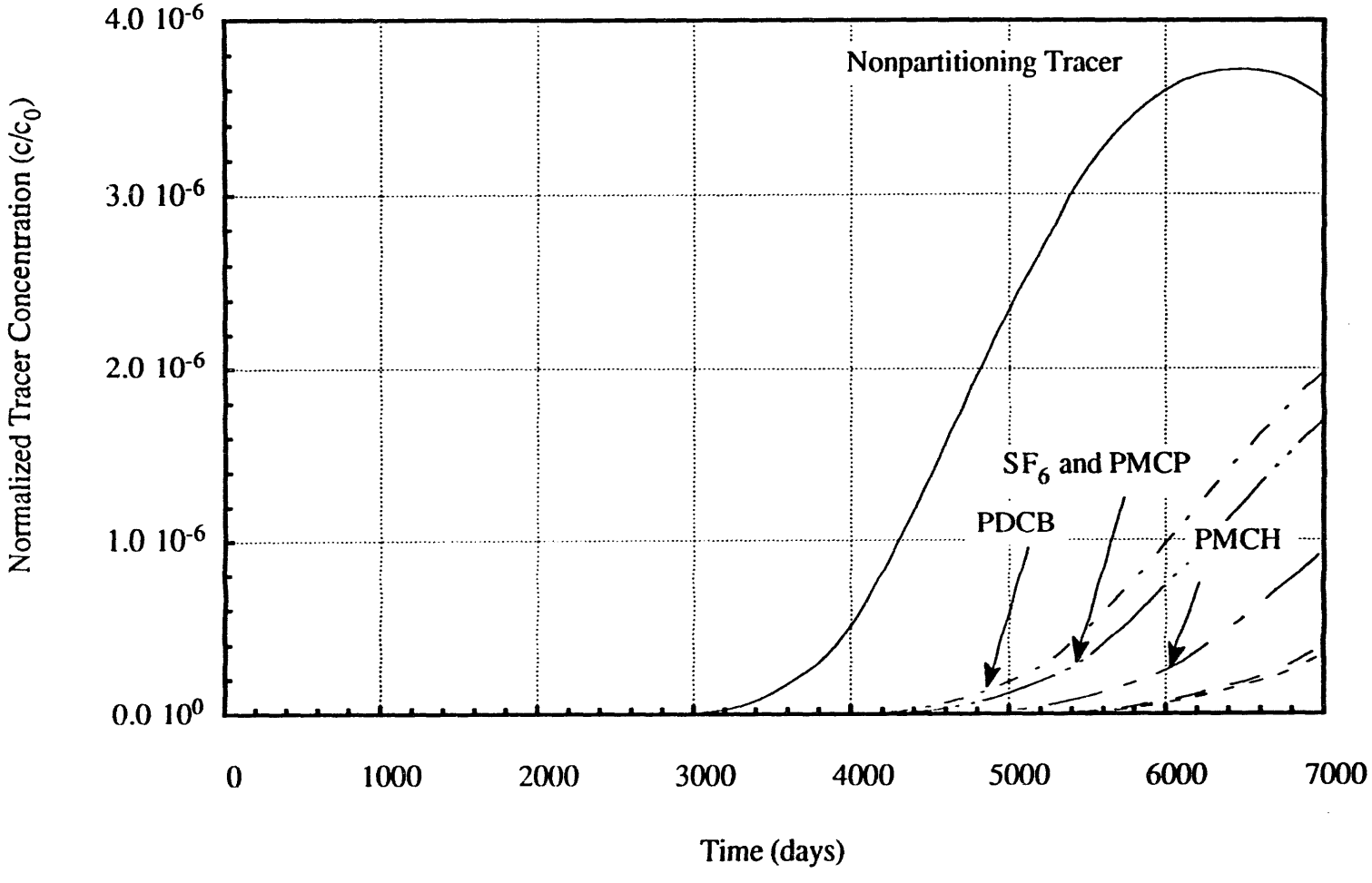

Fig. 11 Simulated tracer concentration history at Well No.384-26R.

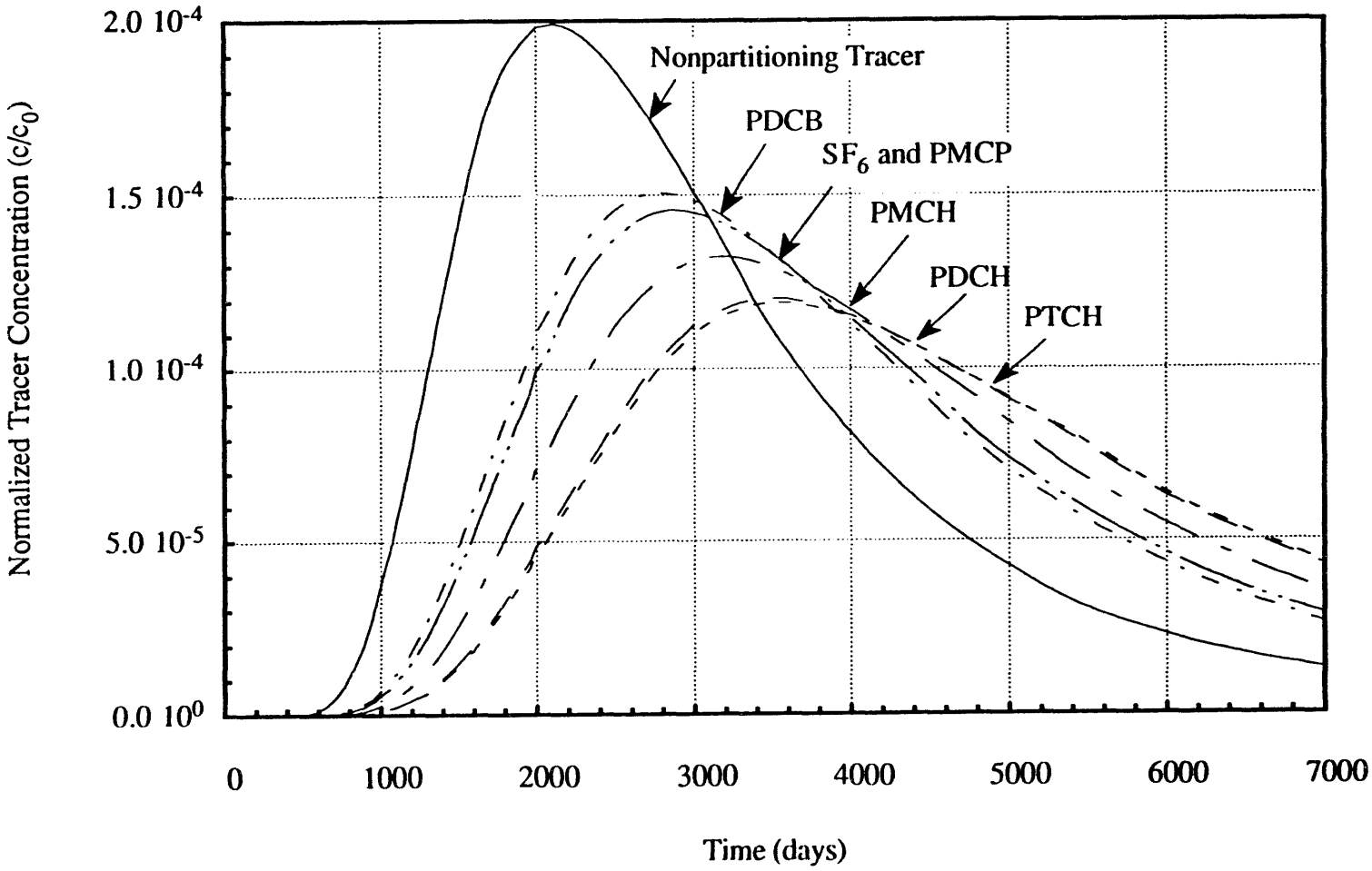

Fig. 12 Simulated tracer concentration history at Well No.386A-26R.

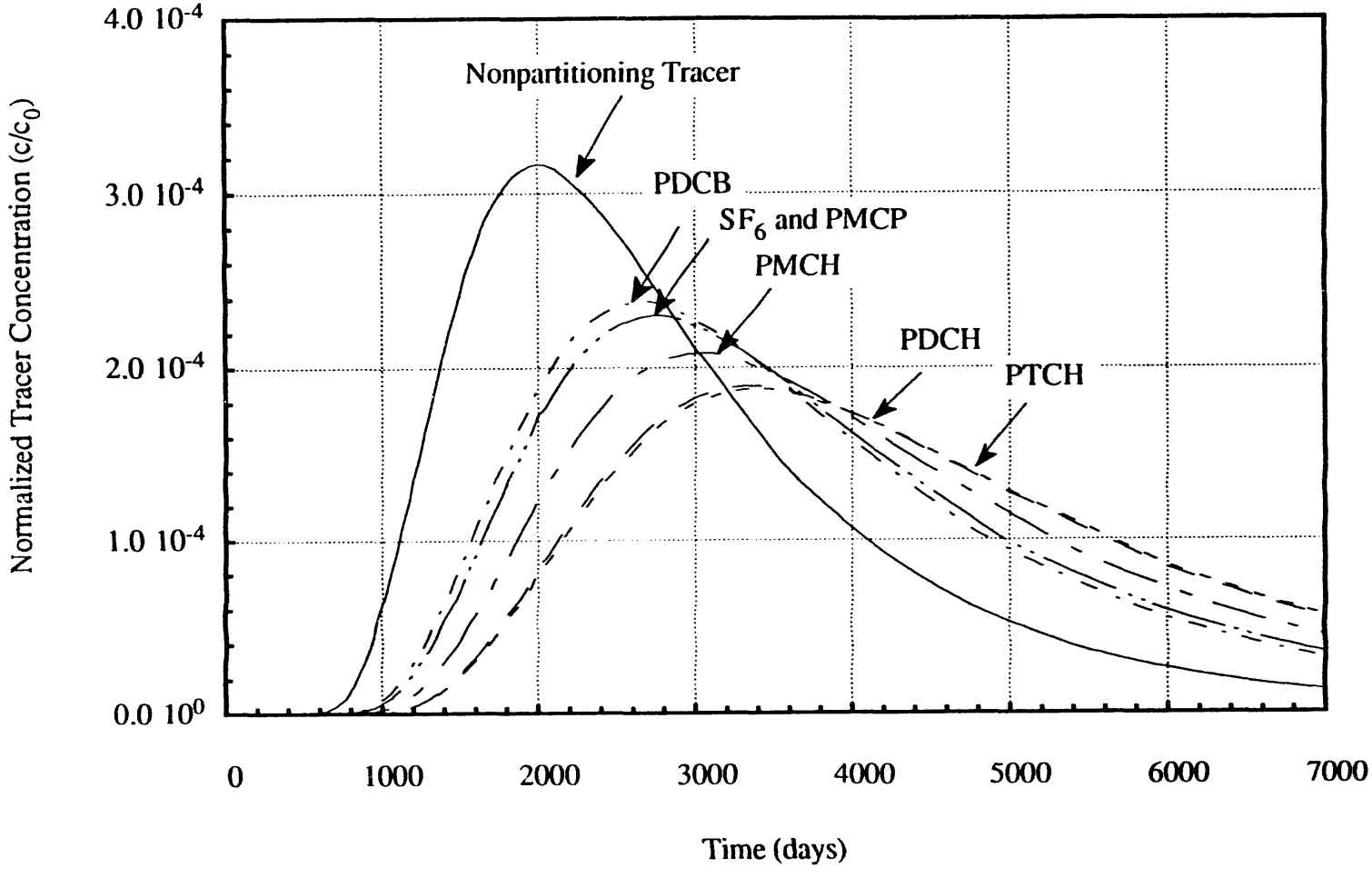

Fig. 13 Simulated tracer concentration history at Well No.358-26R.

NOMENCLATURE

a_i	Amount of tracer i adsorbed (lbm)
$c(t)$	Produced concentration history
$c_0(t)$	Injected concentration history
$c_{st}(t)$	Streamtube concentration response
$\bar{C}$	Adsorbed tracer concentration
$C_{i,\ell}$	Concentration of tracer i in phase ℓ (lbm/ft^3)
cN_{RL}	$\dfrac{158\ u\ \mu_j\ \Delta x}{c_{pcj}\ k_{rj}^{o}\sqrt{\phi\ k_h}}$, Cell Rapoport and Leas number
c_{pcj}	Capillary pressure parameter [psi darcy$^{1/2}$]
cP_e	$\dfrac{\Delta x}{\alpha_l}$, Longitudinal cell Peclet number
$C(\omega)$	Fourier transform of $c(t)$
$C_0(\omega)$	Fourier transform of $c_0(t)$
D_{st}	Retardation factor (pore volume)
e_j	Relative permeability exponent of phase j
f_c	Critical (Nyquist) frequency, 1/t
$h(t)$	Impulse response function
$H(\omega)$	Fourier transform of $h(t)$
k	Permeability [darcy]
k_h	Horizontal (radial) permeability [darcy]
k_{rj}	Relative permeability of phase j
k_{rj}^{o}	Endpoint relative permeability of phase j
k_x	Horizontal permeability, L^2
k_z	Vertical permeability, L^2
K_{Ti}	Partition coefficient for tracer i
L	Length of reservoir [ft]
M^o	Endpoint mobility ratio
$M_{i,\ell}$	Mass transfer coefficient of tracer i in phase ℓ (day^{-1})
n_{pcj}	Capillary pressure exponent
P_{ci}	Critical pressure for component i (psia)
$P_{c,ow}$	Capillary pressure between oil and water [psi]
$P_{e,l}$	$\dfrac{L}{\alpha_l}$, Longitudinal Peclet number
$P_{e,t}$	$\dfrac{W^2}{L\alpha_l}$, Transverse Peclet number
q_{inj}	Injection rate (ml/min)
r_e	Outer radius [ft]
r_w	Wellbore radius [ft]
S_{jr}	Residual saturation of phase j
S_{nj}	Normalized saturation of phase j
S_{wi}	Initial water saturation

S_ℓ	Phase saturation (fraction)
$S_{\ell r}$	Residual saturation of phase ℓ (fraction)
t_D	Pore volumes injected
t_r	Retention time (min)
T	Time required to inject 1 PV, t
T_{ci}	Critical temperature for component i (^oR)
v	Total velocity, L/t
v_x	x-component of velocity, L/t
v_z	z-component of velocity, L/t
V_{ci}	Critical volume for component i (cu ft/lb-mole)
V_{DP}	Dykstra-Parsons coefficient
V_m	Volume of mobile gas (ml)
V_r	Retention volume (ml)
V_s	Volume of stationary oil (ml)
VR_r	Relative retention volume (fraction)
W	Width of reservoir [ft]
Wt_i	Molecular weight for component i (lbm/lb-mole)

Greek symbols

λ_D	$\frac{\lambda_x}{L}$, Dimensionless correlation length
$\sigma^2 \ln$	Variance of log permeability
ρ_g	Rock density (lbm/ft^3)
ϕ	Porosity (fraction)
$\tau(\psi)$	Transit time at the producer, PV
$\tau_a(\psi)$	Areal transit time distribution, PV
ψ	Normalized streamfunction
$\Delta\psi_i$	Size of streamtube i
$\Phi(\omega)$	Phase spectrum
ω_c	Critical angular frequency, 1/t
ω_d	Dimensionless angular frequency at match point
ω_m	Angular frequency at match point, 1/t

Subscripts

avg	Arithmetic mean
i	Component index
j	Phase j
l	Longitudinal
ℓ	Phase index (o, w, g)
o	Oleic phase
r	Rock
t	Transverse
w	Aqueous phase

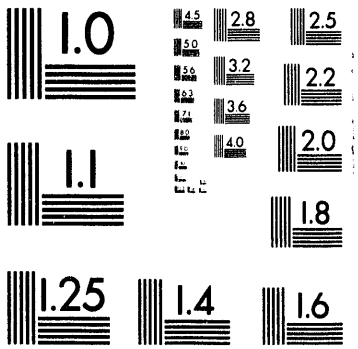
1.0
2.8
2.5
3.2
2.2
3.6
2.0
4.0
1.1
1.8
1.25
1.4
1.6

2 of 2

REFERENCES

Abbaszadeh-Dehghani, M. and W.E. Brigham: "Analysis of Unit Mobility Ratio Well-to-Well Tracer Flow to Determine Reservoir Heterogeneity," U.S. DOE Report SF/11564-1, Feb. 1983, SUPRI TR-36.

Abbaszadeh-Dehghani, M. and W.E. Brigham: "Analysis of Well-to-Well Tracer Flow to Determine Reservoir Layering," *J. Pet. Tech.* (Oct. 1984) **36**, 1753-1762.

Abbaszadeh-Denghani, M. and M. Kamal: "Pressure-Transient Testing of Water-Injection Wells," *SPE Reser. Eng.* (Feb. 1989) **4**, 115-124.

Allison, S.B., G.A. Pope, and K. Sepehrnoori: "Analysis of Field Tracers for Reservoir Description," *J. Pet. Sci. Eng.* (1991) **5**, No. 2, 173-168.

Amott, E.: "Observations Relating to the Wettability of Porous Rock," *Trans.*, AIME (1959) **216**, 156-62

Andersen, M.A., D.C. Thomas, and D.C. Teeters: "A New Formation Wettability Test: The Dynamic Wilhelmy Plate Wettability Technique," paper SPE 17368 presented at the 1988 SPE/DOE Symposium on Enhanced Oil Recovery, Tulsa, OK, April 17-20, 1988.

Anderson, W.G.: "Wettability Literature Survey - Part 1: Rock/Oil/Brine Interactions and the Effects of Core Handling on Wettability," *J. Pet. Tech.* (Oct. 1986a) **38**, 1125-1144.

Anderson, W.G.: "Wettability Literature Survey - Part 2: Measurements of Wettability," *J. Pet. Tech.* (Nov. 1986b) **39**, 1453-1468.

Anderson, W.G.: "Wettability Literature Survey - Part 3: Effects of Wettability on Electrical Properties," *J. Pet. Tech.* (Dec. 1986c) **39**, 1453-1468.

Anderson, W.G.: "Wettability Literature Survey - Part 4: Effects of Wettability on Capillary Pressure," *J. Pet. Tech.* (Oct. 1987a) **39**, 1283-1300.

Anderson, W.G.: "Wettability Literature Survey - Part 5: Effects of Wettability on Relative Permeability," *J. Pet. Tech.* (Nov. 1987b) **39**, 1453-1468.

Arya, A., T.A. Hewett, R.G. Larson, and L.W. Lake: "Dispersion and Reservoir Heterogeneity," *SPE Reser. Eng.* (Feb. 1988) **3**, No. 1, 139-148.

Bear, J.: *Dynamics of Fluids in Porous Media* , Dover, New York (1988).

Bhuyan, D., L.W. Lake, and G.A. Pope: "Mathematical Modelling of High pH Chemical Flooding," paper SPE 17398 presented at the 1988 SPE/DOE Symposium on Enhanced Oil Recovery, Tulsa, OK, April 17-20.

Bhuyan, D.: "Effect of Wettability on Capillary Desaturation Curves," M.S. thesis, The U. of Texas, Austin (May 1986).

Coats, K.H. and B.D. Smith: "Dead-End Pore Volume and Dispersion in Porous Media," *Soc. Pet. Eng. J.* (Mar. 1964) **4**, 73-84; *Trans.*, AIME **231**.

Cockcroff, P.J., D.R. Guise, and I.D. Waworuntu: "The Effect of Wettability on Estimation of Reserves," paper SPE 19484 presented at the SPE Asia-Pacific Conference, Sydney, Australia, Sept. 13-17, 1989.

Cooke, C.E., Jr.: "Method of Determining Residual Oil Saturation in Reservoirs," U.S. Patent 3,590,923 (July 1971).

Craig, F.F.: *The Reservoir Engineering Aspects of Waterflooding*, Monograph Series, Soc. Pet. Eng., Dallas, TX (1971) **3**.

Datta Gupta, A., G.A. Pope, K. Sepehrnoori, and R.L. Thrasher: "A Symmetric, Positive Definite Formulation of a Three-Dimensional Micellar/Polymer Simulator," *SPE Reser. Eng.* (Nov. 1986) **1**, 622-632.

Datta Gupta, A., L.W. Lake, G.A. Pope, and M.J. King: "A Type Curve Approach to Analyzing Two-Well Tracer Tests," paper SPE 24139 presented at the SPE/DOE 8th Symposium on Enhanced Oil Recovery, Tulsa, OK, April 21-24, 1992.

Deans, H.A. and J.R. Bragg: "Method for Determining Fluid Saturations in Reservoirs," U.S. Patent 4,090,398 (Jan. 1977).

Deans, H.A. and L.K. Shallenberger: "Single-Well Chemical Tracer Method to Measure Connate Water Saturation," paper SPE 4755 presented at the 1974 SPE Symposium on Improved Oil Recovery, Tulsa, OK, April 22-24.

Deans, H.A. and S. Majoros: "The Single-Well Chemical Tracer Method for Measuring Residual Oil Saturation, Final Report," DOE/BC/20006-18, Oct. 1980.

Deans, H.A., J.R. Bragg, and L.K. Shallenberger: "In-Situ Determination of Residual Gas Saturation by Injection and Production of Brine," paper SPE 6047 presented at the 1976 SPE Annual Tech. Conf., New Orleans, LA, Oct. 3-6.

Deans, H.A.: "A Mathematical Model for Dispersion in the Direction of Flow in Porous Media," *Soc. Pet. Eng. J.* (Mar. 1963) **3**, 49-52; *Trans.*, AIME **228**.

Deans, H.A.: "Using Chemical Tracers to Measure Fractional Flow and Saturation In-Situ," paper SPE 7076 presented at the Fifth SPE Symposium on Improved Methods for Oil Recovery, Tulsa, OK, April 16-19, 1978.

Deans, H.A.: "Method of Determining Fluid Saturations in Reservoirs," U.S. Patent 3,623,842 (Nov. 1971).

Deans, H.A.: "Using Chemical Tracers to Measure Fractional Flow and Saturation In-Situ," paper SPE 7076 presented at the 1978 SPE Symposium on Improved Oil Recovery, Tulsa, OK, April 16-19.

Delshad, M., D.J. MacAllister, G.A. Pope, and B.A. Rouse: "Multiphase Dispersion and Relative Permeability Experiments," *Soc. Pet. Eng. J.* (Aug. 1985) **25**, 524-534.

Desbrandes, R. and Z. Bassiouni: "In-Situ Formation Wettability Determination in Depleted Zones," paper SPE 21182 presented at the SPE Latin America Petroleum Engineering Conference, Rio de Janeiro, Brazil, Oct. 14-19, 1990.

Desbrandes, R. and Z. Bassiouni: "In-Situ Wettability Determination in Gas Reservoir," paper SPE 19058 presented at the 1989 SPE Gas Technology Symposium, Dallas, TX, April 17-20.

Descant, F.J., III: "Simulation of Single-Well Tracer Flow," M.S. thesis, The U. of Texas, Austin (Aug. 1989).

Donaldson, E.C. and R.D. Thomas: "Microscopic Observations of Oil Displacement in Water-Wet and Oil-Wet Systems," paper SPE 3555 presented at the 1971 SPE Annual Tech. Conf. and Exhibition, New Orleans, LA, Oct. 3-6.

Donaldson, E.C., R.D. Thomas, and P.B. Lorenz: "Wettability Determination and Its Effect on Recovery Efficiency," *Soc. Pet. Eng. J.* (Mar. 1969) **9**, 13-20.

Duffy, C.J. and L.W. Gelhar: "A Frequency Domain Analysis of Groundwater Quality Fluctuations: Interpretation of Field Data," *Water Resour. Res.* (1986) **22**, No. 7, 1115-1128.

Duffy, C.J. and L.W. Gelhar: "A Frequency Domain Approach to Water Quality Monitoring in Groundwater: Theory," *Water Resour. Res.* (1985) **21**, No. 8, 1175-1184.

Duffy, C.J. and S. Al-Hassan: "The Time and Frequency Response of Tracer Experiments," *J. Hydrol.* (1988) **97**, No. 1/2, 59-73.

Dustad, ø., T. Bjørnstad, and I.A. Hundere: "Construction of a Slim-Tube Equipment for Gas-Tracer Evaluation at Simulated Reservoir Conditions," Institutt for Energiteknikk, N-2007 Kjeller, Norway (1991).

Dykstra, H and R.L. Parsons: "The Prediction of Oil Recovery by Water Flood," *Secondary Recovery of Oil in the United States*, API (1950) 160-74.

Earlougher, R.C., Jr.: *Advances in Well Test Analysis*, SPE Monograph Series, Soc. Pet. Eng., Richardson, TX (1977).

Ehrlich, R., H.H. Hasiba, and P. Raimondi: "Alkaline Waterflooding for Wettability Alteration - Evaluating a Potential Field Application," *J. Pet. Tech.* (Dec. 1974) **26**, 1335-43.

Ezekwe, N., S. Smith, M. Wilson, M. Humphrey, and J. Murphy: "Performance of a Peripheral Waterflood Project in the Main Body 'B' Reservoirs (Stevens) at the Elk Hills Oil Field, California," paper SPE 21759 presented at the SPE Western Regional Meeting, Long Beach, CA, Mar. 20-22, 1991.

Ferreira, L.E.A.: "Reservoir Characterization Using Single-Well Tracer Tests," Ph.D. dissertation, The U. of Texas, Austin (Aug. 1992).

Gangwal, S.K., R.R. Hudgins, A.W. Bryson, and P.L. Silveston: "Interpretation of Chromatographic Peaks by Fourier Analysis," *Can. J. Chem. Eng.* (1971) **49**, No. 1, 113-119.

Gelhar, L.W. and C.L. Axness: "Three-Dimensional Stochastic Analysis of Macrodispersion in Aquifers," *Water Resour. Res.* (1983) **19**, No. 1, 161-180.

Gelhar, L.W. and C.L. Axness: "Three-Dimensional Stochastic Analysis of Macrodispersion in Aquifers," *Water Resour. Res.* (1978) **14**, No. 2, 161-180.

Glimm, J. and D.H. Sharp: "A Random Field Model for Anomalous Diffusion in Heterogeneous Porous Media," SUSB preprint no. SUSB-AMS-90-08, 1990.

Goggin, D.J.: "Geologically-Sensible Modeling of the Spatial Distribution of Permeability in Eolian Deposits: Page Sandstone (Jurassic), Northern Arizona," Ph.D. dissertation, The U. of Texas, Austin (1988).

Honarpour, M., L. Koederitz, and A.H. Harvey: *Relative Permeability of Petroleum Reservoirs*, CRC Press, Inc., Boca Raton, FL (1986).

Jennings, H.Y.: "Surface Properties of Natural and Synthetic Porous Media," *Prod. Monthly* (Mar. 1957) **21**, 20-24.

Journel, A.B. and C.J. Huijbregts: *Mining Geostatistics*, Academic Press, New York (1978).

Karl, J.H.: *Introduction to Digital Signal Processing*, Academic Press, San Diego (1989).

Khan, S.A.: "Development of an Expert System," Miscible Gas Flooding, Category C Research, 8th Annual Report of Enhanced Oil and Gas Recovery Research Program, The U. of Texas, Austin (Mar. 1991).

Killins, C.R., R.F. Nielsen, and J.C. Calhoun, Jr.: "Capillary Desaturation and Imbibition in Rocks," *Prod. Monthly* (Dec. 1953) **18**, 30-39.

Koch, D.L. and J.F. Brady: "Anomalous Diffusion in Heterogeneous Porous Media," *Phys. Fluids* (1988) **31**, 965-73.

Koval, E.J.: "A Method for Predicting the Performance of Unstable Miscible Displacement in Heterogeneous Media," *Soc. Pet. Eng. J.* (1963) 145-54.

Lake, L.W.: *Enhanced Oil Recovery*, Prentice Hall, Englewood Cliffs, NJ (1989).

Maini, B.B., E. Ionescu, and J.P. Batycky: "Miscible Displacement of Residual Oil — Effect of Wettability on Dispersion in Porous Media," *J. Cdn. Pet. Tech.* (May-June 1986) **25**, 36-41.

Mantoglou, A. and J.L. Wilson: "The Turning Bands Method for Simulation of Random Fields Using Line Generation by a Spectral Method," *Water Resour. Res.* (1982) **18**, No. 5, 1379-1394.

Mishra, S.M., F.M. Orr, and W.E. Brigham: "Tracer and Pressure Test Analysis for Characterization of Areally Heterogeneous Reservoirs," paper SPE/DOE 17365 presented at the 1988 SPE Symposium on Enhanced Oil Recovery, Tulsa, OK, April 17-20.

Morrow, N.R., P.J. Cram, and F.G. McCaffery: "Displacement Studies in Dolomite With Wettability Control by Octanoic Acid," *Soc. Pet. Eng. J.* (Aug. 1973) **13**, 221-232; *Trans.*, AIME **255**.

Mungan, N.: "Certain Wettability Effects in Laboratory Waterfloods," *J. Pet. Tech.* (Feb. 1966) **18**, 247-52; *Trans.*, AIME **237**.

Mut, A.D. and H.A. Deans: "Alcohol Extraction Technique for the In-Situ Determination of Resident Water Saturation and Resident Brine Salinity," paper SPE 12094 presented at the 1983 SPE Annual Tech. Conf., San Francisco, CA, Oct. 5-8.

Namba, T. and R.N. Horne: "Estimation of Water and Oil Relative Permeabilities From Pressure Transient Analysis of Water Injection Well Data," paper SPE 19829 presented at the 1989 SPE Annual Tech. Conf. and Exhibition, San Antonio, TX, Oct. 8-11.

Owens, W.W. and D.L. Archer: "The Effect of Rock Wettability on Oil-Water Relative Permeability Relationships," *J. Pet. Tech.* (Jul. 1971) **23**, 873-878; *Trans.*, AIME **251**.

Pollock, D.W.: "Semianalytical Computation of Pathlines for Finite-Difference Models," *Ground Water* (1988) **26**, No. 6, 743-750.

Pope, G.A. and K. Sepehrnoori: "Innovative Techniques for the Description of Reservoir Heterogeneity Using Tracers," Quarterly Report for the period Oct. 1990 - Dec. 1990, work performed under contract No. DE-AC22-90BC14653.

Pope, G.A., L.W. Lake, and K. Sepehrnoori: "Modelling and Scale-Up of Chemical Flooding," U.S. DOE Report BC/10846-5 (July 1987).

Priestley, M.B.: *Spectral Analysis and Time Series*, Academic Press, New York (1981).

Rial, M.R.: "Naval Petroleum Reserve No. 1, Kern County, California, 26R Detailed Reservoir Study, Final Report," Scientific Software-Intercomp, Inc., Denver, CO (April 1990).

Rowney, J.D.: "Nonreversing Fractional Flow and Composition Behavior in Porous Media," Ph.D. dissertation, U. of Houston (Aug. 1989).

Saad, N., G.A. Pope, and K. Sepehrnoori: "Application of Higher-Order Methods in Compositional Simulation," *SPE Reser. Eng.* (Nov. 1990) **5**, 623-630.

Saad, N., G.A. Pope, and K. Sepehrnoori: "Simulation of Big Muddy Surfactant Pilot," *SPE Res. Eng.* (Feb. 1989) **4**, No. 1, 24-34.

Salter, S.J. and K.K. Mohanty: "Multiphase Flow in Porous Media: I. Macroscopic Observations and Modeling," paper SPE 11017 presented at the 1982 SPE Annual Tech. Conf. and Exhibition, New Orleans, LA, Sept. 26-29.

Senum, G.I., "Program Proposal 26R Reservoir Tracer Test Project," Brookhaven National Laboratory, Upton, NY (Sep. 12, 1991).

Senum, G.I., R.N. Dietz, T.W. D'Ottavio, R.W. Goodrich, E.A. Cote, and D.J. Spandau: "A Perfluorocarbon Tracer Transport and Dispersion Experiment in the North Sea Ekofisk Oil Field," prepared for the U.S. Department of Energy under Contract No. DE-AC02-76CH00016, Bartlesville, OK (July 1990).

Simmons, C.S.: "A Stochastic-Convective Transport Representation of Dispersion in One-Dimensional Porous Media Systems," *Water Resour. Res.* (1982) **18**, No. 4, 1193-1214.

Smith, J.C., M. Delshad, G.A. Pope, W.G. Anderson, and D. Marcel: "An Analysis of Unsteady-State Displacements Using a Capacitance-Dispersion Model," *In Situ* (1988) **12**, Nos. 1 and 2, 41-78.

Smith, P.J. and C.E. Brown: "The Interpretation of Tracer Test Response From Heterogeneous Reservoirs," paper SPE 13262 presented at the 1984 SPE Annual Tech. Conf. and Exhibition, Houston, TX, Sept. 16-19.

Stalkup, F.I.: *Miscible Displacement*, Monograph Series, Soc. Pet. Eng., Dallas, TX (1983) **8**.

Thomman, R.W.: *Systems Analysis and Water Quality Management*, McGraw-Hill, New York (1972).

Tomich, J.F. and H.A. Deans: "Method to Measure Fluid Drift and Immobile Phase Saturation," U.S. Patent 3,902,326 (Sep. 1974).

Tomich, J.F., R.L. Dalton Jr., H.A. Deans, and L.K. Shallenberger: "Single-Well Tracer Method to Measure Residual Oil Saturation," *J. Pet. Tech.* (Feb. 1973) **25**, 211-218.

Waggoner, J. R., J.L. Castillo, and L.W. Lake: "Simulation of EOR Processes in Stochastically Generated Permeable Media," paper SPE 21237 presented at the 11th SPE Symposium on Reservoir Simulation, Anaheim, CA, Feb. 17-20, 1991.

Wagner, O.R.: "The Use of Tracers in Diagnosing Interwell Reservoir Heterogeneities-Field Results," *J. Pet. Tech.* (Nov. 1977) **29**, 1410-1416.

Wang, F.H.L.: "Effect of Wettability Alteration on Water/Oil Relative Permeability, Dispersion, and Flowable Saturation in Porous Media," paper SPE 15019 presented at the 1986 SPE Permian Basin Gas Recovery Conference, Midland, TX, Mar. 13-14.

Yang, A.P.: "Stochastic Heterogeneity and Dispersion," Ph.D. dissertation, The U. of Texas, Austin (1990).

DATE
FILMED
5/12/94

END